Università degli Studi di Padova

Dipartimento di Geoscienze

SCUOLA DI DOTTORATO IN SCIENZE DELLA TERRA

CICLO XXVIII

READING THE SIGNATURES OF CHANGING ENVIRONMENTAL FORCINGS IN SALT-MARSH BIOGEOMORPHIC SYSTEMS

Direttore della Scuola: Prof. Fabrizio Nestola

Supervisore: Prof. Andrea D'Alpaos

Co-supervisore: Prof. Massimiliano Ghinassi

Dottorando: Marcella Roner

TABLE OF CONTENTS

ABSTRACT

The question on whether actual tidal morphologies are in equilibrium with current environmental conditions or retain signatures of past climatic changes or human interventions is a classical and fascinating one, furthermore being of intellectual as well as practical interest. Understanding the dynamic response of tidal landscapes to past conditions is critical to predict their response to future environmental changes, such as rate of relative sea-level rise and sediment supply. This is an open and fundamentally important point, particularly in times of natural and anthropogenic changes, during which tidal environments are most exposed to possibly irreversible transformations with far-reaching socio-economic and ecological implications worldwide.

The proposed work aims at analyzing the signatures of changing environmental forcings imprinted in the landscape and in the sedimentary record of the Venice Lagoon to refine our knowledge of tidal landforms dynamics. The thesis is developed following a biogeomorphic approach to the study of salt-marsh landscapes. Marsh biomorphological evolution, in response to changes in the environmental forcings, is analyzed investigating the relative role and mutual interactions and adjustments between physical and biological processes shaping the salt-marsh landscape.

This thesis was carried out through a series of extensive temporal and spatial high-resolution morphological, sedimentological, geochronological and elemental analyses, aimed at exploring the main features of sub-surface marsh samples and lagoonal sediment cores.

The study of sub-surface marsh samples highlights the mutual role of inorganic and organic accretion on salt marshes, which is mainly driven by the inorganic component near the channels, while the organic component largely contributes in the inner-marsh portion. The analyses carried out on sediment cores

refine the knowledge of the latest Holocene sedimentary succession of the Venice Lagoon, and furnish a chronostratigraphical model for the evolution over the last two millennia. In particular, for a salt-marsh succession, the analyses highlight the occurrence of a delayed marsh-dynamic response to changing sediment delivery rates.

RIASSUNTO

La questione inerente l'equilibrio delle morfologie tidali con le attuali condizioni ambientali, o se esse conservino tutt'ora i segni dei cambiamenti climatici o degli interventi antropici passati, è un argomento classico ed affascinante nel campo delle Geoscienze, oltre ad essere di interesse sia intellettuale che pratico. Comprendere i meccanismi che governano la risposta di un ambiente a marea a variazioni passate delle forzanti ambientali è fondamentale per prevedere la loro risposta a cambiamenti ambientali futuri, quali il tasso di innalzamento del livello del mare relativo e l'apporto di sedimenti. Si tratta di un tema tutt'oggi sospeso e di fondamentale importanza, soprattutto in tempi di cambiamenti sia naturali che umanamente indotti, durante i quali gli ambienti tidali sono maggiormente esposti a trasformazioni potenzialmente irreversibili, con implicazioni di vasta portata socio-economica ed ecologica in tutto il mondo.

Il presente lavoro si propone di analizzare le *firme* del cambiamento delle forzanti ambientali impresse nella morfologia e nel record sedimentario della Laguna di Venezia, con lo scopo di affinare la conoscenza delle dinamiche tidali. La tesi volge allo studio di sistemi di barena attraverso un approccio biogeomorfologico. L'evoluzione geomorfologica delle barene, in risposta ai cambiamenti delle forzanti ambientali, è analizzata investigando il ruolo relativo, le interazioni reciproche e le regolazioni esistenti tra i processi fisici e biologici che modellano gli ambienti di barena.

Il lavoro è realizzato attraverso una serie di analisi morfologiche, sedimentologiche, geocronologiche ed elementali, eseguite ad alta risoluzione spazio-temporale, volte ad esplorare le principali caratteristiche sia di campioni sub-superficiali di barena, sia di carote di sedimenti lagunari.

Lo studio dei campioni sub-superficiali evidenzia il ruolo reciproco delle componenti organica ed inorganica nell'accrezione delle barene, la quale è

principalmente guidata dalla componente inorganica in prossimità dei canali, mentre la componente organica contribuisce in gran parte nelle porzioni più interne delle barene. L'analisi effettuata sulle carote lagunari implementa la conoscenza della successione sedimentaria tardo-Olocenica della Laguna di Venezia, e fornisce un modello di evoluzione cronostratigrafica degli ultimi due millenni. In particolare, le analisi effettuate su una successione sedimentaria di barena, evidenziano la presenza di una risposta dinamica ritardata dell'ambiente a cambiamenti nei tassi di apporto sedimentario.

CHAPTER 1

INTRODUCTION

1.1 OVERVIEW

This study deals with lagoonal deposits accumulated in the Venice Lagoon (Italy) during the last millennium and aims at defining the main salt-marsh modifications in response to changes in both natural (e.g., Relative Sea Level Rise, hereinafter RSLR) and anthropogenic (e.g., sediment supply) forcings. Two key-areas were investigated to detect the mutual interactions and adjustment between physical and biological processes and their effects on salt-marsh surfaces, and to identify the effects on salt-marsh evolution of changing rates of RLSR and sediment supply enhanced by river diversions.

1.2 STATE OF THE ART

1.2.1 Lagoons and salt marshes

A lagoon is "a coastal basin dominated by tides, separated from the sea by a sandbar but communicating with it through lagoon inlets" (Brambati, 1988). Lagoons exhibit particular physical and biological characteristics, are characterized by extremely high biodiversity and elevated rates of primary productivity, host typical ecosystems and landforms and important socio-economic activities worldwide (e.g., Cronk and Fennessy, 2001; Barbier et al., 2011).

Referring to the vertical position within the tidal frame, supratidal areas are permanently dry, being located above the Maximum High Water Level (MHWL), whereas subtidal areas are always submerged, lying below the Minimum Low

Water Level (MLWL) (Fig. 1.1). Intertidal areas are instead subjected to tidal fluctuations, their elevation ranging between MHWL and MLWL. From a morphological point of view, salt marshes, tidal flats and subtidal platforms represent the three major unchanneled lagoon sub-environments. Salt marshes are topographically the highest, with elevation between Mean Sea Level (MSL) and MHWL. They are populated by a luxuriant halophytic vegetation and display a generally flat weakly concave-up profile (Adam, 1990). Tidal flats are characterized by elevations between MSL and MLWL, they lack any halophytic vegetation but can be populated by seagrass meadows, and are fully exposed to the atmosphere only during exceptionally low tides. Subtidal platforms are located below MLWL, and are therefore perennially submerged (e.g., Allen, 2000).

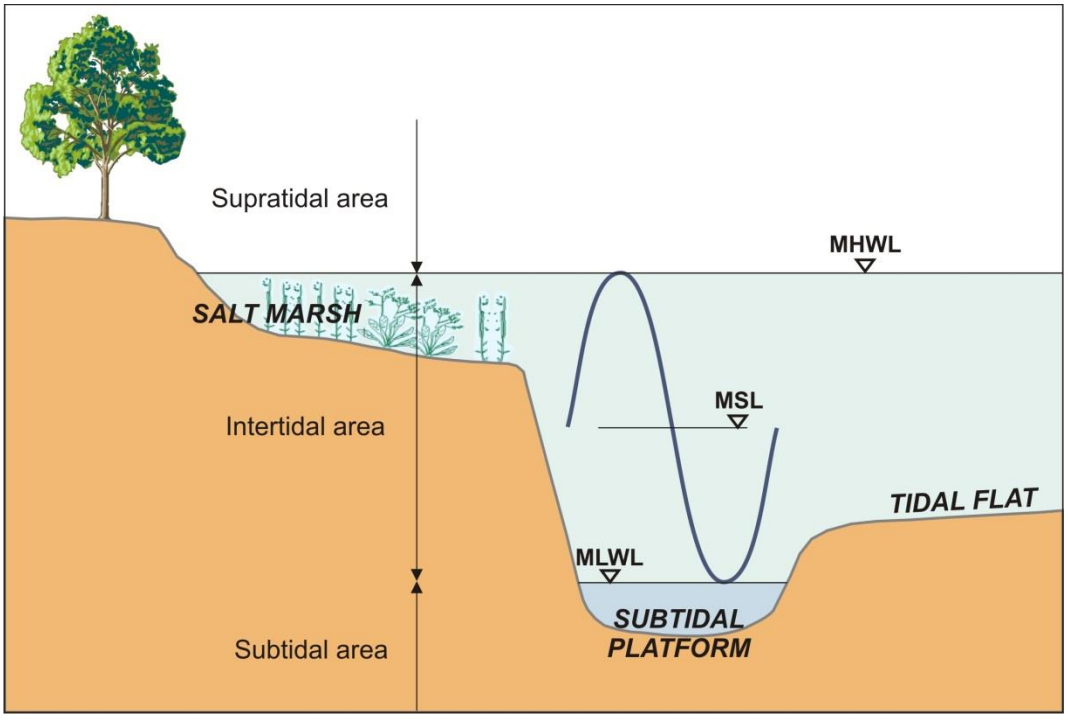

Fig. 1.1. Schematic representation of the subdivision between different sub-environments in the vertical tidal frame.

The unchanneled portions of the tidal landscape are tightly intertwined functionally with the network of channels which cuts through them and exerts a fundamental control on hydrodynamic, sediment and nutrient exchanges within tidal environments (e.g., D'Alpaos et al., 2005) (Fig. 1.2).

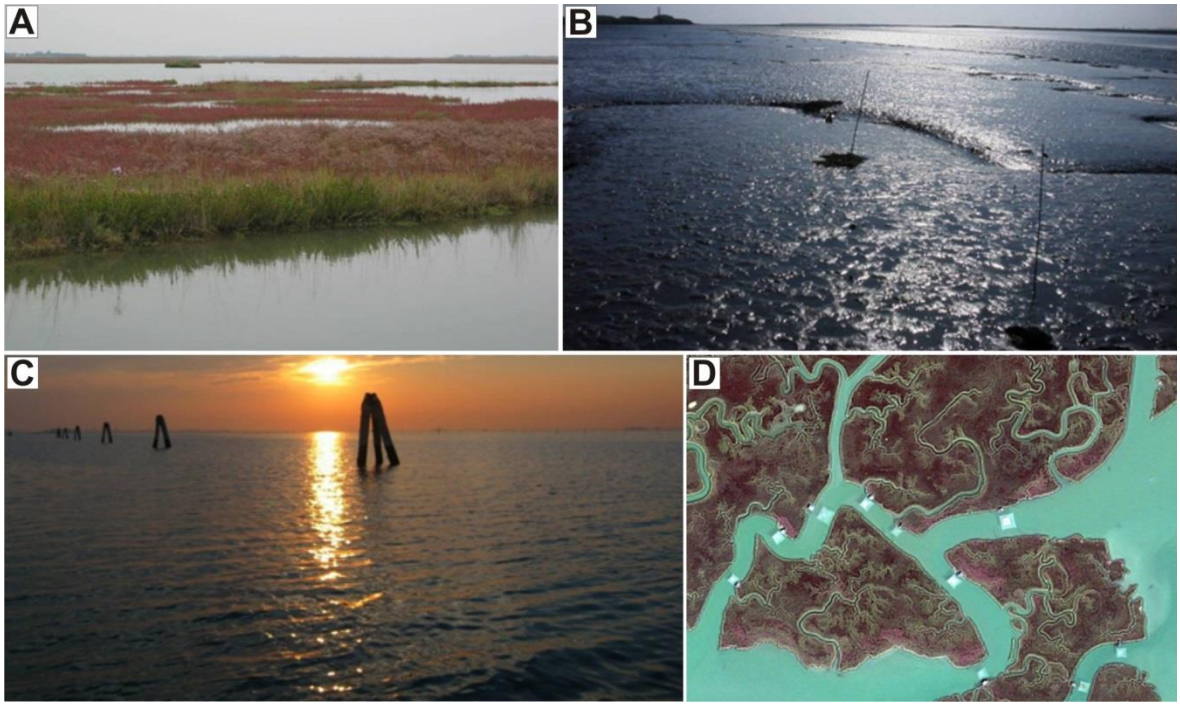

Fig. 1.2. Examples of Lagoon sub-environments: (A) Salt marshes; (B) Tidal flats; (C) Subtidal platforms; (D) Network of channels.

As part of the coastal zone, salt marshes can be defined as "vegetated areas located between coastal hinterlands and daily flooded coastal areas" (Bartholdy, 2012). They thus, represent a transition zone between submerged and emerged environments, occupying the upper margins of the intertidal landscape. They form in low-energy, wave-protected shorelines and are characterized by extremely high primary and secondary production (e.g., Mitsch and Gosselink, 2000; Cronk and Fennessy, 2001; Barbier et al., 2011). Salt marshes exist in all climate zones, from the tropics to high-arctic coastal environments (Bartholdy, 2012), providing a high number of benefits and ecosystem services (e.g., Costanza et al., 1997) to human and, in general, to the entire environment, due to their unique position in the tidal frame. For millennia, humans have relied on marshes for direct provisioning of raw material and food (Davy et al., 2009). Although harvesting of marsh grasses and use of salt marshes as pasture land has decreased nowadays, these services are still important locally in both developed and developing areas of the world (Gedan et al., 2009). Salt marshes provide coastal protection from waves

and storm surges, as well from coastal erosion (e.g., Möller et al., 1999; Davy et al., 2009; Howes et al, 2010; Temmerman et al., 2013; Möller et al., 2014). They reduce impacts of incoming waves by reducing their velocities, height and duration (Gedan et al., 2011; Möller et al., 2014), and they reduce storm surge duration and height by providing extra water uptake and holding capacity in comparison to the sediments of unvegetated tidal flats (Costanza et al., 2008). Salt marshes act as natural filters that purify water from nutrient and pollutants (Mitsch and Gosselink, 2000; Costanza et al, 2007; Larsen et al., 2010;) because as water passes through marshes, it slows due to the baffling and friction effect of marsh vegetation (Morgan et al., 2009). Suspended sediments are then deposited on the marsh surface, facilitating nutrient uptake by vegetation. Salt-marsh ecosystem also provide nursery areas for coastal biota (e.g., Perillo et al., 2009; Silliman et al., 2009) and serve to maintain fisheries by boosting the production of economically and ecologically important fishery species, such as shrimp, oyster, clams and fishes (Boesch and Turner, 1984; MacKenzie and Dionne, 2008). Because of their complex and tightly packed plant structure, marshes provide habitat that is mostly inaccessible to large fishes, thus providing protection and shelter for the increased growth and survival of young fishes, shrimps and shellfish (Boesch and Turner, 1984). As one of the most productive ecosystem in the world, salt marshes serve as an important carbon sink due to their great ability to sequester atmospheric carbon (e.g., Chmura et al., 2003; Duarte et al., 2005; Mcleod et al., 2011; Murray et al., 2011; Sifleet et al., 2011; Kirwan and Mudd, 2012, Ratliff et al., 2015). The sequestered carbon by salt marshes is estimated at millions of tons of carbon annually (Mitsch and Gosselink, 2000), which is stocked in the biomass and in sediments (Duarte et al., 2005; Mcleod et al., 2011; Murray et al., 2011; Sifleet et al., 2011; Duarte et al., 2013). Because of the hypoxic marsh soil conditions, the carbon is buried and preserved for a long time, significantly contributing to the sequestration of "blue carbon" (Nellemann et al., 2009; Mcleod et al., 2011). Blue carbon is sequestered over the short (decennial) time scales in biomass, and over

longer (millennial) time scales in marsh sediments (Duarte et al., 2005), as marshes accrete vertically, leading to its presence both in the short-term and in the long-term carbon cycle. This capability is unique among many of the world ecosystems, where carbon is mostly turned over quickly and does not often move into the long term carbon cycle (Mitsch and Gosselink, 2000; Mayor and Hicks, 2009). Lastly, salt marshes provide important habitat for many other beneficial species, as birds, and are important for tourism, recreation, education and research (Barbier et al., 2011).

The future of these valuable coastal landforms and ecosystems is today at risk, exposed as they are to possibly irreversible transformations due to the effects of climate changes and human interferences (e.g., Delaune and Pezeshki, 2003; Marani et al., 2007; Day et al, 2009; Kirwan et al., 2010; Mudd, 2011; Murray et al., 2011; D'Alpaos et al., 2012; Ratliff et al., 2015). Current human threats to salt marshes include biological invasion, eutrophication, climate change and sea level rise, increasing air and sea surface temperatures, increasing CO_2 concentrations, altered hydrologic regimes, marsh reclamation, vegetation disturbance, and pollution (e.g., Silliman et al., 2009; Barbier et al., 2011).

Approximatively 50% of the original salt marsh ecosystem have been degraded or lost globally (Barbier et al., 2011), and in some areas, such as the West Coast of the US, the loss is >90% (Bromberg and Silliman, 2009; Gedan et al., 2009). However, the extent of salt marshes has dramatically decreased worldwide in the last century (Day et al., 2000; Marani et al., 2003, 2007; Carniello et al., 2009; Day et al., 2009; Gedan et al., 2009; Mcleod et al., 2011) together with their fundamental ecosystem services. For example, salt-marsh areas in the Venice lagoon decreased from about 180 km^2 in 1811 to about 50 km^2 in 2002, a reduction of more than 70% (Marani et al., 2003, 2007; Carniello et al., 2009; D'Alpaos, 2010a). Losses of vast amounts of marsh areas have also been documented for the San Francisco Bay (about 200 km^2, Gedan et al., 2009) over the last century, while vast amounts of

wetlands disappeared in the Mississippi Delta plain (about 4800 km^2, Day et al., 2000, 2009).

The rising sea level and the lack of available sediments are key factors in determining the drowning and disappearance of salt marshes worldwide (Day et al., 2000; Morris et al., 2002; Reed, 2002; Marani et al., 2007; Gedan et al., 2009; Kirwan et al., 2010; D'Alpaos et al., 2011; Mudd, 2011; D'Alpaos and Marani, 2015). In the horizontal plane the prevalence of wind-wave induced lateral erosion over marsh progradation is responsible for the retreat of salt marsh edges (Carniello et al., 2009; Mariotti and Fagherazzi, 2010; Marani et al., 2011; Mariotti and Carr, 2014). Once the marsh drowns or is laterally eroded and converted to tidal flat or to a subtidal platform.

Salt marshes are populated by halophytic vegetation species, adapted to saline environments (Fig. 1.3). The development of vegetation over salt marshes is mainly determined by the frequency and duration of marsh flooding (e.g., Morris et al., 2002; Silvestri et al., 2005; Kirwan and Guntenspergen, 2012), which, in turn, depend on elevation, position and local topography of the marshes.

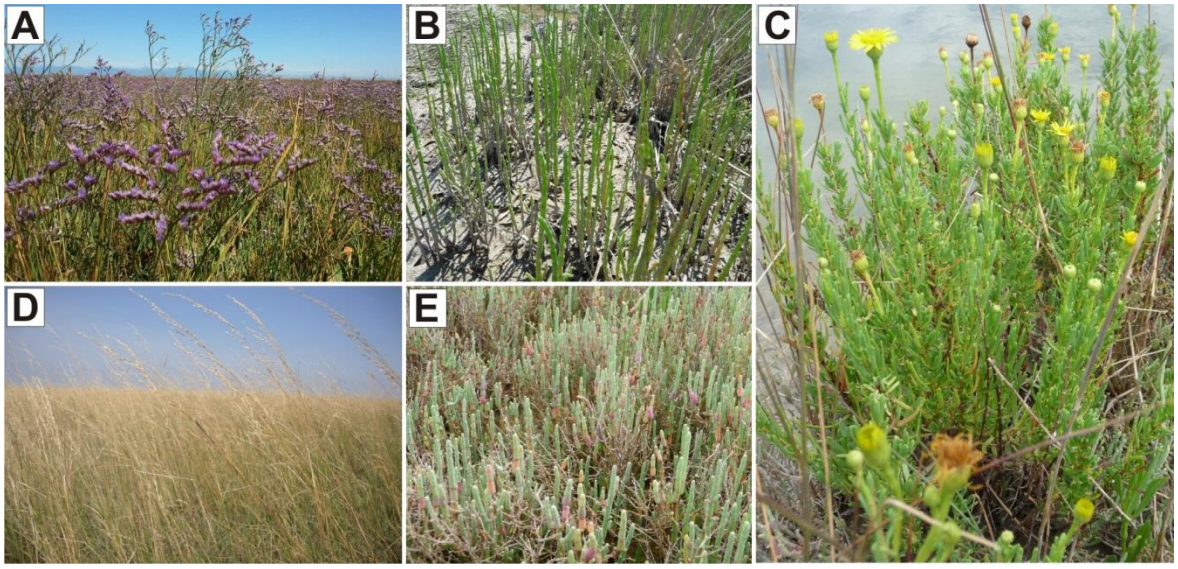

Fig. 1.3. Examples of halophytic species populating the salt marshes of the Venice Lagoon. (A) ***Limonium narbonense*****. (B)** ***Salicornia veneta*****. (C)** ***Inula crithmoides*****. (D)** ***Spartina maritima*****. (E)** ***Sarcocornia fruticosa*****.**

Halophytic vegetation species which populate marsh platforms control sediment trapping efficiency, by enhancing particle settling via reduction of turbulence kinetic energy (e.g., Leonard and Croft, 2006; Mudd et al., 2010), by directly capturing sediment particles (e.g., Leonard and Luther, 1995; Li and Yang, 2009), and determine vertical organic accretion, by directly depositing organic matter due to root growth and litter deposition (Nyman et al., 2006; Neubauer, 2008; Mudd et al., 2009). Halophytes interact with inorganic sedimentation and the rate of Relative Sea Level Rise (RSLR, sea level variations plus local subsidence), their combined effects controlling marsh surface elevation. Surface elevation, in turn, affects the vegetation productivity (e.g., Morris et al., 2002) which influences inorganic sediment deposition and control organic accretion, thus closing the bio-geomorphic feedback.

1.2.2 Biomorphodynamic models of salt-marsh evolution

The development of salt marshes occurs through the sedimentation furnished by both inorganic and organic components, which interact with each other and the rate of sea level. The strong dynamic coupling of biotic and abiotic processes in salt-marsh landscapes gives rise to beautiful and complex biological and morphological patterns, whose non-linear dynamics is a fascinating examples of biomorphodynamics (e.g., Murray et al., 2008). The collective temporal evolution emerging from the mutual interactions and adjustments among hydrodynamic, morphological and biological processes (D'Alpaos et al., 2009). Stemming from the pioneering work by Viles (1988), the long-standing paradigm of physical processes shaping the landscape and dictating the constraints for biological agents, forced to live within those constraints, is being abandoned, in favor of a new perspective in which biota feeds back on, directly modify, and contributes to shape their physical environment (e.g., Jones et al., 1994; Hupp et al., 1995; Dietrich and Perron, 2006; Murray et al., 2008; D'Odorico et al., 2010;

Reinhardt et al., 2010). As for many other fields of science, the biogeomorphological approach has become the new paradigm for studying the form and evolution of the salt-marsh geomorphological and ecosystem structures. As a consequence, in the last few decades a number of studies have analysed salt-marsh biomorphological evolution (e.g., Morris et al., 2002; Mudd et al., 2004; D'Alpaos et al., 2007; Kirwan & Murray, 2007; Marani et al., 2007; Temmerman et al., 2007; Mudd et al., 2009, 2010; D'Alpaos, 2011; D'Alpaos et al., 2012; Fagherazzi et al., 2012; Marani et al., 2013), although a predictive understanding of the two-way feedbacks between physical and biological processes still appears to be elusive. Moreover, analyses of bio-geomorphic feedbacks based on data collected in the field at the marsh scale are rare (Mendelsshon et al., 1981; Day et al., 1998a, 1998b,1999; Morris et al, 2002; Delaune and Pezeshki, 2003; Nyman et al., 2006; Bellucci et al., 2007; Neubauer, 2008), leading to a lack in the characterization of spatial variations in the accretion rates, and, in particular, in the organic soil production.

In addition, the improvement of current understanding of the processes controlling the response and the evolution of salt marshes to changes in the environmental forcings is still an open and fundamentally important issue. A number of models of morphodynamic evolution have been developed (e.g., Allen, 2000; Fagherazzi et al., 2012), which offer a valuable tool to address prediction on the fate of tidal landforms. However, the capability of existing models to provide a comprehensive and predictive theory of tidal-landscape morphodynamic evolution is challenged by the incomplete understanding of the many linkages between the relevant ecological and geomorphological processes (e.g., Murray et al. 2008; Reinhardt et al., 2010). Moreover, in many cases, morphodynamic models resort to the common approximation of a landscape in equilibrium with current forcings, and address predictions on future scenarios using the present observed morphologies as an initial conditions (e.g., Kirwan et al., 2010). For salt-marsh systems, it has recently been observed that marshes might not have yet fully

respond to sea level historical acceleration, and that these tidal morphological features might be out of equilibrium with modern rates of RSLR (Kirwan and Murray, 2005, 2008). Moreover, marshes might not have yet fully responded also to historical decrease in sediment supply inputs and further adjustments in the form of decreasing marsh-platform elevation could be expected (D'Alpaos et al., 2011).

1.2.3 The Venice Lagoon

The Venice Lagoon represents an outstanding example of man-landscape co-existence (Gatto and Carbognin, 1981).

The Venice Lagoon formed over the last 6'000 – 7'000 years as a consequence of the flooding of the upper Adriatic plain which followed the Würm glaciation (Gatto and Carbognin, 1981). The first relevant human settlements within the lagoon dated back to the 5th century AD (e.g., Dorigo, 1983; Ninfo et al., 2009), but a severe human influence started around the 11th century AD and was mainly aimed at hindering the shoaling of the lagoonal bottom and extend the use of navigation channels, causing significant changes in the amount of freshwater and sediment input into the lagoon (e.g., D'Alpaos, 2010a). Thus, as many other tidal landscapes worldwide, the natural environment of the Venice Lagoon has been involved in a drastic hydro-morphodynamic change, which is manifested in the decrease of salt-marsh areas, together with a general expansion and deepening of tidal flats and subtidal platforms over the last centuries (Marani et al., 2003, 2007; Carniello et al., 2009; D'Alpaos 2010a; D'Alpaos et al., 2013).

The Venice Lagoon is about 50 km long and 8 – 14 km wide (Fig. 1.4). It is worth noting that some areas in the northern part of the lagoon represent the lagoonal portion most naturally preserved and, consequently, a large number of studies have been performed in the last decades leading to a large quantity of available data (e.g., Brivio and Zilioli, 1996; Day et al., 1998a, 1999; Marani et al.,

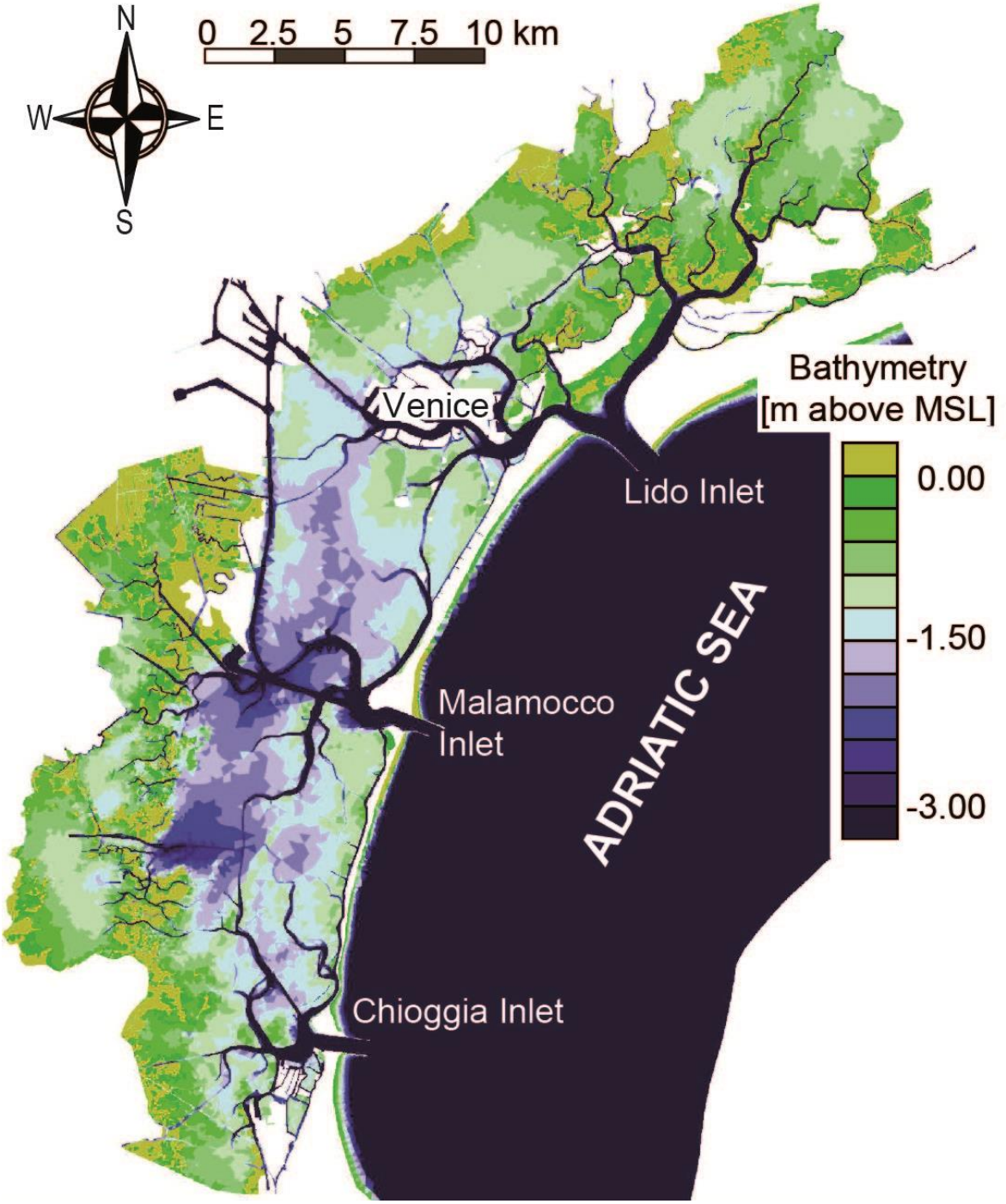

Fig. 1.4. Color-coded bathymetry of the Venice Lagoon.

2003; Silvestri et al., 2003; Silvestri and Marani, 2004; Sfriso et al., 2005; Silvestri et al., 2005; Bonardi et al., 2006; Marani et al., 2006; McClennen et al., 2006; Bellucci et al., 2007; D'Alpaos et al., 2007; Marani et al., 2007; Cola et al., 2008; Rizzetto and Tosi, 2011; Marani et al., 2013; Boaga et al., 2014). On the contrary, the sedimentary succession of southern portion of the Venice Lagoon is still relatively unexplored

(Day et al., 1998a, 1998b, 1999; Lucchini et al., 2001; Bellucci et al., 2007; Brancolini et al., 2008; Zecchin et al., 2008, 2009; Tosi et al., 2009a; Zecchin et al., 2011), and it has been subjected to severe anthropogenic interferences. The main changes occurred during the past 1,000 years and were mainly related to variations in freshwater and sediment input due to repeated re-direction of the Brenta River system. Engineering interventions on the southern Venice Lagoon and the related mainland are exhaustively recorded from historical sources (e.g., topographic maps), whereas their effects, along with their interaction with natural aggravations, are documented in the stratigraphic record, which is considerably expanded given the extraordinary aggradation rate of the southern Venice Lagoon which ranges between 0.03 cm yr^{-1} and 1.5 cm yr^{-1} (Bellucci et al., 2007), up to 2.32 cm yr^{-1} (Day et al., 1998b).

1.3 GOALS OF THE STUDY

The lack of a comprehensive and detailed knowledge on the biomorphodynamic evolution of salt-marsh systems raises queries concerning the processes which control their development over time.

It is therefore of fundamental theoretical and practical importance to improve our understanding of the processes controlling: i) the evolution of salt-marsh bio-geomorphological patterns, and the relative importance of physical and biological processes; ii) the response of salt-marsh systems to changing environmental forcings.

The present work contributes to unravelling these issues by i) analyzing modern sub-surface marsh sediments from the San Felice and Rigà salt marshes (northern Venice Lagoon) to unravel the role of the organic and inorganic components for marshes accretion; ii) analyzing the latest Holocene succession in the Punta Cane area (southern Venice Lagoon) to provide evidences of salt-marsh

system dynamic response to changes in sediment supply (and rates of RLSR) provided by the Brenta River during the last millennium.

1.4 THESIS OUTLINE

The present work is presented through five chapters.

Chapter 2 deals with the analysis of the variations of organic and inorganic deposition on salt marshes to test the role and the effect of the organic and inorganic components for marshes accretion and bio-geomorphological evolution. The results are organized in a journal paper accepted for publication: M. Roner et al., *Spatial variation of salt-marsh organic and inorganic deposition and organic carbon accumulation: Inferences from the Venice Lagoon, Italy*, Advances in Water Resources (2015), http://dx.doi.org/10.1016/j.advwatres.2015.11.011.

Chapter 3 and **Chapter 4** present the results obtained by a study on the latest Holocene depositional history of salt-marsh, tidal-flat, subtidal-platform systems in the southern Venice Lagoon, in the Punta Cane area. In **Chapter 3** the results of sedimentological and chronological analyses are discussed, and a detailed age model for the area over the last two millennia is furnished. **Chapter 4** examines in depth the sedimentological features of the salt-marsh succession to analyze and discuss the evidence of a high delivery rate provided by the Brenta River system. Through the employment of a multidisciplinary approach, the results highlight the occurrence of a dynamic response of the salt-marsh system to changes in the forcings. **Chapters 3** and **4** provide material for two further publications, which are currently in preparation for submission.

Chapter 5 summarizes the main results of this thesis.

CHAPTER 2

SPATIAL VARIATION OF SALT-MARSH ORGANIC AND INORGANIC DEPOSITION AND ORGANIC CARBON ACCUMULATION: INFERENCES FROM THE VENICE LAGOON, ITALY.

2.1 OVERVIEW

This chapter is a journal paper accepted for publication in Advances in Water Resources (http://dx.doi.org/10.1016/j.advwatres.2015.11.011). The manuscript aims at analyzing the variations of organic and inorganic deposition on salt marshes considering a linear spatial variability, to unravel the role of the organic and inorganic components for marshes accretion. Moreover, three different methods are examined for the determination of the organic content, and an estimate of the soil organic carbon for two marshes in the northern Venice Lagoon is provided.

2.2 PAPER

MARCELLA RONER[1], ANDREA D'ALPAOS[1], MASSIMILIANO GHINASSI[1], MARCO MARANI[2,3], SONIA SILVESTRI[3], ERICA FRANCESCHINIS[4], NICOLA REALDON[4]

[1]Dept. of Geosciences, University of Padova, via Gradenigo 6, 35131 Padova, Italy.

[2]Dept. of Civil, Environmental and Architectural Engineering (ICEA), University of Padova, via Marzolo 9, 35131 Padova, Italy.

[3]Division of Earth and Ocean Sciences, Nicholas School of the Environment and Department of Civil and Environmental Engineering, Pratt School of Engineering, Duke University, Durham, North Carolina 27708, USA.

[4]Dept. of Pharmaceutical and Pharmacological Sciences, University of Padova, via Marzolo 5, 35131 Padova, Italy.

2.2.1 Abstract

Salt marshes are ubiquitous features of the tidal landscape governed by mutual feedbacks among processes of physical and biological nature. Improving our understanding of these feedbacks and of their effects on tidal geomorphological and ecological dynamics is a critical step to address issues related to salt-marsh conservation and response to changes in the environmental forcing. In particular, the spatial variation of organic and inorganic soil production processes at the marsh scale, a key piece of information to understand marsh responses to a changing climate, remains virtually unexplored. In order to characterize the relative importance of organic vs. inorganic deposition as a function of space, we collected 33 shallow soil sediment samples along three transects in the San Felice and Rigà salt marshes located in the Venice lagoon, Italy. The amount of organic matter in each sample was evaluated using Loss On Ignition (LOI), a hydrogen peroxide (H_2O_2) treatment, and a sodium hypochlorite (NaClO) treatment following the H_2O_2 treatment. The grain size distribution of the inorganic fraction was determined using laser diffraction techniques. Our study marshes exhibit a weakly concave-up profile, with maximum elevations and coarser inorganic grains along their edges. The amount of organic and inorganic matter content in the samples varies with the distance from the marsh edge and is very sensitive to the specific analysis method adopted. The use of a H_2O_2 + NaClO treatment yields an organic matter density value which is more than double the value obtained from LOI. Overall, inorganic contributions to soil formation are

greatest near the marsh edges, whereas organic soil production is the main contributor to soil accretion in the inner marsh. We interpret this pattern by considering that while plant biomass productivity is generally lower in the inner part of the marsh, organic soil decomposition rates are highest in the better aerated edge soils. Hence the higher inorganic soil content near the edge is due to the preferential deposition of inorganic sediment from the adjacent creek, and to the rapid decomposition of the relatively large biomass production. The higher organic matter content in the inner part of the marsh results from the small amounts of suspended sediment that makes it to the inner marsh, and to the low decomposition rate which more than compensates for the lower biomass productivity in the low-lying inner zones. Finally, the average soil organic carbon density from the LOI measurements is estimated to be 0.044 g C cm^{-3}. The corresponding average carbon accumulation rate for the San Felice and Rigà salt marshes, 132 g C m^{-2} yr^{-1}, highlights the considerable carbon stock and sequestration rate associated with coastal salt marshes.

Keywords: tidal environments, salt marshes, soil organic matter, blue carbon.

2.2.2 Introduction

Coastal salt marshes represent a transition zone between submerged and emerged environments, occupying the upper margins of the intertidal landscape. Because of their unique position in the tidal frame, salt marshes represent a crucially important ecosystem. They offer valuable services, by providing a buffer against wave and storm surges (e.g., Möller et al., 1999; Howes et al, 2010; Temmerman et al., 2013; Möller et al., 2014), nursery areas for coastal biota (e.g., Perillo et al., 2009; Silliman et al., 2009) and filtering of nutrients and pollutants (e.g., Costanza et al, 1997; Larsen et al., 2010). In the last few decades a number of

authors also highlighted the importance of salt marshes serving as an organic carbon sink due to their great ability to sequester atmospheric carbon (e.g., Chmura et al., 2003; Mcleod et al., 2011; Murray et al., 2011; Sifleet et al., 2011; Kirwan and Mudd, 2012). The future of these valuable coastal landforms and ecosystems is today at risk, exposed as they are to possibly irreversible transformations due to the effects of climate changes and human interferences (e.g., Delaune and Pezeshki, 2003; Marani et al., 2007; Day et al, 2009; Kirwan et al., 2010; D'Alpaos et al., 2012; Murray et al., 2011; Ratliff et al., 2015). The extent of these coastal features, in fact, has dramatically decreased worldwide in the last century (Day et al., 2000; Marani et al., 2003, 2007; Carniello et al., 2009; Gedan et al., 2009; Mcleod et al., 2011). For example, salt-marsh areas in the Venice lagoon decreased from about 180 km^2 in 1811 to about 50 km^2 in 2002, a reduction of more than 70% (Marani et al., 2003, 2007; Carniello et al., 2009; D'Alpaos, 2010a). Losses of vast amounts of marsh areas have also been documented for San Francisco Bay (about 200 km^2, Gedan et al., 2009) over the last century, while vast amounts of wetlands disappeared in the Mississippi Delta plain (about 4800 km^2, Day et al., 2000, 2009).

The rising sea level and the lack of available sediments are key factors in determining the drowning and disappearance of salt marshes worldwide (Day et al., 2000; Morris et al., 2002; Reed, 2002; Marani et al., 2007; Gedan et al., 2009; Kirwan et al., 2010; D'Alpaos et al., 2011; Mudd, 2011; D'Alpaos and Marani, 2015). In the horizontal plane the prevalence of wind-wave induced lateral erosion over marsh progradation is responsible for the retreat of salt marsh edges (Carniello et al., 2009; Mariotti and Fagherazzi, 2010; Marani et al., 2011; Mariotti and Carr, 2014). Once the marsh drowns or is laterally eroded and converted to tidal flat or to a subtidal platform, unless the environmental conditions change (i.e. the sediment concentration increases) the re-growth of the marsh platforms is unlikely because the system is characterized by a hysteretic behavior (e.g., Kirwan and Murray, 2007; Marani et al., 2010).

Salt marshes are populated by halophytic vegetation species, adapted to saline environments. The spatial distribution of halophytes over salt marshes is organized in characteristic patches, a phenomenon known as *zonation* (Chapman, 1976; Adam, 1990; Pennings et al, 2005; Silvestri et al., 2005; Marani et al., 2006; Moffett et al., 2010). It has been recently shown that zonation patterns are not just the result of ecological and physiological processes and that their emergence is the consequence of the feedback on soil accretion of organic soil production by plants, which act as a landscape engineer (Marani et al., 2013, Da Lio et al., 2013). The development of vegetation over salt marshes is mainly determined by the frequency and duration of marsh flooding (e.g., Morris et al., 2002; Silvestri et al., 2005; Kirwan and Guntenspergen, 2012), which, in turn, depend on elevation, position and local topography of the marshes. Halophytic vegetation species which populate marsh platforms control sediment trapping efficiency, by enhancing particle settling via reduction of turbulence kinetic energy (e.g., Leonard and Croft, 2006; Mudd et al., 2010), by directly capturing sediment particles (e.g., Leonard and Luther, 1995; Li and Yang, 2009), and determine vertical organic accretion, by directly depositing organic matter due to root growth and litter deposition (Nyman et al., 2006; Neubauer, 2008; Mudd et al., 2009). Halophytes interact with inorganic sedimentation and the rate of Relative Sea Level Rise (RSLR, sea level variations plus local subsidence), their combined effects controlling marsh surface elevation. Surface elevation, in turn, affects the vegetation productivity (Morris et al., 2002) which influences inorganic sediment deposition and control organic accretion, thus closing the bio-geomorphic feedback. In this framework it is clear that the interaction between physical and biological processes acting within salt marsh systems plays a fundamental role in salt-marsh survival or disappearance. Although in the last few decades a number of studies have analysed salt-marsh biomorphological evolution (e.g., Morris et al., 2002; Mudd et al., 2004; D'Alpaos et al., 2007; Kirwan & Murray, 2007; Marani et al., 2007; Temmerman et al., 2007; Mudd et al., 2009; D'Alpaos, 2011; D'Alpaos et

al., 2012; Fagherazzi et al., 2012; Marani et al., 2013), a predictive understanding of the two-way feedbacks between physical and biological processes still appears to be elusive. Moreover, analyses of bio-geomorphic feedbacks based on data collected in the field at the marsh scale are rare (Mendelsshon et al., 1981; Day et al., 1998a, 1998b, 1999; Morris et al, 2002; Delaune and Pezeshki, 2003; Nyman et al., 2006; Bellucci et al., 2007; Neubauer, 2008). The evolution in time of marsh elevation z ($\boldsymbol{x}$, t) (referenced to Mean Sea Level -- hereinafter MSL) at a given site $\boldsymbol{x}$ and at time t, is governed by the sediment continuity equation (where erosion is neglected because of the stabilizing presence of vegetation, see Marani et al., 2010, 2013):

$$\frac{\partial z(\boldsymbol{x},t)}{\partial t} = Q_i\,(\boldsymbol{x},t) + Q_o(\boldsymbol{x},t) - R \qquad [1]$$

where $Q_i(\boldsymbol{x},t)$ and $Q_o(\boldsymbol{x},t)$ are the local rates of inorganic and organic deposition, respectively, and R is the rate of RSLR. In equilibrium conditions, the marsh elevation referenced to MSL is constant over time and therefore the left-hand side term in the above equation vanishes. The sediment balance equation then reads:

$$Q_i\,(\boldsymbol{x},t) + Q_o(\boldsymbol{x},t) = R \qquad [2]$$

Hence, in a stable marsh, if Q_i increases, Q_o needs to decrease by the same magnitude, and vice versa, such that the forcing rate of RSLR is matched everywhere in the marsh. Field observations and numerical models (e.g., Christiansen et al., 2000; Temmerman et al., 2003; D'Alpaos et al., 2007; Kirwan et al., 2008) suggest that marsh inorganic accretion rates, and the related platform elevations, decrease with distance from the main channels. Therefore, the organic accretion should be expected to gradually increase as the distance from the main channel increases for the equilibrium assumption to hold. However, a direct and detailed characterization of spatial variations in the accretion rates, and, in particular, in the organic soil production, is still lacking, and is the focus of the present work.

The paper is organized as follows. In the next section we provide a brief description of our study sites within the Venice lagoon. We then fully describe the methods used to determine the organic and inorganic sediment content, grain size distribution, above-ground biomass. The subsequent Results and Discussion sections analyze the role of physical and biological factors shaping the tidal landscape, and how these factors influence salt-marsh biogeomorphic patterns.

2.2.3 Study area

The Venice lagoon (Fig. 2.1a) is part of a foreland basin located between the NE-verging northern Appenninic chain and the SSE-verging eastern South-Alpine chain (Italy). Located in the northwestern Adriatic Sea, the Venice lagoon is the largest lagoon in the Mediterranean, with an area of about 550 km^2, a mean water depth of 1.5 m, and a semi-diurnal micro-tidal regime (maximum water excursion at the inlets of ± 70 cm around MSL). The Lagoon is connected with the Adriatic Sea via three inlets: Lido, Malamocco and Chioggia (Fig. 2.1a).

The two study areas (Figs. 2.1a, 2.1b, 2.1c) are the San Felice and the Rigà salt marshes, located in the northern Venice lagoon, close to the Lido inlet and adjacent to the San Felice Channel (see Marani et al., 2003, Silvestri et al. 2003, 2005, for a detailed description of the study sites from a geomorphological and ecological perspective). These marshes, about 2 km apart, have been studied for more than 10 years and a large amount of data is available. In addition, it is worth noting that these marshes maintained their main characteristics because of their location in the most naturally preserved portion of the lagoon. The San Felice and the Rigà salt marshes are incised by meandering tidal networks and are colonized by a wide range of halophytic vegetation species: *Salicornia veneta*, *Spartina maritima*, *Limonium narbonense*, *Sarcocornia fruticosa*, *Juncus maritimus*, *Inula crithmoides*, *Puccinellia palustris*, *Halimione portulacoides*, *Suaeda maritima*, *Arthrocnemum macrostachyum*, *Aster tripolium* (Silvestri et al., 2003). The marsh soil

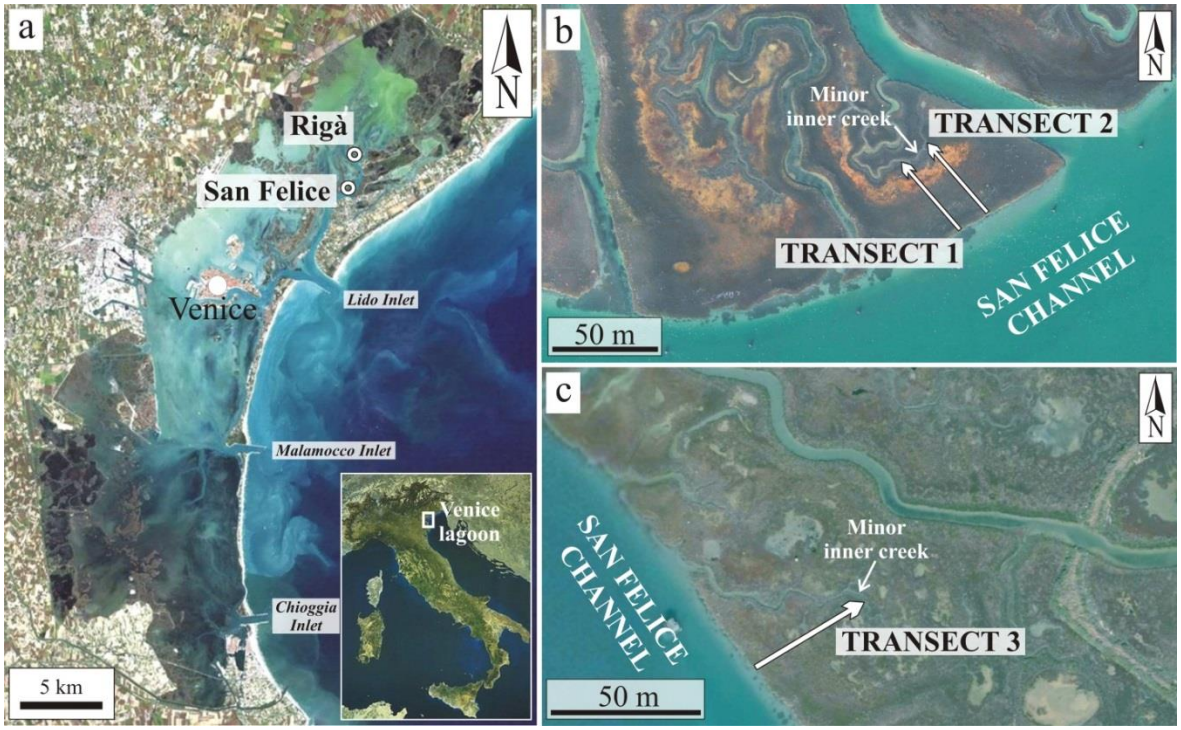

Fig. 2.1. (a) Location of the study sites in the northern Venice lagoon, Italy. (b) San Felice salt marsh. (c) Rigà salt marsh.

is composed of clayey sandy silt and of a large organic fraction. Accretion rates in the San Felice area were estimated in 3.0 mm yr^{-1} by Day et al. (1998a), whereas the rate of sea-level rise is of about 2.0 mm yr^{-1} (Carbognin et al., 2004), and the local subsidence is about 1.0 mm yr^{-1} (Carbognin et al., 2004; Strozzi et al., 2013), for a total rate of relative sea level rise of about 3.0 mm yr^{-1}.

2.2.4 Materials and methods

We collected 33 undisturbed cubic sediment samples with side of 5 cm, delimited at the top by the present-day depositional interface, to study the spatial variations of the soil inorganic and organic matter content, for the determination of the inorganic (Q_i) and the organic (Q_o) accretion rates, respectively. Each sample consists of massive brownish to blackish silt and contains abundant stems and roots. Some of the samples also contained scattered mm-size bivalve and gastropod shells and/or shell fragments. The samples were collected along three 40

m long transects in two salt marshes in the Northern Venice lagoon (Fig. 2.1a). Transect 1 and 2 were located in the San Felice salt marsh, whereas Transect 3 was located in the Rigà salt marsh (Figs. 2.1b, 2.1c). At both sites the transects started on the marsh edge close to the main channel (the San Felice channel) and ended close to a minor inner tidal creek (width of the order of a few tens of centimeters). Samples were collected with a spacing of 2.5 m for the first 10 m from the San Felice channel, whereas the spacing was 5 m for the remaining 30 m. Elevation and geographic location of each sample were determined using two TOPCON GR-3 GPS receivers (dual frequency - L1/L2 - and dual constellation - NavStar/Glonass - with integrated Tx/Rx UHF radio).

A volume of 8 cm^3 from each sediment sample, extract at a depth of 3 cm from the top sample surface, was dried at 60°C for 36 hours, until a constant weight was obtained. The difference in weight between the wet and dry samples was used to estimate the sediment dry bulk density, where the value of the total dry mass was corrected for the presence of saline water (Dadey et al., 1992).

The amount of inorganic (Q_i) and organic fraction (Q_o), together with the grain size and the above-ground biomass distribution, were measured and analyzed for each sample in order to provide a complete characterization of the processes acting on the salt-marsh surface. Finally, an analysis of the soil organic carbon content was performed in order to estimate the carbon stock potential of these marshes.

2.2.4.1 Determination of the organic fraction: three different analyses

Because all the methods available for the determination of soil organic matter have their own specific limitations, different methodologies were used to determine the organic matter content in the samples: 1) a treatment with hydrogen peroxide (H_2O_2); 2) treatments with H_2O_2 and, in succession, sodium hypochlorite (NaClO); 3) Loss On Ignition (LOI) analyses. It should be emphasized that the

chemical treatments to determine the organic matter content are not frequently used, mainly because they are time consuming. However, they allow the preservation of the original grain size of the inorganic fraction for grain-size analysis, contrary to the LOI procedure, where sample crumbling and heating modifies the size of clastic particles. The LOI approach is broadly applied in the literature, it is faster than chemical methods and permits the simultaneous analysis of a large number of samples. Moreover, the organic carbon content in a soil is usually defined in the literature on the basis of LOI measurements, providing a wider context for direct comparisons. However, an accepted standardized LOI procedure is still lacking. The need for a standard LOI procedure has been widely acknowledged (Heiri et al, 2001), but the scientific community continues to use heterogeneous procedures in terms of ignition temperatures, exposure times, sample sizes, position in the muffle furnace, etc. (Heiry et al., 2001; Barillé-Boyer et al., 2003). The results from these different procedures cannot be directly compared, and may underestimate or overestimate the actual organic matter content depending on the specific sample type of organic matter present. For example, during combustion the samples may lose structural water in the range of temperatures from 450°C to 600°C (Ball, 1964; Howard and Howard, 1990) in sediments characterized by high clay content, thereby significantly affecting soil organic matter estimates (Mook and Hoskin, 1982; Dankers and Laane, 1983; Barillé-Boyer et al., 2003). Between 425°C and 520°C a potential loss of CO_2 can occur in minerals or in sediments containing inorganic carbon, such as siderite ($FeCO_3$), magnesite ($MgCO_3$), rhodocrosite ($MnCO_3$) and dolomite ($CaMg(CO_3)_2$) (Weliky et al., 1983; Howard and Howard, 1990; Southerland, 1998; Santisteban et al., 2004). Overall, a LOI test at 550°C leads to a large overestimation of the loss of organic matter mass (Frangipane et al., 2009).

2.2.4.2 H_2O_2 and NaClO treatments

The sub-samples, each characterized by a volume of 8 cm^3, were treated with 35% H_2O_2 for 36 hours. At the end of the oxidation, when no visible frothing occurred, dilution with deionized water, decantation (for 24 hours), siphoning, and drying were carried out. The weight of each sample was again measured after drying. A further treatment with 5% NaClO was subsequently applied (for 24 hours) in order to remove the remnant organic matter, which mainly occurred under the shape of sub-millimetric plant debris. After this second treatment, the weight of each dried sample was measured again. The loss in weight affecting each sample during these procedures provided an estimation of the amount of organic matter dissolved during each treatment. The results of our analyses will be expressed as soil organic matter density (computed as the ratio between the amount of organic matter after each treatment and the total volume), and inorganic sediment density (ratio between the amount of inorganic residual after each treatment and the total volume).

2.2.4.3 Loss On Ignition

Our choice of the temperature and duration of ignition in the LOI process was made on the basis of the existing literature (Ball, 1964; Frangipane et al., 2009; Protocol of SFU Soil Science Lab, 2011). A total amount of 2 g of dry sediment for each sample, dried at 60°C for 36 hours, was used to perform LOI analyses. The sediment was crumbled in a ceramic mortar and placed in a dry ceramic crucible. The LOI process started with a temperature increase of 5°C/min until reaching 375°C, and continued at a constant temperature for 16 hours (Ball, 1964; Frangipane et al., 2009; Protocol of SFU Soil Science Lab, 2011). The difference in weight, before and after the process, was used to estimate the amount of organic matter which was combusted. As for the soil organic matter determined through

the chemical treatments described above, the LOI soil organic content will be expressed as the density of soil organic matter computed from the sediment dry bulk density at the end of the procedure (because of in the LOI analysis the samples volume was unknown, we estimated the volume of these samples by the ratio between the total mass of each sample and the sediment dry bulk density for the same sample previously calculated for the chemical treatments).

The results obtained from LOI measurements were subsequently used to determine the content of soil organic carbon in each sample according to the relationship proposed by Craft et al. (1991):

$$\text{Organic Carbon} = 0.40\ (\text{LOI}) + 0.0025\ (\text{LOI})^2 \qquad [3]$$

2.2.4.4 Particle size analysis

The inorganic particle size distribution was performed after the removal of the organic matter through the H_2O_2 + NaClO treatment. In samples mainly composed by silt, where a large amount of organic matter is bound to the mineral matrix, the removal by chemical reagents is a common pretreatment for this analysis (Gee and Bauder, 1986; Allen and Thornley, 2004; Gray et al., 2010), although the benefits brought by the use of chemical agents are not clear. Allen and Thornley (2004) state that there are no advantages from the treatment with H_2O_2 before laser granulometry. On the contrary, Gray et al. (2010) recommend the employment of H_2O_2 treatment on samples with moderate to large amount of organics composed of stem pieces, root fragments and seeds.

On San Felice and Rigà samples, the particle size analysis was performed on the residual inorganic sediment fraction obtained after the H_2O_2 + NaClO treatment. Deionized water was added to each sample to obtain a dispersed particulate sample. The particle size analysis was carried out using a Mastersizer 2000 (Version 5.40, MALVERN INSTRUMENTS). The Mastersizer 2000 uses laser diffraction to measure the size of particles, by measuring the intensity of light

scattered as a laser beam passes through the dispersed particulate sample. These data are then analyzed to calculate the size of the particles that created the scattering pattern. The grain size results will be presented as D_{10}, D_{50} and D_{90} distribution.

2.2.4.5 Above-ground biomass

Each sampling site was centered in a 14 Megapixel resolution photograph covering an area of about 100x80 cm. The vegetation density in each photo (a proxy for the above-ground biomass) was evaluated through the superposition of a regularly spaced grid. The grid contained 100 nodes, and the occurrence of plant cover or soil was evaluated for each node, providing a percentage of vegetation cover for different sampling site (see examples in Fig. 2.2).

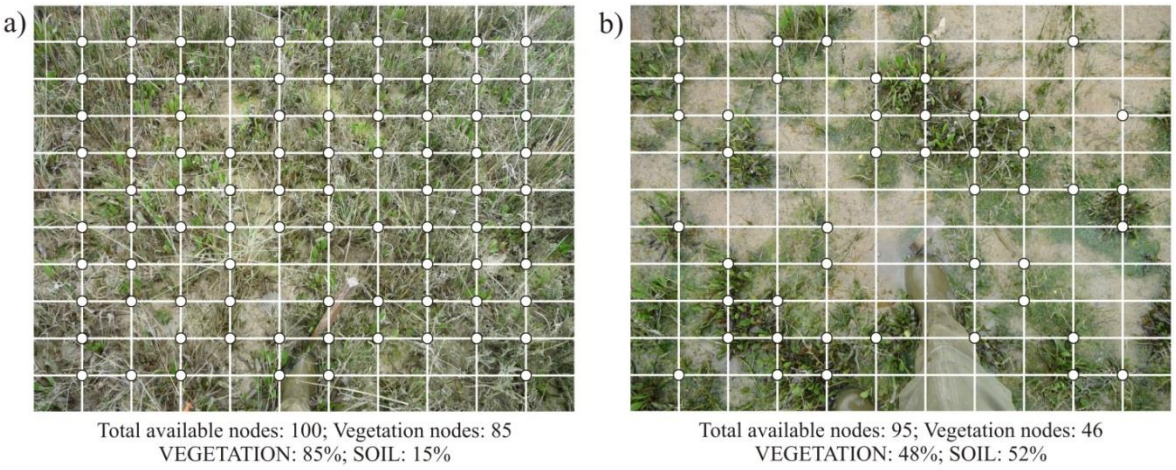

Fig. 2.2. Estimation of the vegetation cover. The white circles indicate the presence of vegetation on the grid nodes. (a) Example of the site at 2.5 m from the San Felice channel along transect 2. (b) Example of the site at 25 m from the San Felice channel along transect 2.

2.2.5 Results

2.2.5.1 Elevation

GPS field surveys show that marsh surface elevations (Figs. 2.3a, 2.4a, 2.5a) are highest near the marsh edge close to the San Felice channel levees (maximum elevation along the transects was equal to 32.1 cm above MSL). Toward the inner marsh, platform elevations decrease, reaching minimum values at about 30 m from the edge, where stagnant pools exist (minimum elevation along the transects was equal to 16.9 cm above MSL). Soil elevations at the end of the transects are slightly higher than in the inner portion of the marsh due to the presence of the levees of two small tidal creeks which cut through the marsh platform (see Fig. 2.1).

2.2.5.2 Sediment dry bulk density, inorganic sediment density and grain size

The average sediment dry bulk density (Figs. 2.3b, 2.4b, 2.5b) across all the samples is 0.89 g cm^{-3}. Dry bulk density is maximum at the edge of the marshes, where its values range from 1.16 to 1.56 g cm^{-3}. The rapid decrease in the bulk density occurs in the first 5 – 7.5 m away from the main channel, where the values range between 0.53 and 0.84 g cm^{-3}. We also observed that, in transect 1 (Fig. 2.3b) and 3 (Fig. 2.5b), the sediment dry bulk density rapidly decreases with distance from the San Felice channel and it then edges up and down when moving towards the inner portion of the marsh. On the contrary, along transect 2 (Fig. 2.4b) sediment dry bulk density rapidly decreases with distance from the main channel, but it tends to increase when moving towards the inner portion of the marsh although being characterized by values smaller than on the marsh edge. In the last 5 m of the transects the sediment dry bulk density increases again, its values ranging from 0.73 to 1.34 g cm^{-3}.

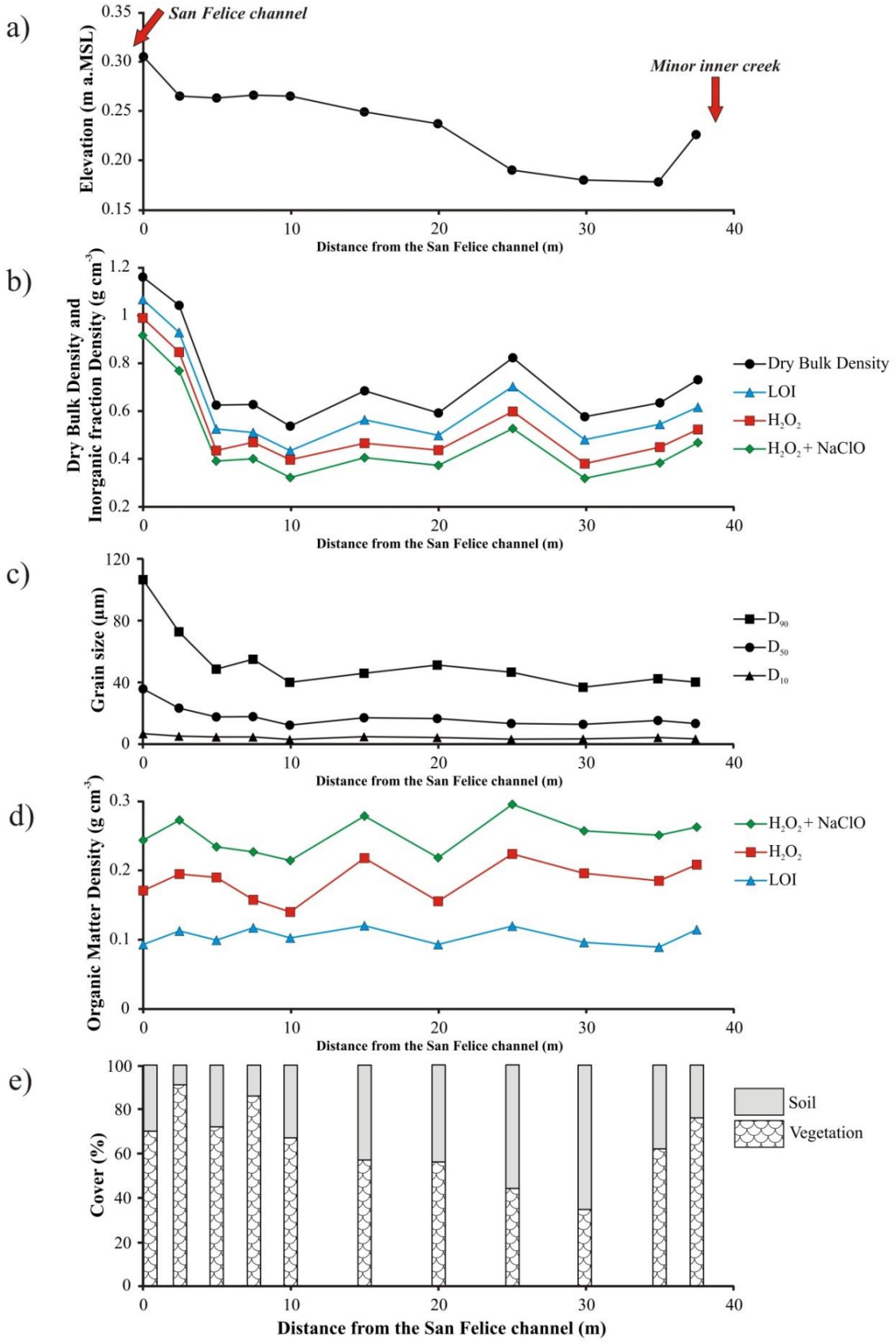

Fig. 2.3. Transect 1 in the San Felice salt marsh. Spatial variations, measured along the distance from the San Felice channel, of: (a) marsh surface elevation; (b) dry bulk density and density of the inorganic fraction sediment; (c) grain size distribution; (d) density of the organic matter; (e) vegetation or soil cover.

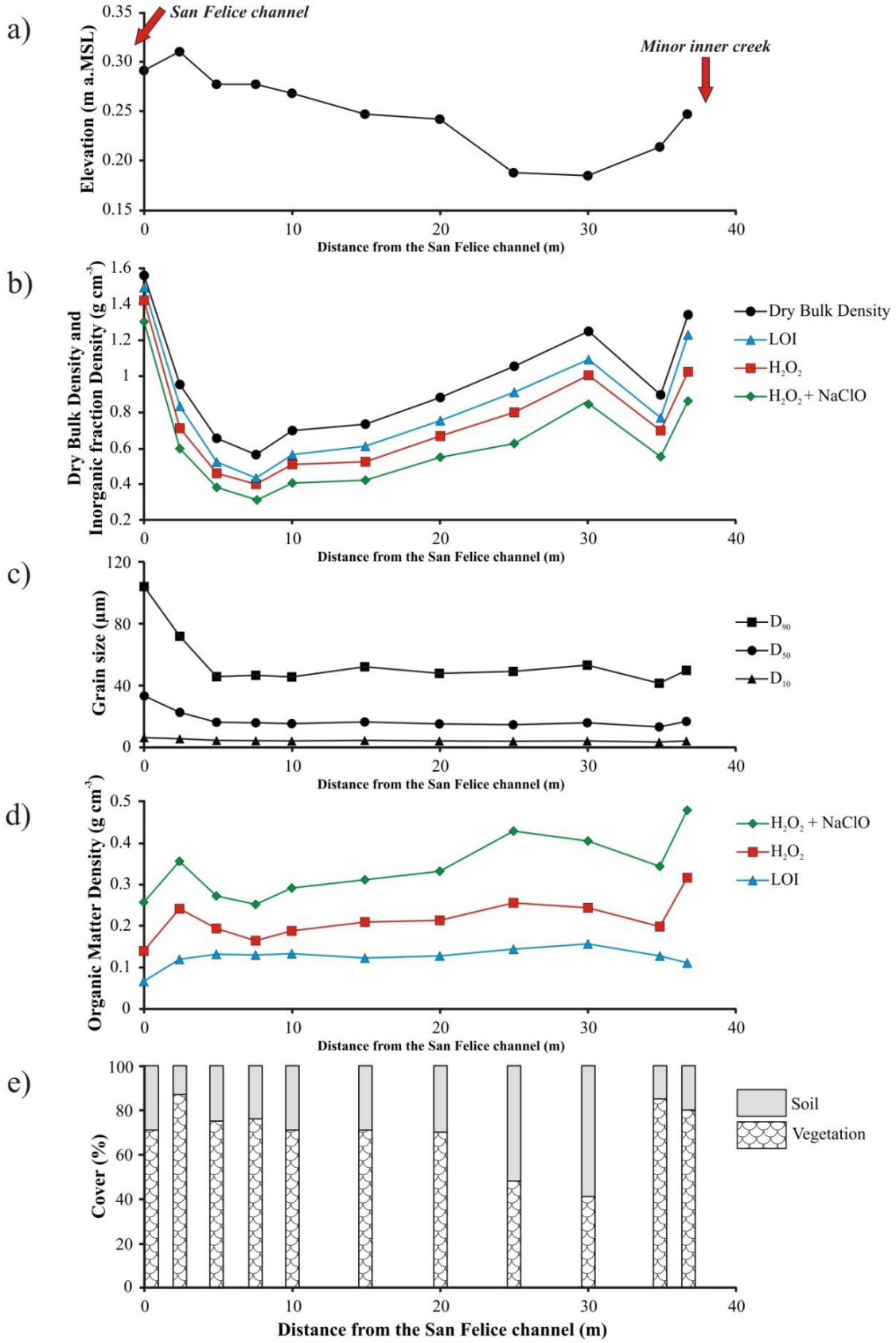

Fig. 2.4. Transect 2 in the San Felice salt marsh. Spatial variations, measured along the distance from the San Felice channel, of: (a) marsh surface elevation; (b) dry bulk density and density of the inorganic fraction sediment; (c) grain size distribution; (d) density of the organic matter; (e) vegetation or soil cover.

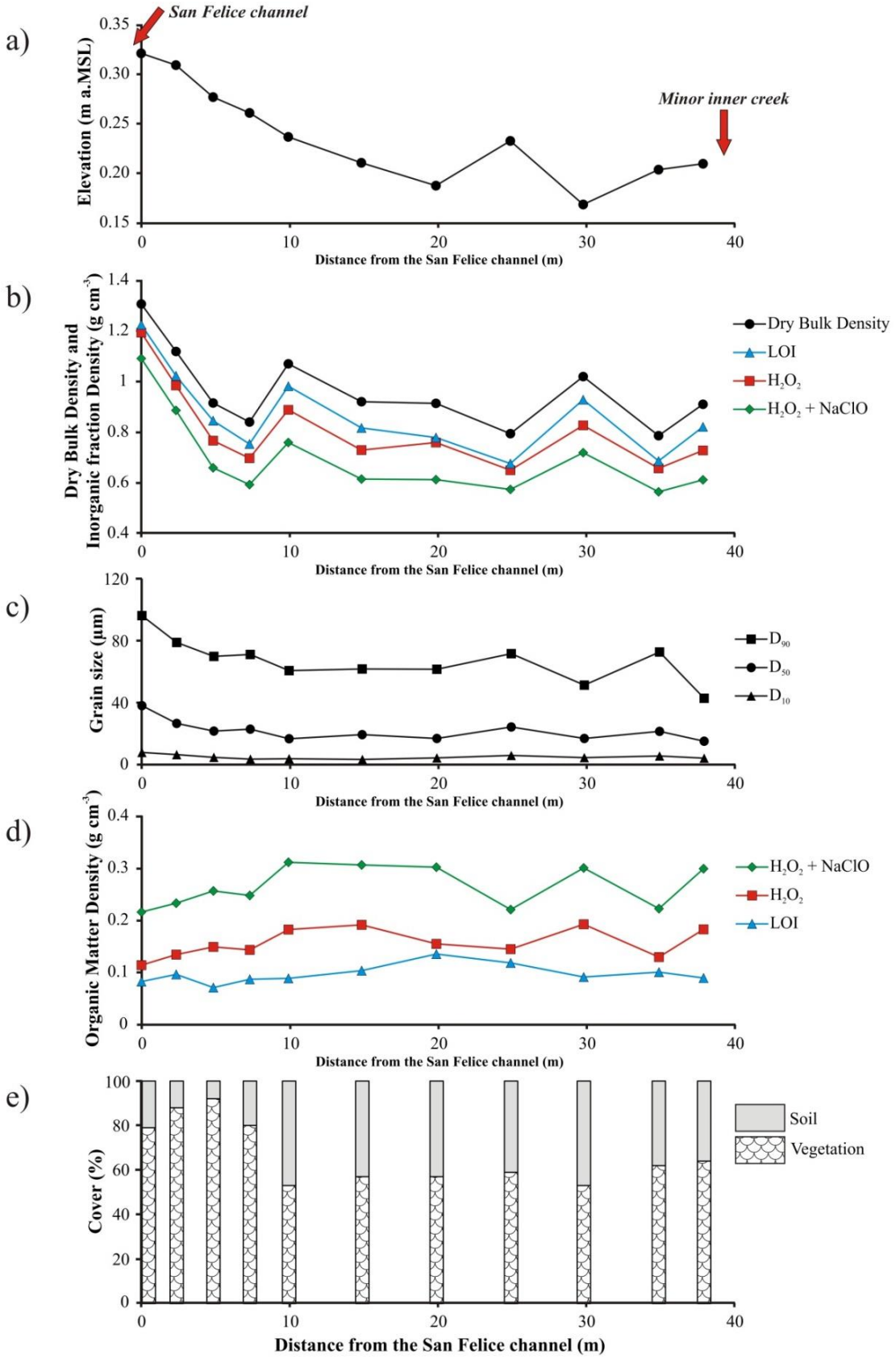

Fig. 2 5. Transect 3 in the Rigà salt marsh. Spatial variations, measured along the distance from the San Felice channel, of: (a) marsh surface elevation; (b) dry bulk density and density of the inorganic fraction sediment; (c) grain size distribution; (d) density of the organic matter; (e) vegetation or soil cover.

The amount of inorganic sediment, calculated for each sample by subtraction from the organic content through the three different methods, is reported as inorganic sediment density (Figs. 2.3b, 2.4b, 2.5b). The results show that its trend along each transect, regardless of the method used, follows a trend analogous to that displayed by the sediment dry bulk density along the same transect. The average value along the transects obtained by LOI, H_2O_2 and H_2O_2 + NaClO is equal to 0.78, 0.70 and 0.60 g cm^{-3}, respectively.

The Mastersizer recorded a range of grain size values for the inorganic sediment fraction comprises between 831.76 μm (maximum value) and 0.63 μm (minimum value). On average, the grain size shows a variable distribution between a medium sand (average coarser value: 400 μm) and a clay (average finer value: 0.63 μm). The D_{10} distribution (Figs. 2.3c, 2.4c, 2.5c) is almost constant along the three transects and ranges between 3 μm toward the inner portion of the marshes, and 6÷7.6 μm on the marsh edges. As to the distribution of the median grain size, D_{50} (Figs. 2.3c, 2.4c, 2.5c), we observe coarser grains along the marsh edges (i.e. along the tidal channel levees) with a median grain size D_{50} in the range 33÷38 μm. The median grain size then becomes finer toward the inner marsh with a median grain size in the range 12÷24 μm. The decrease in grain size with distance from the San Felice channel reveals to be quite rapid and occurs in the first 5 – 10 m from the marsh edge. In the remaining portion of the transect the values of the D_{50} remain rather stable. On the San Felice salt marsh, from x=10 m up to the end of the transects, values of the D_{50} are lower (12÷17 μm) than those which characterize the Rigà salt marsh (15÷24 μm). The distribution of the D_{90} emphasizes the presence of coarser grains along the marsh edges. In the San Felice salt marsh the decrease in D_{90} occurs rapidly, in the first 5 m from the San Felice channel, from values of 103÷106 μm (on the marsh edge) to 45÷48 μm. From 5 m to the end of these two transects the values fluctuate weakly up and down, with values ranging from 37 μm to 55 μm. On the Rigà salt marsh the decrease in the D_{90} values occurs slowly in the first 10 m from the San Felice channel, from 106 μm

on the marsh edge to 60 μm. From 10 to 20 m away from the channel the values are stable, and tend to fluctuate up and down over the last 10 m of the transect, with values between 72 μm and 42 μm.

2.2.5.3 Soil Organic Matter

The values of soil organic matter density (Figs. 2.3d, 2.4d, 2.5d) obtained by using the three methods described above show important differences for each sample and the trends along the transects follow a non-monotonically increase or a decrease.

Results obtained on the basis of LOI suggest small variations in soil organic matter density along the transects, except for the samples collected on the marsh edges where organic density values are lower and tend to weakly increase in the first 2.5 – 5 m from the marsh edge. In the remaining portion of the transects, values of organic density remain almost stable, with some small peaks between 15 and 30 m away from the main channel. The average organic matter density value along the transects obtained by LOI is equal to 0.11 g cm^{-3}.

Results obtained through H_2O_2 treatments show values higher than those obtained with the LOI method, for all samples, with an average value over the three transects of 0.18 g cm^{-3}. As a whole, the values weakly increase along the transects, although non-monotonically, from the marsh edge toward the inner marsh, with some oscillations. An analysis of transect 1 (Fig. 2.3d) shows the presence of two minimum values of organic matter density at 10 and 20 m away from the channel (0.14 and 0.15 g cm^{-3}, respectively), which seem to divide the transect into three sub-intervals (from 0 to 10 m; from 10 to 20 m, and from 20 m to the end of the transect).The maximum density values occur at 15 and 25 m from the marsh edge, with values of 0.22 g cm^{-3}. In the case of transect 2 (Fig. 2.4d) the peaks in organic matter density are located at 2.5, 25, and 38 m from the channel (with organic matter density values of 0.24, 0.26, 0.32 g cm^{-3}, respectively). The

trend is characterized by two intervals delimited by minimum density values, in which, with different slopes, the organic matter density increases, reaches a peak and decreases (intervals from 0 to 7.5 m; from 7.5 m to 35 m). In the case of transect 3 (Fig. 2.5d) two peaks of 0.19 g cm^{-3} occur at 15 and 30 m away from the San Felice channel. The minimum values of organic matter density at 0, 25, 35 m from the marsh edge, split the line in two intervals (from 0 to 25 m; from 25 to 35 m).

The results obtained with the H_2O_2 + NaClO treatment for each transect show, in general, similar trends compared to the case of the H_2O_2 treatment (Figs. 2.3d, 2.4d, 2.5d). However, values obtained for the organic density are even higher, the average value for the three transects being equal to 0.28 g cm^{-3}. As to the locations of the minimum and maximum values of organic matter density, these are the same as those obtained with the H_2O_2 treatment and, along each transect, the peaks emphasize the higher accumulation of organic matter in the samples collected in correspondence of the low-lying pools (i.e. areas of minimum surface elevations Fig. 2.1). The difference between the two methods tends to be much larger in the samples that contain more organic matter.

The percentage amounts of organic matter, obtained by the different methods at each given sampling site and calculated by the ratio between the mass of the organic matter and the total mass for each sample (Fig. 2.6), further explain the trends displayed by the organic matter for the different transects. The average values for each method show well-defined and similar trends, regardless of the method used. The organic matter percentage is minimum along the marsh edge (6.2%, 10.8% and 18% for LOI, H_2O_2 and H_2O_2 + NaClO, respectively) and increases rapidly to 17.3%, 25.4% and 36.7% for LOI, H_2O_2 and H_2O_2 + NaClO, respectively, at about 5 – 7.5 m from the channel. The organic matter percentage then tends to fluctuate up and down with no evident trend, the average values from 5 m to the end of the transects being equal to 14.4%, 24% and 36% for LOI, H_2O_2 and H_2O_2 + NaClO, respectively.

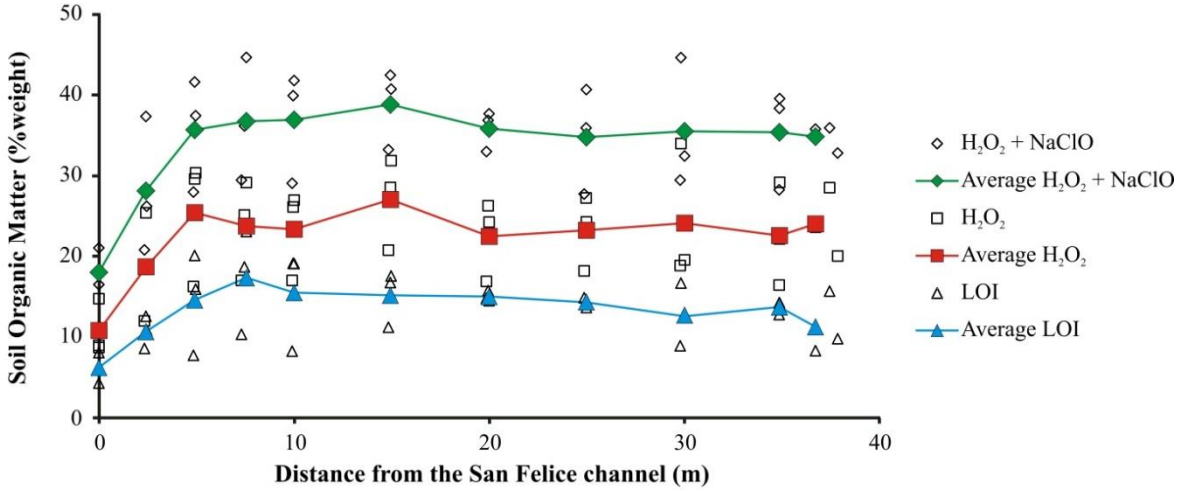

Fig. 2.6. Variability in the amount of soil organic matter, expressed as a percentage, with distance from the San Felice channel. The empty markers represent the soil organic matter values obtained by the three different methods, for each point along the transects. The full-colored markers show the average of soil organic matter values for each point, for each method.

2.2.5.4 Above-ground biomass

The density of the vegetation cover (Figs. 2.3e, 2.4e, 2.5e) is maximum at 2.5 – 5 m away from the main channel (about 90%). From 10 to 30 m far from the channel the density of the above-ground biomass shows lower and variable values, with minimum values around 25 – 30 m from the marsh edges (values range from 35% to 50%). Toward the end of the transects, in the last 10 m located in the inner portion of the marshes, values of the above-ground biomass increase noticeably for the two transects of the San Felice salt marsh, whereas the increase is limited in the case of the Rigà transect. As a whole, the percentage amount of vegetation cover may decreases more than 50% from the marsh edge toward the inner marsh.

2.2.5.5 Soil Organic Carbon

In each transect the soil organic carbon density follows a different trend (Fig. 2.7) but, as a whole, in the first 5 m from the San Felice channel it is lower than in the inner part of the marshes. In the case of transect 1 the values fluctuate up and down with minimum values of 0.037 g cm^{-3} on the marsh edge and 20 m away from the channel, and a maximum value of 0.048 g cm^{-3} at 15 and 25 m from the channel. In the case of transect 2 the increasing trend toward the inner marsh is more defined and the values are spread over a wider range. The soil organic carbon density is minimum on the marsh edge (0.027 g cm^{-3}) and reaches a peak 30 m from the channel (0.063 g cm^{-3}). In the case of transect 3 (minimum value of 0.028 g cm^{-3} at 5 m), the values increase up to a distance of 20 m from the edge (peak of 0.054 g cm^{-3}) and decrease over the last 20 m. The average value of soil carbon density along the three transects is 0.044 g cm^{-3}.

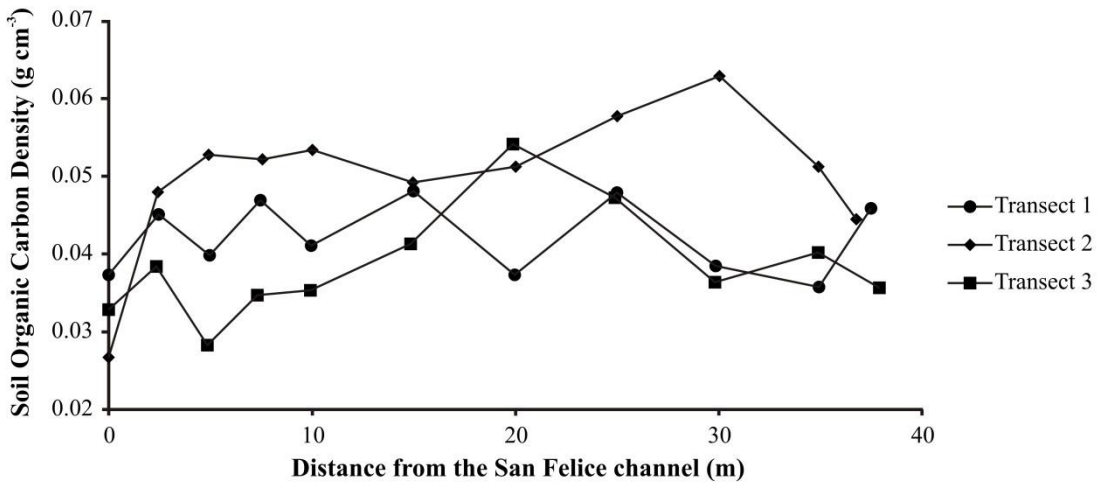

Fig. 2.7. Soil organic carbon density trend, for each transect, as a function of the distance from the marsh edges toward the inner marsh.

2.2.6 Discussion

The marsh elevations along the three transects considered show that the San Felice and Rigà salt marshes display a weakly concave-up profile, as commonly observed elsewhere (e.g., Allen, 2000; Bartholdy, 2012; Sheehan & Ellison, 2014). Field observations and model results show that sedimentation patterns are characterized by a decrease in inorganic deposition with increasing distance from the channels (French et al., 1995; Reed et al., 1999; Christiansen et al., 2000; Temmerman et al., 2004; D'Alpaos et al., 2007). This behavior emerges as a consequence of the progressive sediment settling as water moves towards the inner marsh areas during the tidal flooding and of the concurrent decrease in transport capability of tidal flows over the marsh as water approaches the no-flux boundaries.

The sediment dry bulk density along the transects co-varies tightly with the inorganic sediment content, which, in turn, is controlled by tidal advection of suspended sediment. The inorganic sediment suspended by wind waves in the shallow tidal flats (e.g., Carniello et al., 2011) is transported and deposited in the proximity of the channel banks. The dense vegetation cover encountered by tidal flood flows overspilling from the tidal channels, rapidly decreases flood current velocities (e.g., Leonard and Luther, 1995; Yang, 1998) and turbulent kinetic energy (Leonard and Croft, 2006; Mudd et al., 2010), thus promoting the sedimentation of coarser suspended fraction in proximity of the channel edges (Christiansen et al., 2000; Yang, 1998). Only finer sediment particles can therefore be transported towards the inner portion of the marsh, as attested by the progressive decrease in grain size along the transects in Figs. 2.3c, 2.4c, 2.5c. The increasing elevations at the end of each of the transects are due to the presence of two secondary tidal creeks, which, cutting through the inner parts of the marshes, transport relatively fine-grained inorganic material that is deposited along their banks. The formation of levees along these minor creeks shows that fine sediments

are transported through the smaller and inner reaches of the channel network and are deposited on the marsh when water floods the platform.

The deposition of inorganic sediment plays an important role especially along the marsh edges, where it dominates over organic accretion. If the marsh is in equilibrium conditions, as suggested (see equations [1] and [2]), the total accretion rate ($Q_i + Q_o$) needs to locally balance the rate of RSLR (that can be assumed constant at the marsh spatial scale). Larger rates of inorganic deposition should therefore be associated with lower rates of organic accretion. We note that the decrease in the inorganic deposition with distance from the channel, already suggested by both field observations and modeling results (French et al., 1995; Reed et al., 1999; Christiansen et al., 2000; Temmerman et al., 2004; D'Alpaos et al., 2007), is not always associated with a corresponding clear increase in the organic content. LOI results show an almost constant organic matter content along the transects, with the exception for the first meters along the channel levees Interestingly, H_2O_2 and H_2O_2 + NaClO treatments, generally give a non-monotonic increasing trend in the soil organic matter density and yield larger values of the soil organic content than LOI. Moreover, they show that the maximum organic density values occur at 15 and 25 m from the marsh edge. The fraction of organic matter is minimum along the marsh edge, but it increases quite rapidly away from the channel. In the inner part of the marsh, starting at about 5 – 7.5 m from the channel levees, the ratio between the mass of the organic component and the total mass, although much higher than on the channel levee, becomes almost constant, suggesting that the organic component quickly becomes an important soil component away from the main channel. The organic matter deposition is controlled by plant productivity, but the organic matter accumulation in the soil is not controlled just by the vegetation. The highest values in above-ground biomass are observed on the channel levees (2.5 – 5 m away from the marsh edge), where the elevation is higher and the organic content in the sub-surface samples is lower. On the contrary, where the surface elevation is minimum, the density of the

vegetation cover is lower (a 50% decrease is observed – see Figs. 2.3e, 2.4e, 2.5e), but the organic matter density in the samples is higher than near the edge. We interpret this apparent contrast by noting that where the elevation of the marsh is lower the soil is flooded for longer periods, possibly leading to increased soil saturation and to hypoxic conditions. Without oxygen, the degradation of the organic matter is much slower, such that a larger refractory fraction of the original biomass persists, thus compensating for the reduced plant productivity. On the contrary, the marsh edge, which is characterized by higher elevations, is flooded for shorter periods and mainly during high tides. More prolonged drainage conditions lead to more oxidized soils and to a faster organic matter degradation, leading, in turn, to a lower organic accumulation in the soil.

In addition, it is worth emphasizing that the evaluation of the soil organic matter content based on different methods highlights their different advantages and the potential. The LOI method at temperatures between 350 and 375 °C is likely to underestimate the amount of organic matter, in agreement with Frangipane et al. (2009), because of its incomplete ashing (Donkin, 1991). The treatment with NaClO following H_2O_2 turns out to be more effective in removing the organic matter than H_2O_2 alone, although the effects of these two reagents on the mineral fraction is still unknown.

Salt marshes, together with other coastal ecosystems like mangroves and seagrass beds, are able to sequester CO_2 from the atmosphere stocking high quantities of carbon in the biomass and in sediments (Duarte et al., 2005; Mcleod et al., 2011; Murray et al., 2011; Sifleet et al., 2011). This is because organic carbon in the hypoxic marsh soils conditions is buried and preserved for a long period of time, significantly contributing to the sequestration of "blue carbon" (Nellemann et al., 2009; Mcleod et al., 2011). Blue carbon is sequestered over the short (decennial) time scales in biomass, and over longer (millennial) time scales in marsh sediments (Duarte et al., 2005), as marshes accrete vertically. Although they cover an area <2% of the ocean surface, salt marshes, mangroves and seagrass beds

contribute close to half of the carbon burial in the coastal and global ocean (Duarte et al., 2005). Unlike terrestrial forests, where the organic carbon stores are dominated by the living trees, in vegetated coastal ecosystems the organic carbon is stored in their organic-rich soils (Chmura et al., 2003; Duarte et al., 2005; Mcleod et al., 2011; Murray et al., 2011). For example, salt-marsh systems by themselves lead to a carbon burial rate more than two orders of magnitude higher than the one observed in the tropical forest (Mcleod et al., 2011). When these fundamental coastal ecosystems are degraded or converted to other uses by natural and/or anthropogenic modifications, the sediment carbon is destabilized or exposed to oxygen and it is released to the atmosphere or in the water column in the form of CO_2 (Pendleton et al., 2012). The organic carbon storage on salt marshes, depending on their accretion rates, is geographically variable. In the case of the northern Venice lagoon, considering that the San Felice salt marsh seems to be in equilibrium with the forcing rate of RSLR (Carbognin et al., 2004; Marani et al., 2007), an accretion rate of about 0.3 cm yr^{-1} can be expected (Day et al., 1998a). As a consequence, from our measurements (see equation [3] for the determination of the organic carbon), the average carbon accumulation rate for the San Felice and Rigà salt marshes is estimated to be approximately equal to 132 g C m^{-2} yr^{-1}. This value is comparable with the results obtained by Chmura et al. (2003) for salt marshes in the Gulf of Mexico, NE and NW Atlantic ocean, NE Pacific ocean (average soil organic carbon: 0.039 g cm^{-3}; average organic carbon accumulation in the soil: 210 ± 20 g C m^{-2} yr^{-1}), by Delaune and Pezeshki (2003) for coastal marshes in Louisiana (183 g C m^{-2} yr^{-1}) and by Duarte et al. (2005) who found, from a compilation of previous reports published by Woodwell et al. (1973) and Chmura et al (2003), an average carbon burial at the global scale for salt marshes of 151 g C m^{-2} yr^{-1}. Considering the loss in salt-marsh extension of about 110 km^2 in the Venice Lagoon which occurred over the last 100 years, and considering only the organic carbon stocked in the topmost 1 m soil layer of the eroded marshes, it is possible to estimate a release of almost 5 Tg of carbon in about 100 years. Again

considering only the topmost 1 m soil layer, the Venice lagoon salt marshes still retain today a large carbon stock, amounting to about 2 Tg of C.

It is worth recalling that our estimates of soil organic carbon stocks and fluxes were based on the results of the LOI analysis, in order to make them comparable with previous and current literature results. Because LOI is found to likely underestimate organic matter content compared to chemical treatments, the evaluations of organic carbon accumulation and stock presented may constitute an underestimation of the actual ones.

2.2.7 Conclusions

We analyzed variations in organic and inorganic soil production processes at the marsh scale, a critical issue to improve our understanding of the mutual feedbacks among processes of physical and biological nature in salt-marsh landscapes and of the responses of salt marshes to a changing climate.

Our results emphasize that surface elevations, inorganic and organic sediment content, and grain size distribution along marsh transects are tightly related. In particular, our results show that coarser sediments are found along channel levees (with a median grain size D_{50} in the range 33÷38 μm), while the inner portion of the marsh is reached only by finer sediments (with a median grain size in the range 12÷24 μm). This suggests that the tidal network which cuts through the tidal landscape largely controls inorganic sediment transport over the platform and further supports previous field observations and modelling results emphasizing the occurrence of concave-up marsh surfaces with higher elevations along the channel banks and progressively decreasing elevations towards the inner portion of the marsh.

We also find that the amount of soil organic matter and inorganic content in a sample is very sensitive to the specific analysis method (LOI, H_2O_2, H_2O_2 + NaClO): LOI at 375°C for 16 hours underestimates the amount of the organic

sediment, while NaClO treatment (following H_2O_2 treatment) is likely to overestimate it. Interestingly, we find that the measured organic matter density provided by the H_2O_2 + NaClO method more than doubles the density estimates obtained through LOI. To our knowledge this is the first study in which the results obtained by using the above recalled methods are compared. We deem this to bear important implications, as consequences it shows that the quantification of marsh soil organic content and, consequently, of carbon stocks and, accumulation rates is heavily dependent on the specific analysis method adopted.

We provide evidence that the accumulation rates of the organic and inorganic components are related to the position on the salt marsh and to the distance from the channels. In particular, we find that salt-marsh accretion is mainly driven by the inorganic component in proximity of the channels, whereas the organic component becomes important in the inner part of the marsh. We suggest that our results, and similar determinations of the spatial distribution of soil organic content, will prove useful to quantitatively inform and test marsh biomorphodynamic models. The spatial distribution of organic soil can, in fact, better constrain model representations of organic soil production and decomposition, currently based on few point observations. In this respect, our results show that the accumulation of organic matter in the soil does not increase with biomass production, generally higher along the channel banks and lower in the inner part of the marsh. This observation is consistent with the organic matter accumulation in the soil being governed by the interplay of plant biomass productivity and decomposition. This interplay is, in turn, modulated by soil aeration, favoring decomposition, which is highest near the marsh edge and lowest in the low-lying inner zones, where the reduced decomposition rate compensates the lower biomass productivity.

Finally, our analyses provide the first estimates of soil organic carbon density from LOI measurement (estimated on average to be 0.044 g C cm^{-3}) and of the carbon accumulation rate for marshes in the Venice lagoon (132 g C m^{-2} yr^{-1} on

average in the San Felice and Rigà salt marshes). These results highlight the importance of salt marshes as sites of high atmospheric CO_2 sequestration, and carbon stock.

The proposed methodologies to determine the amount of soil organic matter and inorganic content can be applied to other salt-marsh systems and provides an effective method to study the coupled effects of physical and biological processes at the marsh scale. We therefore believe our findings to be of general interest and that the underlying biogeomorphic interactions shaping salt marshes in Venice, which served as an illustrative case, are also responsible for the evolution of salt-marsh systems worldwide.

Acknowledgements

This work was supported by the CARIPARO Project titled "Reading signatures of the past to predict the future: 1000 years of stratigraphic record as a key for the future of the Venice Lagoon", and by the "Fondazione Ing. Aldo Gini", that are gratefully acknowledged.

This manuscript benefits of the constructive comments from Andrea Rinaldo (Editor), Brad Murray and two anonymous reviewers.

CHAPTER 3

LATEST HOLOCENE DEPOSITIONAL HISTORY OF THE SOUTHERN VENICE LAGOON

3.1 OVERVIEW

This chapter is a journal paper in preparation. Sedimentological and morphological analyses, integrated with chronostratigraphical data, were carried out on salt-marsh, tidal-flat, subtidal-platform environments in the southern portion of the Venice Lagoon. The results allow us to provide a detailed description of the depositional history of the lagoonal sedimentary succession and a detailed age model for the area over the last two millennia. This is a new aspect that had not previously been provided for the Venice Lagoon, despite the large body of literature which analyzed the history and evolution of the Lagoon.

3.2 PAPER

MARCELLA RONER[1], ANDREA D'ALPAOS[1], MASSIMILIANO GHINASSI[1], MARIAELENA FEDI[2], LUCIA LICCIOLI[2], LUCA GIORGIO BELLUCCI[3], LARA BRIVIO[1]

[1]Dept. of Geosciences, University of Padova, via Gradenigo 6, 35131 Padova, Italy.

[2]INFN Section of Florence, Via Rossi 1, 50019 Sesto Fiorentino, Italy.

[3]ISMAR-CNR, Via Gobetti 101, 40129 Bologna, Italy.

3.2.1 Abstract

The Venice Lagoon represents an outstanding example of man-landscape co-existence. Among the typical lagoonal features, salt marshes are governed by the interaction between physical and biological processes. Because of their unique position in the tidal frame, salt marshes represent a crucially important ecosystem providing valuable services to the environment. In the Venice Lagoon salt marshes are currently exposed to possibly irreversible transformations due to the effects of climate changes and human interferences, as in other cases worldwide. Analyzing signatures of landscape changes in the stratigraphic record is crucial to refine our knowledge of tidal landform dynamics and it represents a first step towards the development of a predictive morphodynamic model. The southern Venice Lagoon, where remarkable changes in extent of salt marshes and tidal flats have been documented by historical sources, is suited to analyze modifications in the depositional environment and, consequently, in the sedimentary record. We collected 25 cores along a NE-SW linear transect about 5 km long cutting through salt marshes, tidal flats and subtidal platforms. High resolution sedimentological analyses defined the spatial arrangement of the four different deposits along the transect, whose cores were dated through radiocarbon, ^{210}Pb and ^{137}Cs geochronological analyses.

The study succession testifies an evolution from a palustrine fresh-water environment to a lagoonal environment over the last 2'000 years. The depositional history started with accumulation of palustrine peat which progressively evolved into a salt-marsh environment in the 14th century. Salt-marsh aggradation is characterized by different rates of accretion through time and occurred in parallel with the decrease in the salt-marsh extent and tidal-flat expansion. Indeed, where salt-marsh deposits were locally flooded and impacted by wind waves, a lag deposit developed. As a consequence of the progressive water deepening, organic rich mud accumulated above the lag. The results, as well as providing the first

accretion model for the latest Holocene succession in the southern Venice Lagoon, highlight that the disappearance of salt marshes in this area of the Lagoon has to be ascribed to the lateral erosion of their margins, rather than to a progressive drowning due to the decrease in marsh elevation referred to MSL.

3.2.2 Introduction

Lagoon and estuarine environments are characterized by extremely high biodiversity and elevated rates of primary productivity, host typical ecosystems and landforms and important socio-economic activities worldwide (e.g., Cronk and Fennessy, 2001; Barbier et al., 2011). Referring to the vertical position within the tidal frame, supratidal areas are permanently dry, being located above the Maximum High Water Level (hereinafter MHWL), whereas subtidal areas are always submerged, lying below the Minimum Low Water Level (MLWL). Intertidal areas are instead subjected to tidal fluctuations, their elevation ranging between MHWL and MLWL. From a morphological point of view, salt marshes, tidal flats and subtidal platforms represent the three major unchanneled lagoon sub-environments. Salt marshes are topographically the highest, with elevation between Mean Sea Level (hereinafter MSL) and MHWL. They are populated by a luxuriant halophytic vegetation and display a generally flat weakly concave-up profile (Adam, 1990). Tidal flats have an elevation between MSL and MLWL, they lack any halophytic vegetation and are fully exposed only during exceptionally low tides. Subtidal platforms are located below the MLWL, and are therefore perennially submerged (e.g., Allen, 2000) These three environments are tightly intertwined functionally and their morphological evolution, in both space and time, is strictly related. For example, the extent, shape and elevation of tidal-flat and subtidal-platform profiles in front of salt-marsh platforms can affect the characteristics of wind-wave fields impacting salt-marsh boundaries and promoting their erosion (e.g., Marani et al., 2010; Mariotti and Fagherazzi, 2013;

Hu et al., 2015). On the other hand the extent of salt marsh areas in front of tidal flats or subtidal platforms controls fetch dimensions, thus directly influencing the intensity of the wind-induced wave field (Mariotti and Carr, 2014). In addition, sediments eroded from the bottom of tidal flats can be transported over the marsh platforms by waves and tides and settle therein, while sediments eroded from salt-marsh boundaries can be redistributed over the adjacent tidal flats or subtidal platforms (Carniello et al., 2009). In the tidal frame, salt marshes represent an important ecosystem providing valuable services to the environment (Mitsch and Gosselink, 2000; Chmura et al., 2003; Costanza et al., 2008; MacKenzie and Dionne, 2008; Perillo et al., 2009; Davy et al., 2009; Gedan et al., 2009, Morgan et al., 2009; Silliman et al., 2009; Barbier et al., 2011; Gedan et al., 2011; Mcleod et al., 2011; Temmerman et al., 2013; Möller et al., 2014). The combined effects of natural changes, such as sea level rise, subsidence, erosion, and human interferences, such as reduced sediment supply, expose these ecosystems to possibly irreversible transformations. These effects turned out in an extensive loss of global marshlands, especially during the last century (e.g., Day et al., 2000; Marani et al., 2007; Gedan and Silliman, 2009; Gedan et al., 2009; Kirwan et al., 2010; Marani et al, 2010; Mudd, 2011; Pendleton et al., 2012).

The same fate afflicts salt marshes in the Venice Lagoon, a process also associated to a general expansion and deepening of tidal flats and subtidal platforms (Marani et al., 2007; Carniello et al., 2009; D'Alpaos 2010a; D'Alpaos et al., 2013). The current morphology of the Venice Lagoon is the result of a Pleistocene – Holocene evolution affected by both changes in the environmental forcings and, in the last millennium, by intense human modifications. The Holocene history of the Venice Lagoon has been well documented in recent studies and has arisen from the employment of very high-resolution seismic data integrated with core analyses (Brancolini et al., 2008; Zecchin et al., 2008, 2009, 2011, 2014; Tosi et al. 2009a; Madricardo and Donnici, 2014). Although the accumulation of the lagoonal succession started around 7'000 – 6'000 years B.P.,

only during the last 2'000 years the main changes in depositional patterns were strongly influenced by the interaction between natural processes, such as local subsidence and sea level rise (e.g., Day et al., 1999; Carbognin and Tosi, 2002; Tosi et al., 2002; Brambati et al., 2003; Carbognin et al., 2004, 2005; Teatini et al., 2005, 2012) and human interventions, such as river diversions and channel dredging (e.g., Gatto and Carbognin, 1981; Favero, 1985; Carbognin, 1992; Ravera, 2000; Brambati et al., 2003; Tosi et al., 2009a, 2009b; D'Alpaos, 2010a, 2010b; Bondesan and Furlanetto, 2012). During the last century, the exploitation of underground water significantly contributed to dramatic changes in subsidence of the Venice Lagoon (e.g., Carbognin, 1992; Brambati et al., 2003; Carbognin et al., 2005) and further activities associated with land reclamation and fish-breeding caused a significant decrease in the lagoon surface.

The main environmental and morphological changes occurred in the Venice Lagoon over the past centuries are well known from historical sources, which are represented by historical maps and archive documents (Dorigo, 1983; Favero et al., 1988; Dorigo, 1994; D'Alpaos, 2010a, 2010b). Nevertheless, relatively poor attention has been paid to detecting the signature of these changes in the lagoonal sedimentary record, which commonly appears to be significantly expanded given the remarkable accumulation rate (i.e., 0.25 cm yr^{-1}) that characterizes the Venice area (Bellucci et al., 2007). Lucchini et al. (2001) analyzed physical and chemical features of sediments (such as grain size, mineralogy, major and trace elements, organic carbon and total nitrogen) and the mechanism which control them within the topmost 60 cm of sediment cores within salt-marshes, tidal flats, and subtidal platforms in the Venice Lagoon They pointed out that sediment characteristics from the Northern Venice Lagoon reflect the occurrence of steady conditions for sediment supply and hydrodynamic and wave forcings, while sediment characteristics from the central and southern Venice Lagoon reflect an opposite trend. Bellucci et al. (2007) determined the depositional history of salt-marsh deposits accumulated over the past century analyzing five cores recovered from

different sites in the lagoon. They suggested that, on the long term, the rate of relative sea level rise is the driving forcing for marsh accretions, whereas, on the short term, variations in wind patterns, storm frequency and climate are the driving forcings for salt-marsh accretion rates in the Venice Lagoon.

The present paper focuses on the latest Holocene sedimentary succession of the southern Venice Lagoon, where remarkable changes in extent of salt marshes and tidal flats have been documented by historical sources (e.g., D'Alpaos, 2010a, 2010b). This work aims at detecting the signature of these changes in the stratigraphic record through a multidisciplinary approach based on sedimentological and geo-chronological analyses. Specifically, the aim of the paper is twofold: i) to define the sedimentary features and stratigraphic architecture of the lagoonal succession; ii) to provide a detailed age model for the latest Holocene salt-marsh succession.

3.2.3 Geological setting

The Venice Lagoon (Fig. 3.1A) is located in a foreland region comprised between the NE-verging northern Apennine and the SSE-verging eastern South-Alpine chains. It is a shallow (average depth 1.5 m) lagoon with a total extent of 550 km^2, and a semi-diurnal micro-tidal regime with maximum water excursion of ± 70 cm around Mean Sea Level (hereinafter MSL). The Venice Lagoon is connected to the Adriatic sea through three inlets: from north to south, Lido, Malamocco and Chioggia.

The Venice Lagoon formation started about 7'000 – 6'000 years B.P. in correspondence of the maximum marine transgression triggered by the Holocenic sea level rise (Fontana et al., 2004), which produced flooding of a late Pleistocene alluvial system developed during the Last Glacial Maximum. During the marine ingression, between 10'000 and 6'000 years B.P., longshore drift currents triggered the formation of a barrier island that delimited the Venice paleo-Lagoon

(Brancolini et al., 2008). The Holocene sedimentary succession unconformably overlays the late Pleistocene alluvial deposits and is composed of three main seismic units separated by major stratal surfaces (Zecchin et al., 2008). The first unit accumulated under transgressive conditions and resulted from the infill of estuarine and/or fluvial channels. The second unit accumulated during highstand conditions and is composed of a prograding wedge consisting of shoreface-shelf deposits and ebb tidal deltas, which pass landward into back-barrier sediments. The third unit also accumulated during the highstand phase and mainly consists of lagoonal deposits associated with development of a complex tidal network.

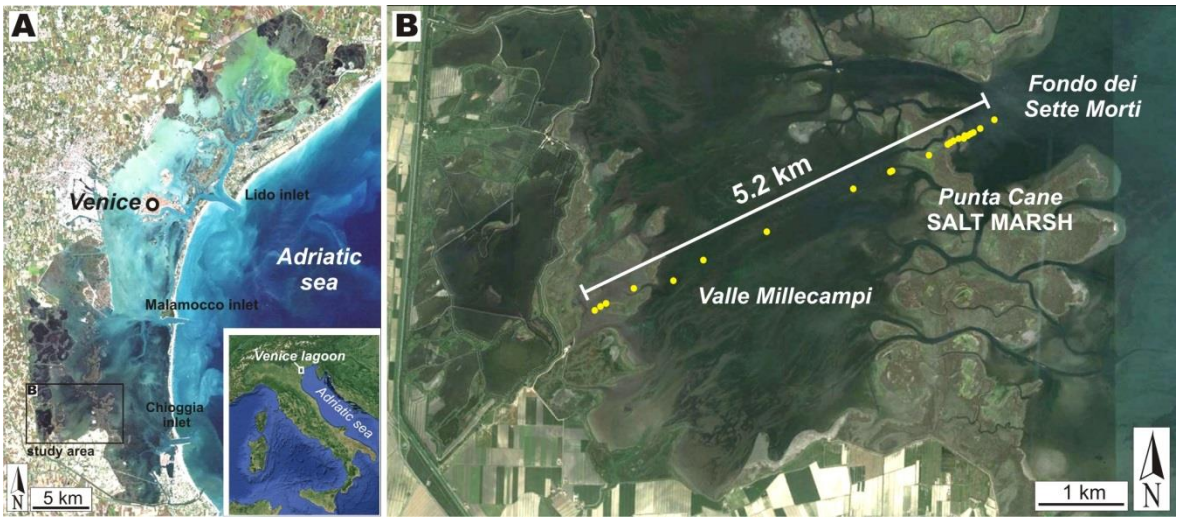

Figure 3.1. (A) Location of the study area in the southern Venice Lagoon, Italy. (B) Location of the 25 cores in the areas of Valle Millecampi, Punta Can salt marsh, Fondo dei Sette Morti.

The study area is located in the southern portion of the Venice Lagoon (Fig. 3.1A), where the Holocene transgression took place from ~10'000 to 6'000 years B.P. (Zecchin et al., 2009) accumulating a 20-22 m thick sedimentary succession (Tosi et al., 2007a, 2007b; Brancolini et al., 2008; Zecchin et al., 2008, 2009). During the past millennium, this area received considerable amount of clastic sediments from the Brenta River (e.g., Fontana et al., 2004; Tosi et al., 2007b; Amorosi et al., 2008; Tosi et al., 2009a), which was repeatedly diverted from and re-introduced in the lagoon (e.g., D'Alpaos, 2010a, 2010b; Bondesan and Furlanetto, 2012) during the last centuries. The diversion of the main rivers out of the Venice Lagoon

caused remarkable changes in salt marsh extent: salt-marsh areas, in fact, decreased from about 180 km^2 in 1811 to about 50 km^2 in 2002, with a reduction of more than 70% (Marani et al., 2003, 2007; Carniello et al., 2009; D'Alpaos, 2010a)

3.2.4 Methods

A total number of 25 sedimentary cores (1.0 to 1.5 m long) was recovered along a NE-SW trending, 5.2 km long transect (Fig. 3.1B). This transect crosses the Punta Cane salt marsh and the Valle Millecampi and Fondo dei Sette Morti tidal flat and subtidal platforms (Fig. 3.1B). Study cores were recovered from different setting (Fig. 3.2A): 11 cores from salt marshes; 5 cores from tidal flats; 9 cores from subtidal platforms. Cores are 10 cm in diameter and up to 1.5 m long, and were obtained stabbing vertically a cylindrical steel corer into the sediment. Complete recover of the core was allowed by a mechanical system, which shut off of the bottom of the corer. Recovering of cores with a diameter of 10 cm was required in order to collect a significant volume of sediment for geochronological analyses (e.g. find enough charcoal/wood fragments for radiocarbon dating). Since vertical stabbing of the corer caused sediment compaction, and additional core was recovered for each site using an auger corer (3 cm diameter), which prevents sediment compaction. Comparison between the two cores allowed us to define the original thickness of different sediment layers in the main core. If not differently specified, de-compacted thicknesses are used in the text. Elevation and geographic location of each core were determined using two TOPCON GR–3 GPS receivers (dual frequency - L1/L2 - and dual constellation - NavStar/Glonass - with integrated Tx/Rx UHF radio). Each core was halved lengthwise in laboratory. The first half was used for sedimentological and geochronological analyses, whereas the second one was archived.

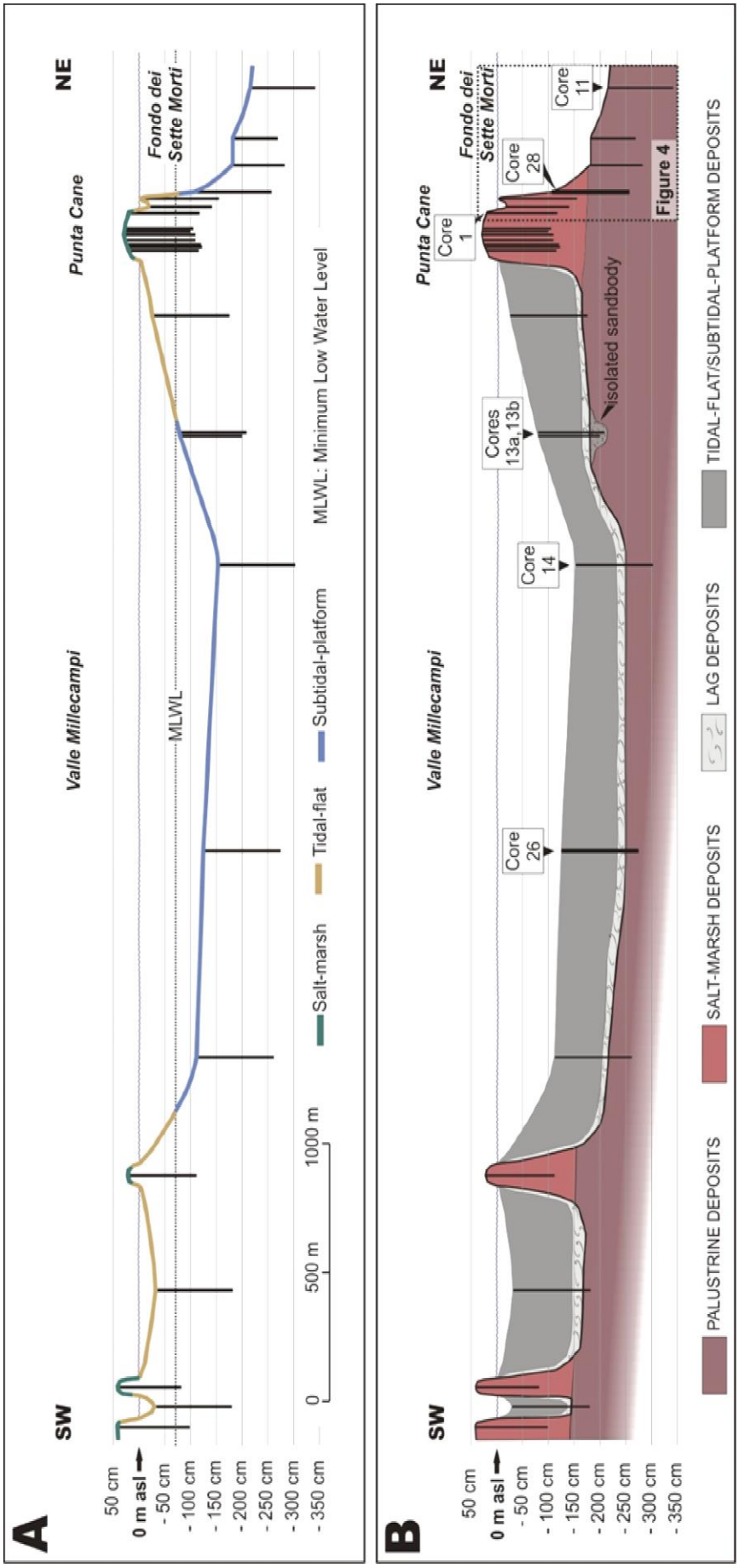

Figure 3.2. (A) Distribution of the 25 cores along the study transect. The three line colors represent the three different unchanneled lagoon sub-environments from a morphological point of view: green lines represent salt-marsh cores, yellow lines are for tidal-flat cores, blue lines symbolize subtidal-platform cores. The length of each line represents the core length after the de-compaction process which arises from the calibration of the deposits depth with uncompacted guide-cores. (B) Interpretation of the study transect built on the basis of the sedimentological features and the spatial distribution of the 4 different sedimentary deposits.

3.2.4.1 Sedimentological analysis

A high-resolution sedimentological analysis was carried out on the study cores through the principles of modern facies analysis in order to define the distinctive features of different types of deposits and to link them with corresponding sedimentary processes and depositional environments. Different types of deposits were differentiated basing on their color, grain size, texture, sedimentary structures and macroscopical biogenic content, that mainly consisted of shells, plant debris and *in situ* vegetal remains. An high-resolution stratigraphic framework was finally obtained correlating different types of deposits and related bounding surfaces along the transect.

3.2.4.2 Geochronological analyses

The Punta Cane and Fondo dei Sette Morti areas (Fig. 3.1B) were selected for geochronological analyses, since density and depth of core data allow one to investigate the maximum thickness of deposits with a remarkable resolution (Figs. 3.2A, 3.2B). Geochronological analyses were performed through radiocarbon and radionuclides (^{137}Cs and ^{210}Pb) analyses, which were performed on three selected cores (cores 1, 28, 11). These cores can be laterally correlated in order to define a composite core with an overall thickness of about 3.5 m. The Valle Millecampi area was selected for determining the radiocarbon dating of the onset of tidal flat/subtidal platform deposits on samples arising from core 14.

3.2.4.2.1 Radiocarbon analyses

Samples for radiocarbon analyses were collected from cores recovered in the Valle Millecampi (2 from core 14), in the Punta Cane (3 from core 1; 3 from core 28) and in the Fondo dei Sette Morti (1 sample from core 11) areas. Samples from Valle Millecampi were picked up to establish the onset of tidal flat/subtidal

platform deposition, whereas those from Punta Cane and Fondo dei Sette Morti were collected through the whole study succession in order to frame in time the main changes in depositional dynamics and sediment aggradation rate. Samples, consisting either of charcoals or vegetal remains (e.g., fragments of reeds, wood pieces, fragments of stems from halophytic plants in life position) were measured by ^{14}C – AMS (Accelerator Mass Spectrometry). The datable materials were recovered by directly picking from the cores for the coarser material and by floating for the finer fragments.

Before the AMS measurement, samples were cleaned using the so-called Acid-Base-Acid (ABA) procedure that allows one to remove any natural contaminations possibly due to carbonates and humic traces. Then carbon was first extracted as gaseous CO_2 by combustion and finally converted to solid graphite by reaction with hydrogen, in the presence of iron powder as catalyst. According to the typical laboratory quality check procedure, two graphite pellets were prepared from each of the pre-treated samples. AMS measurements were performed exploiting the dedicated beam line at the 3 MV Tandem accelerator installed at INFN-Labec, Florence (Fedi et al., 2007). $^{14}C/^{12}C$ isotopic ratios were measured in unknown, standard and blank samples, as well as $^{13}C/^{12}C$ ratios (to correct for isotopic fractionation). After verifying their consistency from the statistically point of view, for each sample, the best estimate of the radiocarbon concentration, and as a consequence of the radiocarbon age, was calculated as the weighted average of the two measured pellets.

3.2.4.2.2 Radionuclides ^{210}Pb and ^{137}Cs

Geochronological analyses through ^{210}Pb and ^{137}Cs were carried out on the uppermost 70 cm sedimentary interval of core 1. This thickness is referred to the compacted core, and corresponds to 85 cm of de-compacted salt-marsh deposits.

Alpha spectrometry of ^{210}Po was used for ^{210}Pb determinations, assuming secular equilibrium between the two isotopes. ^{210}Po was extracted from the sediment with hot HNO_3 and H_2O_2, in the presence of ^{209}Po as a yield monitor, to account for extraction and counting efficiencies. After separation of the leachate from the residue, the solution was evaporated to near dryness and the nitric acid was eliminated using concentrated HCl. The residue was dissolved in 1.5 N HCl, and Po was plated onto a silver disk overnight, at room temperature. Iron was reduced using ascorbic acid (Frignani and Langone, 1991), and alpha decays were counted by a silicon surficial barrier detector connected to a multichannel analyser. The analyses of the same sample with the two different ^{209}Po internal standards used at ISMAR (Bologna) and MSRC (Stony Brook) gave nearly identical results, thus suggesting that the analyses were accurate. Nevertheless, the accuracy of ^{210}Pb analyses was estimated also by repeated measurements of the certified standard sediment IAEA 300 (Baltic Sea sediment) and the results were within the standard uncertainties. In addition a successful intercalibration in the framework of the Euromarge-NB project was carried out (Sanchez-Cabeza et al., 1994). Precision, calculated from independent analyses of the same sample, was 4.6%.

^{137}Cs was measured by non-destructive gamma spectrometry of dry samples in standard vessels of suitable geometries. The analytical accuracy was periodically checked by counting the international certificate standard IAEA Baltic Sea sediment, and the results were within the standard uncertainties. In addition, two international intercalibrations (IAEA Proficiency test: Determination of Anthropogenic g-emitting Radionuclides in a Mineral Matrix, 2002; IAEA Proficiency test: Determination of γ-emitting Radionuclides, 2006) yielded ^{137}Cs activities within 4.1% and 1.6% of the IAEA accepted values, respectively. Precision, estimated by repeated analyses of the same sample, ranged between 2.05 and 3.07%. Efficiencies on 10 ml geometries (3.12-3.18%) were calculated through a series of standards obtained by spiking old sediment with a known

amount of the Amersham QCY58 multi-peak standard solution. The analytical detection limit for ^{137}Cs was 3 Bq kg^{-1}.

3.2.4.3 Accretion model

Calibration of the measured radiocarbon ages was performed exploiting the Bayesian inference. For the samples of the Punta Cane and Fondo dei Sette Morti areas, a chronological model was a priori built using both the information about the chronological order of the events and the sampling depth of the dated materials. The OxCal 4.2 (Bronck Ramsey, 2008) software was used. Because we can expect that the deposition process was random, the P_Sequence model was applied. In this model, we assume that, along the dated succession, the deposition rate may have random fluctuations (according to Poisson statistics). We can choose the guessed number of the accumulation events per unit depth (the so-called k parameter in OxCal): the higher is k, the more uniform is the expected sedimentation rate. In this case, we assumed a k parameter of 0.1 cm^{-1} (corresponding to 1 accumulation event per 10 cm depth). In defining our model, we also allowed the model to estimate the age distributions of probability of events that had not to be directly dated, considering them every 20 cm. The IntCal13 calibration curve (Reimer et al., 2009) was used in OxCal as reference.

Finally, our likelihood was build integrating the radiocarbon data with samples dated by ^{137}Cs and ^{210}Pb series.

3.2.5 Results

The study transect is characterized by an overall topographic relief of about 2.5 m below MSL (Fig. 3.2A). Salt marsh areas show an elevation ranging between 16 and 41 cm above MSL, with the lower values located in the Punta Cane area. Salt marshes are surrounded by bare tidal flats which extend up to 70 cm below

the MSL (Fig. 3.2A). A maximum water depth of 1.3 and 2.16 m below the MSL was measured in the Valle Millecampi and Fondo dei Sette Morti, respectively, where constantly flooded subtidal platforms develop (Fig. 3.2A).

3.2.5.1 The study deposits

3.2.5.1.1 Sedimentology

Five types of deposits were recognized through sedimentological analysis . The deposits are described and interpreted in the following.

i. Palustrine deposits

They are at least 2 m thick and consist of peat with abundant fragment of reeds, which can be up to 15 cm long (Fig. 3.3A). They occur in all the cores exceeding about -1.5 m below MSL (Fig. 3.2B). Peat consists of comminuted plant debris, is massive and contains a minimum amount of dispersed mud and very fine sand. Rare reeds in sub-vertical positions have been recovered from core 10. The peat can either grade upward into salt-marsh mud or be abruptly overlain by a shell-rich lag. The basal part of the peat was not encountered in any core.

In the NE sector of the Valle Millecampi subtidal platform, two adjacent cores show that sandy deposits occur laterally to the peat (cores 13a and 13 b in Fig. 3.2B). Only a 15 cm thick layer of sandy deposits has been recovered and consists of medium sand grading upward into a very fine sand (Fig. 3.3C). Medium sand is well-sorted and contains scarce matrix, whereas fine sand is rich in mud and contains abundant plant debris.

Peat deposits are interpreted to be formed in a palustrine setting, where vegetal remains were transported as debris or produced *in situ*, as attested by the occurrence of sub-vertical reeds, which probably were buried in life position. In this framework, the sandy deposits occurring in the NE sector of the Valle Millecampi area could represent the infill of a fluvial/distributary channel

draining a densely vegetated coastal plain. The occurrence of a progressive fining-upward of the sandy unit, suggesting the progressive deactivation of the channel, supports this hypothesis.

ii. Lag deposits

These deposits are up to 15 cm thick and occur only in cores located in subtidal platforms and tidal flat areas. They consist of fine sand fining upward into muddy silt. Sand is very rich in shells and shell fragments (Fig. 3.3B). Bivalves are commonly disarticulated, although few specimens of *Cerastoderma edule* have been found in life position. Sand is mainly massive, although a subtle horizontal layering can be locally distinguished. Wood fragments, up to 1 cm in size, are also common. Bioturbation is intense, although distinct burrows can be rarely distinguished. These shell-rich sand overlay palustrine peat and grade upward into muddy subtidal platform deposits. They can be followed for several hundred meters along the study transect (Fig. 3.2B).

The absence of mud and concentration of shells are consistent with lag deposits produced by wave winnowing. The occurrence of fragmented and disarticulated shells, along with the considerable lateral extent, the fining-upward grain size trend and the abrupt basal surface, strongly support this hypothesis.

iii. Tidal-flat/subtidal-platform deposits

They are up to 1.30 m thick and consist of dark, organic-rich mud with subordinate sandy layers (Figs. 3.3D, 3.3E). Mud is massive and contains scattered plant fragments. Shells can be isolated or form localized concentrations (Fig. 3.3D). Bivalve *Cerastoderma edule* frequently occurs in life position. Sandy layers are up to 2-3 cm thick and commonly show a lenticular geometry with a flat base and wavy top (Fig. 3.3E). They consist of fine to very fine moderately to well-sorted sand and are frequently disturbed by intense bioturbation. These deposits occur only in cores located in subtidal platforms and tidal flat areas and conformably overlie shell-rich lag sand.

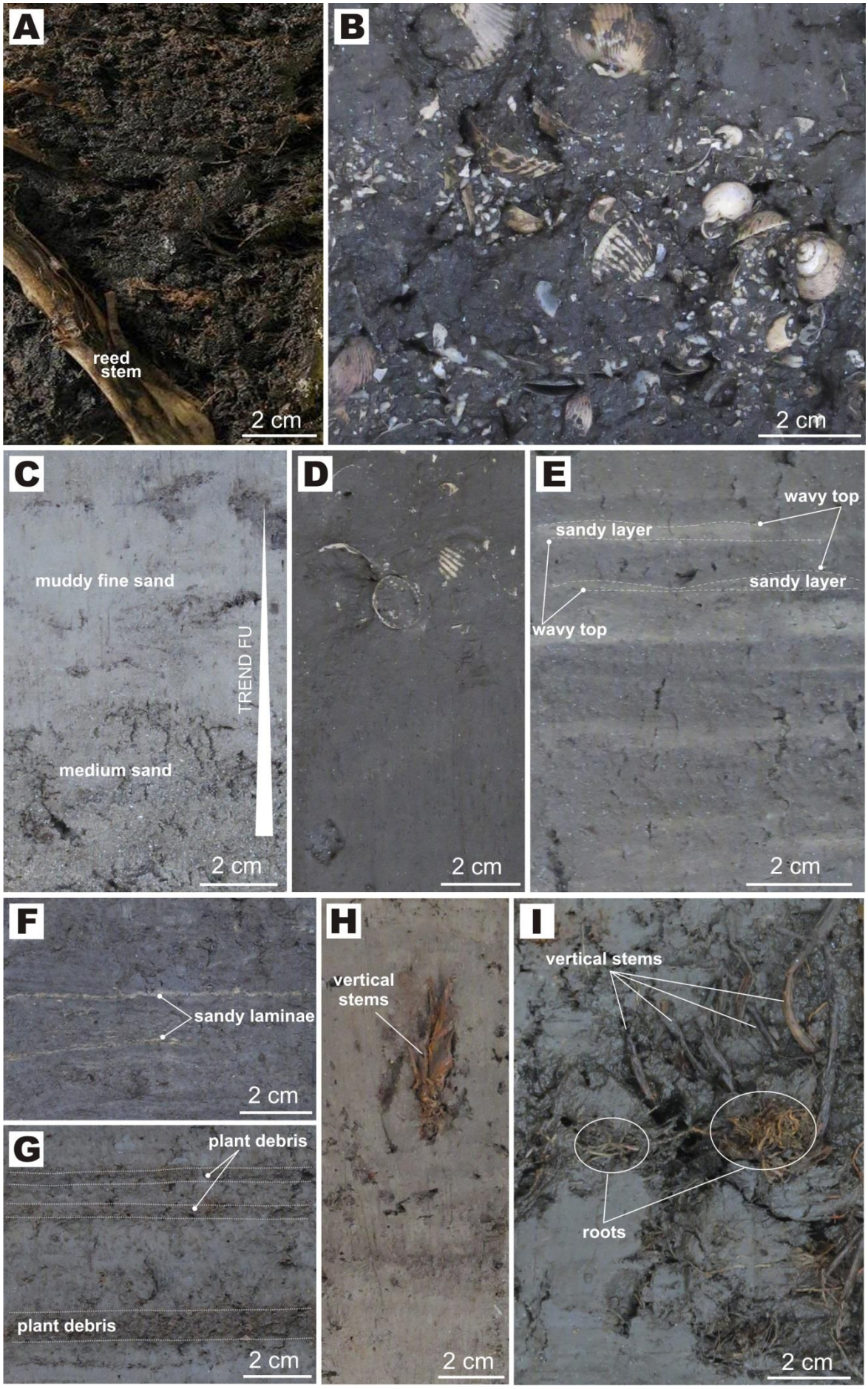
A
reed stem
2 cm
B
2 cm
C
muddy fine sand
TREND FU
medium sand
2 cm
D
2 cm
E
wavy top
sandy layer
sandy layer
wavy top
2 cm
F
sandy laminae
2 cm
G
plant debris
plant debris
2 cm
H
vertical stems
2 cm
I
vertical stems
roots
2 cm

Figure 3.3. Sedimentary facies of the study deposits. (A) Peat deposit with fragment of reeds from millimetric to decimetric in size. (B) Shell-rich lag deposit. (C) Sandy to muddy-sandy paleo-channel deposit. (D) Massive tidal-flat/subtidal-platform deposit with shells. (E) Laminated tidal-flat/subtidal-platform deposit. (F) Sub-millimetric fine-medium sand layers in salt-marsh brownish silt deposit. (G) Organic material organized in layers in salt-marsh brownish silt deposit. (H-I) Plant debris in life position in the salt-marsh brownish deposit.

Dominance of mud indicates settling from sediment suspension in a low-energy setting, which is consistent with a tidal-flat or subtidal-platform depositional environment. Sandy layers and localized shell concentration developed during storm events, when wave-generated currents suspended the mud causing concentration of the coarser deposits on the depositional interface. The wavy top of sandy layers indicates local preservation of wave-generated ripple forms and supports the previous interpretation.

iv. Salt-marsh deposits

These deposits are up to 2.0 m thick and occur only in cores recovered in salt-marsh areas. They consist of a horizontally-laminated, bioturbated, brownish mud, with a variable amount of fine to very fine sand (Figs. 3.3F, 3.3G). Several mud laminae are dark brown and appear to be very rich in plant debris (Fig. 3.3G) and wood fragments. Sand is mainly concentrated in millimetric, whitish, horizontal laminae (Fig. 3.3F), which are characterized by a good grain-size sorting. Roots and vertical stems up to 0.5 cm in diameter are common (Figs. 3.3H, 3.3I).

These deposits accumulated in salt-marsh environment, in the highest portion of the intertidal zone that was commonly affected by subaerial exposure allowing the growth of a dense halophytic vegetation. Muddy deposits likely settled down around high water slack, at the transition between flood and ebb tide. Sandy laminae were generated during storm events in high tide conditions, when wind-generated waves winnow the salt-marsh surface, suspending mud

and concentrating sand. Textural sorting of sandy laminae and lack of a muddy matrix support this hypothesis.

3.2.5.1.2 Stratigraphy

The substrate of the study succession is made of palustrine peat, that is documented almost along the whole transect (Fig. 3.2B). Above the basal peat both salt-marsh and tidal-flat deposits are documented. In the Valle Millecampi area, the peat is abruptly overlaid by the shell-rich lag deposit (see, for example, core 26 in Fig. 3.4), which shows maximum thickness in the central, deepest parts of the depression and becomes thinner toward its margins (Fig. 3.2B). The lower boundary of the shell-rich lag is commonly disrupted because of intense bioturbation (e.g., core 26 in Fig. 3.4). Muddy tidal flat/subtidal platform deposits

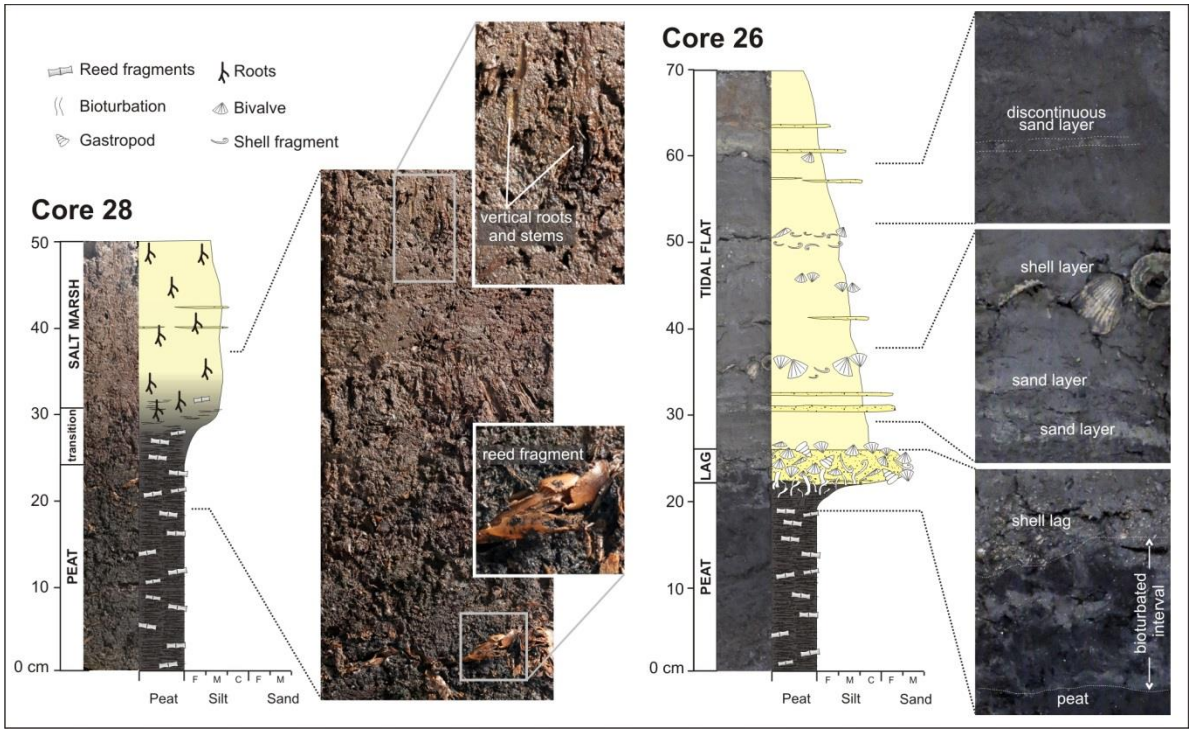

Fig. 3.4 Sedimentological log of core 28: this core exhibits the transition between the basal peat and the salt-marsh deposit, which is characterized by a gradual decrease in the reeds content and an equivalent increase in the mud and halophytic roots content. Sedimentological log of core 26, typical tidal-flat and subtidal-platform core of Valle Millecampi. The presence of widespread bioturbation marks the passage from the basal peat to the shell-rich lag, the latter representing the base of the organic-rich, blackish, massive or laminated mud.

are widespread in the Valle Millecampi area above the shell-rich lag. These deposits are characterized by an overall fining-upward grain size trend from fine sand to mud (e.g., core 26 in Fig. 3.4). Where salt marshes are well developed, the basal peat grades upward into salt-marsh deposits. The transition occurs within about 20 cm and is characterized by a gradual decrease in content of reed fragments, which occurs in parallel with an increase in root traces and mud content (i.e., core 28 in Fig. 3.4). In the Fondo dei Sette Morti area, the shell-rich lag and overlying mud are missing, and the basal peat and salt marsh deposits are exposed at the depositional interface (Fig. 3.2B).

3.2.5.2 Radiocarbon datings

Table 3.1 shows the experimental results of ^{14}C-AMS measurements performed in Valle Millecampi, Punta Cane and Fondo dei sette Morti areas. For each sample, the best estimate of the radiocarbon concentration, and the corresponding radiocarbon age, were calculated as the weighted average of the two measured graphite pellets (see the Lab. codes column in Table 3.1). Only in the case of samples 14.30 and 1.112, the low amount of the residual mass after the ABA pre-treatment allowed us to prepare just a single graphite pellet. Data are quoted at 1 sigma uncertainty.

Samples from Valle Millecampi, that were collected from the shell-rich lag to establish the onset of the deposition in this basin, provided low-quality results. This is probably due to the reworking of charcoal and wood materials during the formation of the wave-winnowed lag. As a whole, despite the significant errors in the calibrated ages (sample 14.33: 240^{+85}_{-105} cal AD; sample 14.30: 265^{+155}_{-125} cal AD, ages expressed as mode value in the interval at 68% of probability), these results would suggest that the age of lag deposits would span between the 2nd and 5th century.

Recovering area	Sample	Lab. codes	Depth (cm referred to MSL)	^{14}C conc. (pMC)	Radiocarbon age (years BP)
Valle Millecampi	14.33	14Fi2560 14Fi2566	-250.0	80.05 ± 0.57	1790 ± 55
	14.30	14Fi2569	-241.0	80.6 ± 1.1	1730 ± 110
Punta Cane	28.33	14Fi2627 15Fi2632	-208.0	90.32 ± 0.47	820 ± 40
	28.19	14Fi2561 14Fi2565	-165.2	92.64 ± 0.54	615 ± 45
	28.11	14Fi2638 14Fi2640	-140.7	94.25 ± 0.38	475 ± 30
	1.112	14Fi2553	-113.3	94.50 ± 0.68	455 ± 60
	1.80	14Fi2625 15Fi2628	-75.5	96.49 ± 0.36	287 ± 30
	1.70	14Fi2624 14Fi2629	-63.7	96.82 ± 0.49	260 ± 40
Fondo dei Sette Morti	11bottom	14Fi2559 14Fi2564	-342.0	77.70 ± 0.50	2030 ± 50

Table 3.1. Experimental data of ^{14}C-AMS measurements.

In the Punta Cane and Fondo dei sette Morti areas, the seven dated samples are distributed along the composite core 1-28-11 at different depths (Fig. 3.5), which are referred to MSL. The age for each sample is represented by the mode value of the calibrated age quoted at 68%. As a whole, radiocarbon datings show that the oldest peat deposits occur at about 3.40 m below MSL, and that they are dated at about 0±60 cal AD. The transition between palustrine and salt-marsh deposits is dated at 1355^{+40}_{-45} cal AD.

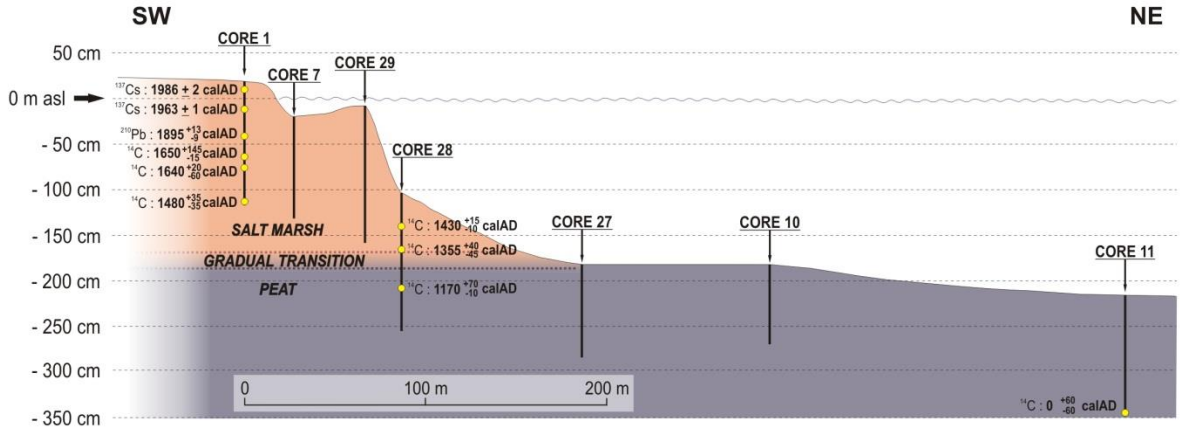

Figure 3.5. Detailed representation of the seaward part of the study transect. The sedimentary succession involves the peat deposit which gradually passes to the salt-marsh deposit. The yellow dots represent the uncompacted depths of the dated samples. Each age reports the employed geochronological method (^{14}C, ^{210}Pb, ^{137}Cs), the mode value obtained from the age distribution, and the errors of the calibrated ages interval at 68% of probability (see Table 3.2).

3.2.5.3 Radionuclides ^{210}Pb and ^{137}Cs

The ^{210}Pb activity-profile of core 1 (Fig. 3.6A) reaches, on the compacted core, the equilibrium depth at 55 cm from the core top and allows us to set the 1900 ± 10 AD at 50 cm, that corresponds to 60 cm from the core top of the de-compacted one. The ^{137}Cs activities show a clear trend (Fig. 3.6B) and the peaks at 7.5 cm and at 25.5 cm (9 cm and 30.5 cm on the de-compacted core, respectively) are associated to 1986 AD (fallout from the Chernobyl accident) and to 1963 AD (maximum ^{137}Cs fallout from nuclear testing), respectively.

3.2.5.4 Accretion model

As already recalled above, calibration of the measured radiocarbon ages was performed using the P_Sequence model and adding to the dated succession the more recent samples dated by Pb and Cs series: Pb 1900±10 AD, Cs1 1963 AD, Cs2 1986 AD. Running the model gives us satisfying results: the agreement index is indeed 99%, with the individual agreement index of each sample well above the

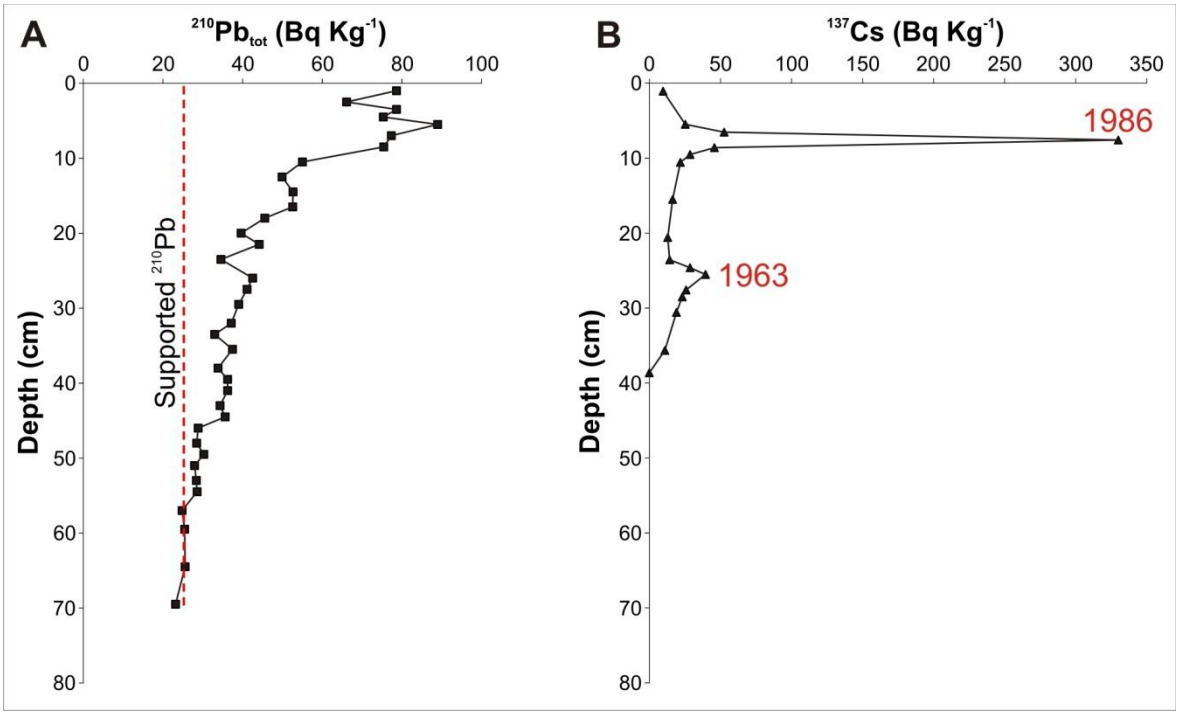

Figure 3.6. ^{210}Pb and ^{137}Cs activity-depth profiles in core 1.

threshold of 60%. Table 3.2 shows the calculated intervals for the calibrated age of the measured samples, quoted at both 68% and 95% probability levels. The depths of the samples, referred to MSL, were calculated on the basis of the de-compaction process after calibration of the depth of the different deposits.

Figure 3.7 shows the data evaluated applying the P_Sequence model using the mode of the calculated distribution of probability for each sample. In fact, even though it is well known that there is no good point estimation of the true calendar age of a sample dated by radiocarbon, the mode of the distribution may be taken as an acceptable approximation (MichczyÒski, 2007). We can therefore use this information to evaluate the sedimentation rate. The figure clearly shows that the accumulation rate is not constant over the last two millennia.

Sample	Depth (cm referred to MSL)	Cal Age (BC/AD) 68% prob.	Cal Age (BC/AD) 95% prob.
11bottom	-342.0	-60 – 60	-165 – 80
28.33	-208.0	1160 – 1240	1045 – 1085 (8%) 1125 – 1135 (1%) 1150 – 1270 (86%)
28.19	-165.2	1310 – 1395	1290 – 1405
28.11	-140.7	1420 – 1445	1405 – 1450
1.112	-113.3	1445 – 1515	1430 – 1585
1.80	-75.5	1580 – 1595 (3%) 1615 – 1660 (65%)	1525 – 1665
1.70	-63.7	1635 – 1670 (61%) 1785 – 1795 (7%)	1545 – 1595 (4%) 1615 – 1685 (74%) 1735 – 1805 (17%)
Pb	-41.1	1886 – 1908	1877 – 1917
Cs1	-11.6	1962 – 1964	1960 – 1965
Cs2	10.0	1984 – 1988	1982 – 1990

Table 3.2. Calibrated ages of the measured samples, quoted at both 68% and 95% probability levels, as calculated applying the P_Sequence model. When more than one interval was calculated for each level of confidence, the probability for each definite interval is also shown in brackets.

The aggradation trend, derived from the age model shown in Figure 3.8A, is portrayed in Figure 3.8B, in which the total accretion rate is plotted as a function of the depth along the succession (the inset shows the accretion rate as a function of time). The mode and the errors employed are represented by the result of the calibrated ages intervals at 68% of probability.

As a whole, the sedimentation rate along the study succession considering the mode values tends to gradually increase from the bottom to 1480 AD, with increasing values starting from 0.11, 0.23, 0.33, up to 0.55 cm/yr. During the 16th century, framed from a depth of 113 cm to a depth of 75 cm below MSL along the

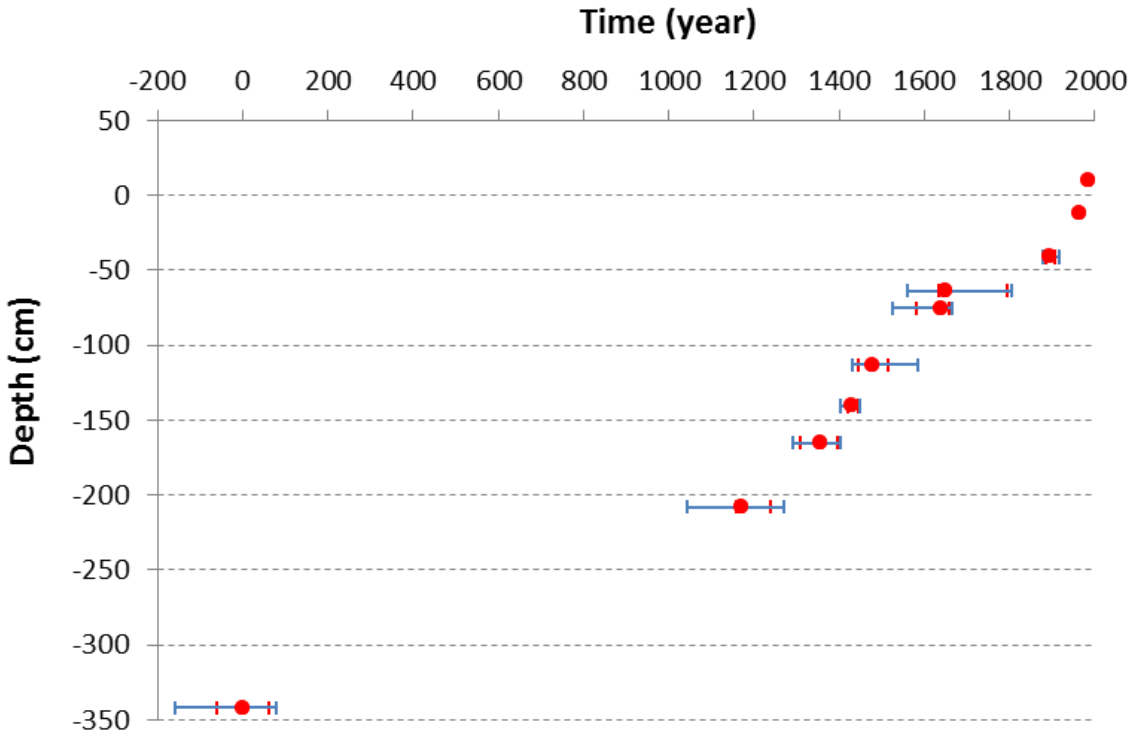

Fig. 3.7. Calibrated ages of the measured samples plotted versus the sampling depth. For each sample the mode of the posterior distribution of probability as determined applying the P_Sequence model is shown; error bars indicate the extremes of the calibrated ages interval at both 68% (in red) and 95% (in blue) of probability.

succession, the accumulation rate decreased to 0.24 cm/yr. The above interval is characterized by an important increase in the accumulation rate which reaches values of 1.18 cm/yr, and it is later followed by a significant decrease. During the ages from 1650 AD to 1986 AD the sedimentation rate increases again, changing from values of 0.09 cm/yr until the end of the 19th century, to values of 0.43 cm/yr from 1900 AD to 1963 AD, up to 0.94 cm/yr in the years between 1963 AD and 1986 AD. From the year of Chernobyl accident to nowadays the accretion rate on Punta Cane salt marsh is equal to 0.33 cm/yr, which is much smaller compared to the value of 2.32 cm/yr obtained by Day et al. (1998b) for the same study area.

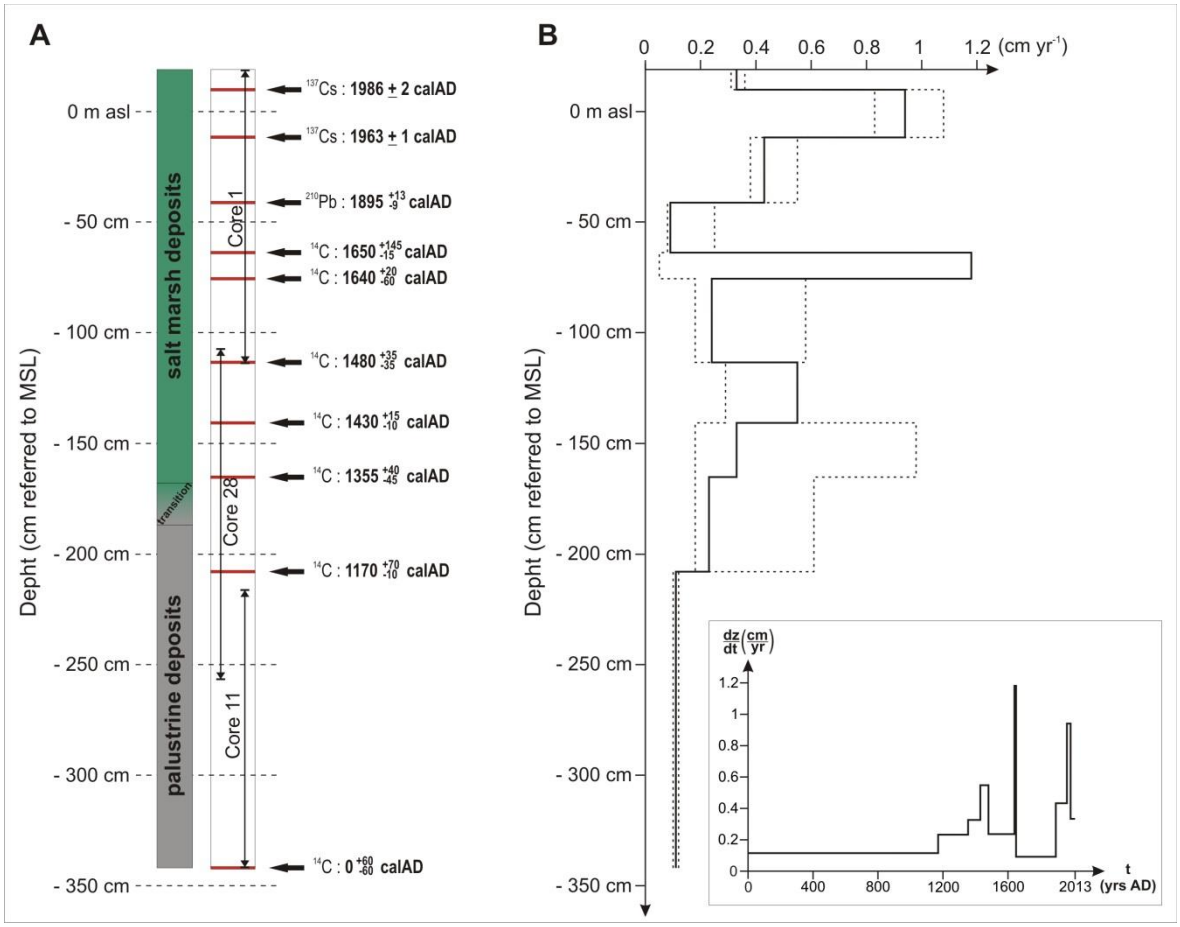

Figure 3.8. Accumulation rate model. On the left (A) the depths of each dated sample are represented in a schematic continuous sedimentary succession built up from cores 1, 28 and 11, after the de-compaction process. Each sample age is expressed as the mode value in the distribution and the two errors represent the ages interval at 68% of probability. On the right (B) the accumulation rates are plotted versus the depth intervals. The black line represents the accumulation trend considering the mode values; the two dashed lines represent the minimum and the maximum accumulation rates considering the result of the calibrated ages intervals at 68% of probability. The inset shows the accretion rate as a function of time.

3.2.6. Discussion

3.2.6.1 Depositional history of the Punta Cane area

The radiocarbon age of the deepest sample indicates that, during the 1st century BC, the NE sector of the study transect (i.e., the Punta Cane area) was characterized by peat accumulation in a palustrine environment. Palustrine sedimentation persisted for about 1,400 years allowing the accumulation of about 2.0 m of peat. Continuous peat sedimentation indicates that organic deposition

faced the increase in accommodation space also during the 12th and 13th century, when combination between sea-level rise and local subsidence caused an increase in mean sea level. Sandy deposits which were observed in the SW part of Punta Cane area (see cores 13a and 13b in Fig. 3.2B) suggest that clastic sediment probably remained confined within distributary channels (e.g., Horne et al., 1978). The presence of peat and of small sandy deposits, agrees with information derived from historical sources pointing out that the Brenta River was active (although being characterized by the presence of different reaches and different outlets within the Lagoon), during the 1st century BC, during the Roman age, and between the 5th and the 9th century AD (Mozzi et al., 2004). Moreover, across the studied transect (Fig. 3.1B), the presence of a generally peaty continental substratum of Roman age and the presence of organic and salt-marsh deposits of Late-Roman – Medieval age, lying above this substratum (Tosi et al., 2007b), confirms the presence of an active reach of the Brenta River, although it is difficult to establish which Brenta reach they belong to.

During the 14th century, the palustrine environment gradually experienced a transition into a salt marsh system. Transitions of this type might be the result of a decrease in the rate of relative sea level rise, of an increase in sediment supply, or both (Marani et al., 2010; Kirwan et al., 2011; Mudd, 2011). We are not aware of relative sea level reconstructions dating back to this period, nor of diversions of the Brenta River likely promoting an increase in the availability of sediment. In addition, in the case of the Venice Lagoon, to our knowledge, no historical maps of the Lagoon exist dating back to before 1556 AD (Cristoforo Sabbadino Map, Fig. 3.9A). Interestingly, our results document, for the first time, the transition from a palustrine to a salt-marsh system in this portion of the Venice Lagoon. Salt marsh deposition persisted until the present day allowing the accumulation of about 1.80 m of sediment in about 650 years, although the accretion rates over time are not constant.

3.2.6.2 Depositional history of the area landward of Punta Cane

As to the Valle Millecampi area (see Figs. 3.2A, 3.2B), located landward of the Punta Cane area, the basal peat is overlaid by a lag deposit over which a mud deposit further accumulated. The age of the wave-winnowed lag deposits suggests that flooding of the Valle Millecampi area occurred between the 2nd and 5th century AD. As noted above, the first historical map showing the presence of a tidal flats in this area dates back to the 1556 (Cristoforo Sabbadino map, Fig. 3.9A). During the 16th century, the Valle Millecampi basin was already well-developed, thus suggesting that the fetch and water depth were large enough for the development of waves capable to produce bottom shear stresses promoting resuspension of sediments from the bottom (Fagherazzi et al., 2006; Francalanci et al., 2013; Mariotti and Fagherazzi, 2013). Although radiocarbon calibrated ages are affected by a remarkable error, they are consistent with observations derived solely based on historical maps. (e.g., D'Alpaos 2010a, 2010b). The overall fining-upward grain size trend of the deposits overlying the lag points (see core 26 in Fig. 3.4) are ascribed to a progressive increase in water depth, which was not large enough to hinder wave winnowing of the tidal flat bottom (Fagherazzi et al., 2006), as attested by storm-generated, sandy layers in the uppermost part of the muddy succession (core 26 in Fig. 3.4). The constant wave reworking of the bottom of the tidal flats in the Valle Millecampi area, causing suspension and removal of fine sediments, is consistent with a maximum sediment accumulation of 1.30 m over the last 1'600 – 1'900 years.

The correlation between sedimentary cores recovered from modern tidal flats (see the Valle Millecampi areas in Figs. 3.2A, 3.2B) allows us to relate the stratigraphic record (described for the first time in this work) to the historical record derived from the detailed topographic map of Augusto Dénaix, (1809 – 1811, Fig. 3.9B). This map, which is the oldest map describing in details the bathymetric characteristics of the Venice Lagoon (the older maps, e.g., Fig. 3.8 A,

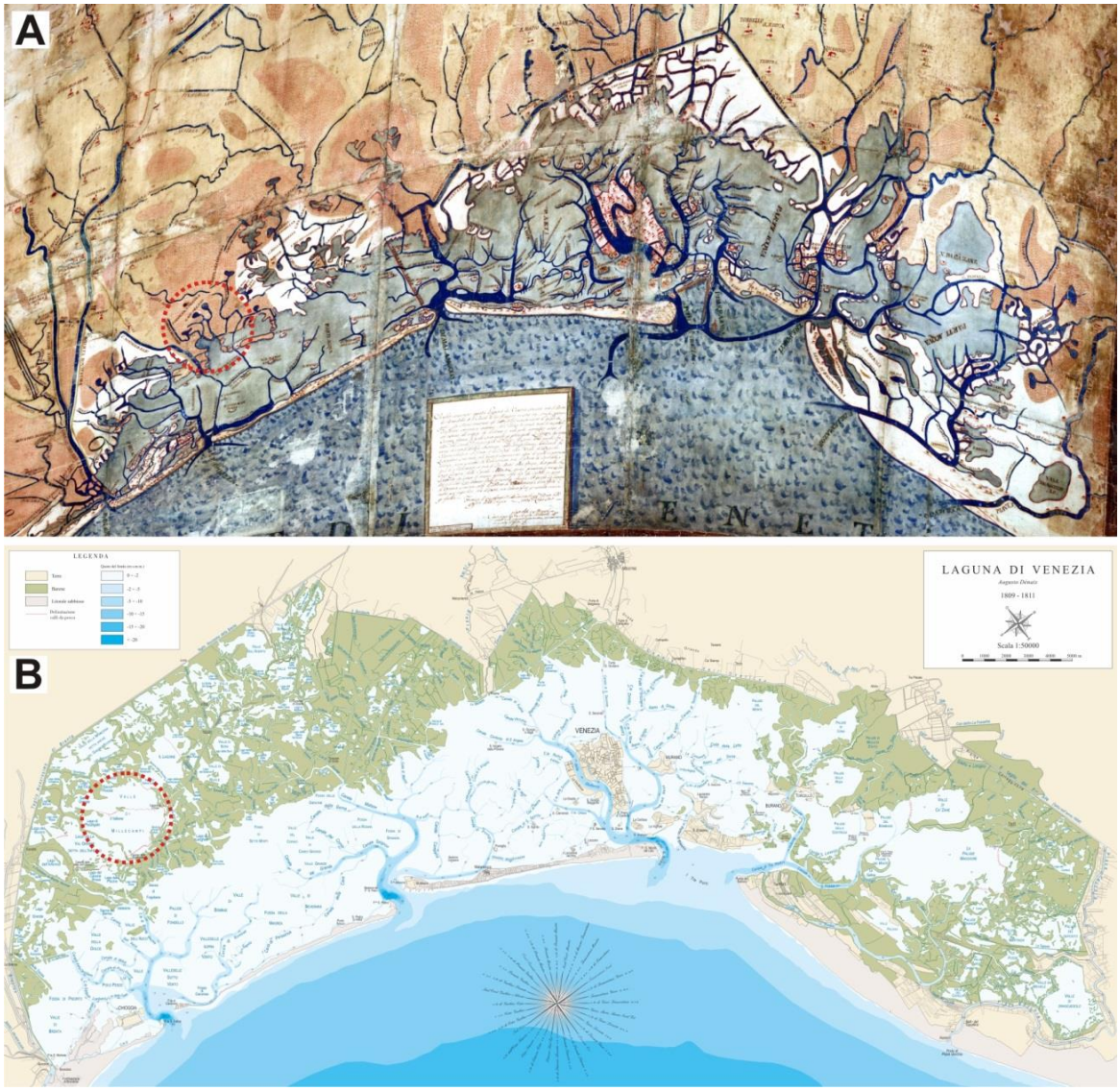

Fig. 3.9. (A) Map of Cristoforo Sabbadino (1556). (B) Map of Augusto Dénaix, (1810). The red circle in the two maps highlights the Valle Millecampi area (after D'Alpaos, 2010b, modified).

reported only qualitative information about the morphological characteristics of salt marshes, tidal flats and channels), shows that most of the modern tidal flats, presently cover areas which were previously colonized by salt marshes: i.e., the width of the Valle Millecampi basin (*sensu* Mariotti and Fagherazzi, 2013) was much smaller in 1810 than nowadays. Interestingly, none of the sediment cores recovered in these tidal flats highlight the presence of salt-marsh deposits below the wave-generated shell lag (Fig. 3.2B, core 26 in Fig.3.4). This suggests that these deposits were entirely removed by waves, which promoted deepening of tidal flats and lateral erosion of salt-marsh edges thus increasing the width of the Valle

Millecampi basin, at least, during the last two centuries. It is worth emphasizing that, in this case, marshes did not disappeared due to drowning promoted by the exceedance of a threshold rate of RSLR. On the contrary, the transition from a salt-marsh to a tidal-flat landscape was triggered by the positive feedback between the increase in wave power and the increase in the basin width and depth (Francalanci et al., 2013; Mariotti and Fagherazzi, 2013). Larger fetches and increasing water depths lead to increased wave height, wave power and lateral erosion, which further promoted tidal-flat deepening and increase in the fetch, thus closing the feedback. The extension of tidal-flat areas therefore occurred in parallel with the decrease in salt-marsh extent, and the progressive water deepening led to bottom elevations lower than MLWL and, consequently, to the conversion of tidal flats in subtidal-platforms. The presence of typical tidal-flat deposits on the subtidal-platform part of Valle Millecampi confirms the common origin of the sediments in this area in which wind-wave erosion played a fundamental role on the marsh platforms.

3.2.6.3 Depositional history of the area seaward of Punta Cane

Seaward of the Punta Cane salt marsh, the tidal flat which connects the marsh with the subtidal platform of Fondo dei Sette Morti does not show a succession similar to that observed for Valle Millecampi, but rather it presents a salt-marsh succession similar to that observed for Punta Cane. The presence of typical salt-marsh deposits which lie below MSL (core 7: elevation 20 cm below MSL; core 29: elevation 8 cm below MSL; see Fig. 3.5) highlights that this seaward part of the Punta Cane salt marsh is currently under lateral erosion. Day et al. (1998b) found, by direct measurements in this area over 25 months, that the seaward edge of Punta Cane salt marsh retreated at a rate of 0.6 ÷2.2 m yr^{-1}. In this area the action of the wind waves is particularly strong because of both its exposure toward NE (Bora wind direction), the presence of quite a large fetch

(about 9 km of unlimited water surface between the Punta Cane salt marsh and the littoral barrier) in the same direction, and the large water depths. As suggested by Marani et al. (2011), the rate of edge erosion is linearly related to the incident wave power density. Moreover, the erosion condition of the seaward part of the marsh is also confirmed by the presence of a very steep scarp (much steeper than the one which characterizes the sheltered portion landward of Punta Cane). As suggested by Mariotti and Fagherazzi (2010), the scarp formation is a consequence of the lowering of the tidal flat, which increases the height of the incoming waves reaching the marsh edge and is responsible of an increase in marsh regression by wave impact and bank failures (Francalanci et al., 2013), thus accelerating erosion.

3.2.7 Conclusions

In this study we provide the first accretion model of the latest Holocene succession of the southern Venice Lagoon (transect through Valle Millecampi – Punta Cane – Fondo dei Sette Morti). Our study succession testifies an evolution from a palustrine freshwater environment to a lagoonal environment over the last ~2'000 years. The depositional history started with accumulation of peat deposits in a deltaic setting which progressively evolved into a salt-marsh environment in the 14th century. The aggradation of the salt-marsh system has been stemmed out from both mud settling and organic accumulation, and occurred in parallel with the decrease in the salt-marsh extent and the tidal-flat expansion. Indeed, where salt-marsh deposits where locally flooded and impacted by wind waves, wave erosion played a fundamental role, and a lag deposit developed. As a consequence of the progressive water deepening, organic-rich mud accumulated above the lag, originating tidal-flat deposits.

This study highlights also that the disappearance of salt marshes in this area of the Venice Lagoon has to be ascribed to the lateral erosion of their margins rather than to a progressive decrease in marsh elevations referred to MSL and the

following marsh drowning. Our observational evidence support the Mariotti and Fagherazzi (2013) conceptual model based on the positive feedback between tidal flat deepening and expansion and salt marsh retreat.

Acknowledgements

This work was supported by the CARIPARO Project titled "Reading signatures of the past to predict the future: 1000 years of stratigraphic record as a key for the future of the Venice Lagoon", that is gratefully acknowledged.

CHAPTER 4

DYNAMICS OF SALT-MARSH LANDSCAPES UNDER HIGH SEDIMENT DELIVERY RATES: THE CASE OF THE SOUTHERN VENICE LAGOON

4.1 OVERVIEW

This chapter is a journal paper in preparation and it deals with the dynamic response of a salt-marsh system to changes in sediment availability from a fluvial source. The sedimentary succession of the Punta Cane salt marsh (southern Venice Lagoon) was investigated through detailed sedimentological and elemental analyses, together with the determination of the organic content and inorganic grain size along the cores. The results were therefore wedged with the chronological model proposed in Chapter 3, in order to detect the signatures of the diversions of the Brenta River in/from the Lagoon.

4.2 INTRODUCTION

Tidal landforms are currently threatened by natural climate changes and increasing human interferences, and are possibly subjected to potentially irreversible transformations with far-reaching ecological, social and economic implications worldwide (e.g., Costanza et al., 1997; Day et al., 2008; Barbier et al., 2011). To address issues of conservation of tidal landforms, exposed to the effects of climate changes and often to increasing human pressure, it is therefore of critical importance to improve current understanding of the processes controlling the response of these landforms to changes in the environmental forcings. This issue is deemed of both intellectual as well as practical interest.

Tidal landscapes are shaped by physical and biological processes which act over overlapping spatial and temporal scales, thus making the analysis of their response to changes in the forcing a challenging task. Numerical modeling is an effective tool to not only improve our theoretical understanding but also for practical environmental management issues of tidal landscape evolution. A number of models of morphodynamic evolution have been developed (e.g., Allen, 2000; Fagherazzi et al., 2012), which potentially offer a valuable tool to predict the fate of tidal landforms: this is particularly interesting at sites which have been exposed for centuries to natural climatic changes and severe human interventions. However, the capability of existing models to provide a comprehensive and predictive theory of tidal-landscape morphodynamic evolution seems to be challenged by the incomplete understanding of the many linkages between the relevant ecological and geomorphological processes (e.g., Murray et al. 2008; Reinhardt et al., 2010). Moreover, in many cases, morphodynamic models resort to the common approximation of a landscape in equilibrium with current forcings and address predictions on future scenarios using the present observed morphologies as an initial conditions (e.g., Allen, 1990; Kirwan et al., 2010).

Tidal environments are known to be highly dynamic systems in which salt marshes, tidal flats, subtidal platforms and channel network represent a complex intertwined system. Among the three unchanneled tidal sub-environments, salt marshes represent a crucially important ecosystem due to their unique position in the tidal frame (e.g., Mitsch and Gosselink, 2000; Chmura et al., 2003; Costanza et al., 2008; MacKenzie and Dionne, 2008; Davy et al., 2009; Gedan et al., 2009; Morgan et al., 2009; Perillo et al., 2009; Silliman et al., 2009; Barbier et al., 2011; Gedan et al., 2011; Mcleod et al., 2011; Francalanci et al., 2013; Temmerman et al., 2013; Möller et al., 2014). Effects of natural changes and human interferences on these ecosystems are the responsible of possibly irreversible transformations, which are manifested in a significant decrease in marsh extent worldwide, especially during the last century (e.g., Day et al., 2000; Marani et al., 2003, 2007;

Carniello et al., 2009; Gedan et al., 2009; Mcleod et al., 2011). The rising sea level and the lack of available sediments are suggested to be the key factors which determine the drowning and disappearance of salt marshes worldwide (Day et al., 2000; Morris et al., 2002; Reed, 2002; Marani et al., 2007; Gedan et al., 2009; Kirwan et al., 2010; D'Alpaos et al., 2011; Mudd, 2011; D'Alpaos and Marani, 2015).

Salt marsh growth, development and maintenance occur through the accretion rates provided by both inorganic and organic components, which interact with each other and with the rate of sea level (e.g., Morris et al., 2002; D'Alpaos et al., 2007; Marani et al., 2007; Li and Yang, 2009; Mudd et al., 2009; Marani et al., 2010; Mudd et al., 2010; D'Alpaos 2011; D'Alpaos et al., 2011; Da Lio et al., 2013; Marani et al., 2013). Marsh vertical growth within the tidal frame is a function of the rates of inorganic and organic sedimentation, of the rate of sea-level, and of the rate of sediment autocompaction (Allen, 1990; Bartholdy, 2012). While inorganic and organic fractions and autocompaction terms are marsh-elevation dependent (e.g., Allen, 2000; Mudd et al., 2009), only the relative sea-level term is independent (Allen, 1990). As a consequence, measurements of sea-level movements from salt-marsh accretion rates could be not authentic and they could be characterized by a lag effect in which measured accretion rates either over-estimate or under-estimate the rate of sea-level changes (Allen, 1990). It has recently been observed, through mathematical modelling, that marsh morphology, and its effect on biological productivity and vertical accretion, could lag century-scale sea-level rise rate oscillations by several decades (Kirwan and Murray, 2005, 2008). As a consequence, salt marshes might not have been in equilibrium with the Holocene sea level and they might currently be out of equilibrium with modern rates of sea level rise, reflecting environmental conditions of the past (Kirwan and Murray, 2008). Kirwan and Temmerman (2009), on the basis of a point model, observed that marsh elevations adjust to a step change in the rate of sea-level rise in about 100 years (although this needs to depend also on sediment availability), but in the case of a continuous acceleration in the rate of sea-level rise, modeled

accretion rates lag behind sea-level rise rates by about 20 years, and never obtain equilibrium. However, changing rates of sea-level rise may not be the dominant factor determining the evolution/degradation of some marshes (Kirwan and Temmerman, 2009; Kirwan et al., 2011). D'Alpaos et al. (2011) showed, on the basis of an analytical point model, that the time-lag characterizing the response of marshes to perturbations in the environmental forcings depends not only on RSL oscillations but also on sediment availability and tidal range. Moreover, marshes are more resilient to a decrease rather than an increase both in the rate of RSLR and in the sediment availability. As a consequence, a lag has also to be expected between changes in sediment availability and new equilibrium conditions, in analogy to the case of changes in the rate of RSLR. Kirwan et al. (2011) document an example of rapid salt marsh expansion during the 18th and 19th centuries due to increased rates of sediment delivery following deforestation associated with European settlement in the Plum Island Estuary (Massachusetts, US). The authors also suggest that current marsh degradation in the North America coast may represent a slow return to pre-settlement marsh extent with a natural state.

The Venice Lagoon, as observed in other lagoons and tidal environments worldwide, is currently threated by a severe decrease in salt-marsh area, together with a general expansion and deepening of tidal flats and subtidal platforms. Salt-marsh areas decreased from about 255 km^2 in 1611 to about 180 km^2 in 1810. The decrease peaked in the last century when the marsh areas decreased to about 50 km^2 in 2002, with a reduction of more than 70% compared to marsh extent in 1810 (Marani et al., 2003, 2007; Carniello et al., 2009; D'Alpaos, 2010a). Moreover, marshes might not have yet fully responded also to historical decrease in sediment supply and further adjustments in the form of decreasing marsh-platform elevation could be expected (D'Alpaos et al., 2011).

In the Venice Lagoon, the most severe changes in terms of sediment supply, together with large amounts of freshwater inputs, occurred in the last millennium due essentially to the diversion, carried out by the "Serenissima" (as the Republic

of Venice used to call itself), of the main rivers which used to debouch into the lagoon. These measures were undertaken to avoid the infilling of the Lagoon with sediments. An outstanding number of sedimentological and modelling investigations has been carried out in the Venice Lagoon aiming at defining the stratigraphy of the Holocene sedimentary succession (e.g., Madricardo et al., 2007; Tosi et al., 2007a, 2007b; Brancolini et al., 2008; Zecchin et al., 2008; Tosi et al., 2009a; Zecchin et al., 2009, 2011; Madricardo and Donnici, 2014; Zecchin et al., 2014) and the morphodynamic changes of the modern lagoonal environment (e.g., Marani et al., 2007; Carniello et al., 2009; Amos et al., 2010). However, the higher sedimentological resolution focused mainly on environmental changes occurred at the millennium scale (e.g., McClennen and Housley, 2006; Madricardo et al., 2007; Tosi et al., 2007a, 2007b; Brancolini et al., 2008; Zecchin et al., 2008, 2009, 2011; Madricardo and Donnici, 2014), leaving a major gap regarding the past 1,000 years, which were characterized by the highest human interventions on the lagoonal system. The knowledge of the response of tidal environments to changes in the forcings at centennial – decadal scale is therefore an important and critical issue for the determination of a detailed evolution of these systems.

In this work we focus on the response of a salt-marsh system in the Venice Lagoon, located in an area deeply involved in sediment supply and freshwater input changes during the last millennium because of the repeated diversion of the Brenta River system into the lagoon. The goal of this study is twofold: i) to detect the signature of the Brenta River in the Punta Cane salt-marsh sedimentological succession through a multidisciplinary approach based on the integration between sedimentological, stratigraphical, geochronological, and elemental data; ii) to verify through field measurements and analyses the existence of a time-lag between the flowing of the Brenta River into the lagoon and the morphodynamic response of the Punta Cane salt-marsh system.

4.3 GEOLOGICAL AND GEOMORPHOLOGICAL SETTING

4.3.1 The southern Venice Lagoon

The Venice lagoon is an elongated and arched waterbody located in the northwestern Adriatic Sea (Fig. 4.1A). It is the largest lagoon in the Mediterranean with an area of about 550 km^2, a mean water depth of 1.5 m, and a semi-diurnal micro-tidal regime (maximum water excursion at the inlets of ± 70 cm around MSL). The three inlets of Lido, Malamocco and Chioggia permit the exchange of water and sediments with the Adriatic Sea.

The Venice Lagoon originated by flooding of the upper Adriatic plain due to rising sea levels that followed the Last Glacial Maximum, and formed over the last 7'000 – 6'000 years. The formation of the Venice Lagoon occurred diachronically, starting from the south, where the oldest sediments are dated at about 7'000 years ago. In the central part of the lagoon, sedimentation started around 6'000 years ago (Favero and Serandrei Barbero, 1978, 1980).

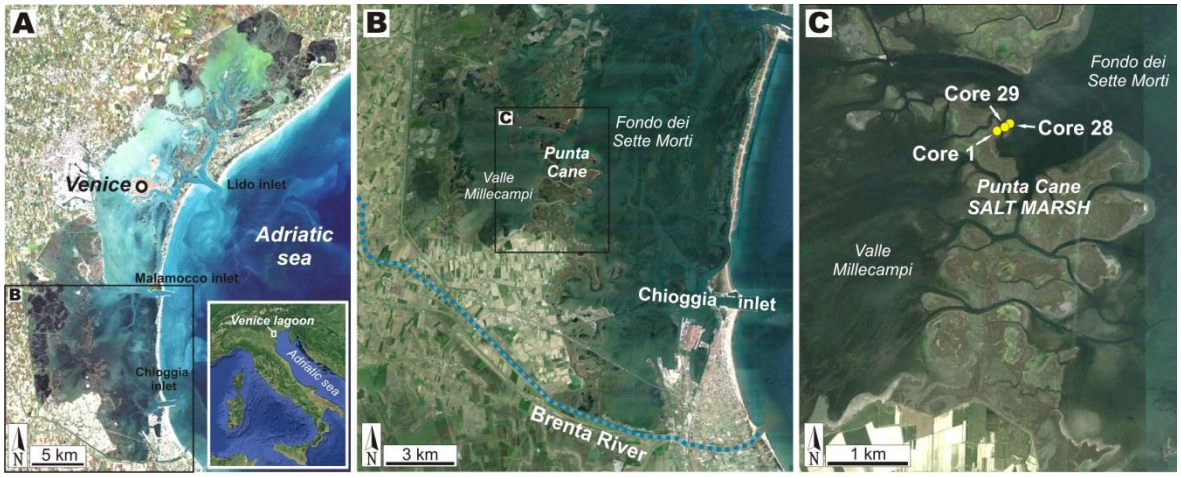

Fig. 4.1. (A) Location of the study site in the southern Venice Lagoon. (B) Punta Cane salt marsh area and current path of the Brenta River. (C) Location of the three sediment cores, object of this study, in the Punta Cane area.

The southern portion of the Venice Lagoon contains a ~20 m thick Holocene sedimentary succession (Tosi et al., 2007a, 2007b; Brancolini et al., 2008; Zecchin et al., 2008, 2009) which overlays Pleistocene continental deposits accumulated

during the Last Glacial Maximum (LGM). The Holocene succession is composed of three main seismic units, separated by key stratal surfaces (Zecchin et al., 2009). The surface topping the LGM deposits is an unconformity surface generated by fluvial incision. Accordingly, the Holocene sedimentary succession is made of three main units. The first unit consists of incised valley fills passing upward into lagoonal deposits which are abruptly overlain by shoreline deposits, associated with the maximum marine ingression occurred at around 6'000 years BP. During this ingression, the shoreline shifted from 4 km (Fondo dei Sette Morti area) to up to 15 km (Adige River area) landward (Favero and Serandrei Barbero, 1980). The second Holocene unit represents the regressive phase started after the maximum marine ingression. It consists of delta plain, swamps and marshes deposits landward, and prodelta, shoreface and beach ridge deposits seaward. At this stage, sediment supply from the mainland caused the seaward shift of the shoreline, which reached the current position around 2'500 years BP (Favero and Serandrei Barbero, 1980). The irregular surface which marks the passage from the second to the third Holocene unit is younger than 2'000 years and corresponds to the base of the recent lagoonal deposits. It represents the erosive base of channelized deposits and, outside of the channels, to a surfaces which marks an abrupt change in the depositional style. The uppermost Holocene unit is, in fact, associated to the deposition of tidal-channel, tidal-flat, subtidal-platform deposits that follow the generalized drowning of the southern part of the Venice area, and a parallel remarkable change in the hydrodynamics, primarily due to human interventions (Zecchin et al., 2009)

4.3.2 The Brenta River

The Late Pleistocene – Holocene evolution of the southern part of the Venice Lagoon (Fig. 4.1B) is strongly influenced by the sediment and water supply from the Brenta River, especially during the Latest Holocene, when the river was

repeatedly diverted in/from this area. The Brenta River is one of the major watercourses draining the Dolomites (Southern Alps). It has origin from Caldonazzo lake (south-eastern part of Trentino-Alto Adige region) and flows into the Adriatic sea, northern of the Po River, at Brondolo mouth, although a minor small reach (the Naviglio Brenta) is still active and flows towards the central part of the Venice Lagoon at Fusina mouth. The Brenta River has a length of 174 km and a drainage basin of 1567 km^2. Its mean annual discharge is about 71 $m^3\ s^{-1}$, while the flood peak discharge is 2400 $m^3\ s^{-1}$ (Surian et al., 2009). As for the hydrological characteristics of its watershed, the mean annual precipitation is 1313 mm and runoff at the basin outlet is 105%. This high value of runoff is due to the contribution of karst springs, which are located in the lower part of the drainage basin (Surian and Cisotto, 2007). The course of the Brenta River can be divided into two reaches: an upper reach, 70 km long, where the river flows within the mountain area, and a lower reach, 104 km long, where it flows in the Venetian Plain. In the mountain area, the Brenta River collects water from the Cismon creek, which is its main tributary. These two watercourses drain two catchment basins of about 650 km^2 each. Along more than half of its course, from the source up to the Upper Venetian Plain, the Brenta River channel bed is composed of coarse material, whereas sand and silt are found in the lowest reach. Different types of rock crop out in the drainage basin: in the upper part of the basin, gneiss, phyllite, granite and volcanic rocks (andesite, rhyolite, etc.) and subordinate limestone and dolomite are found, whereas limestone and dolomite are predominant in the lower part (Surian and Cisotto, 2007).

The current lower course of the Brenta River (from the Padova area to the mouth) has been strongly modified by anthropic interventions, being the result of a series of diversions and hydraulic arrangements carried out over the last millennium. During 16^{th} and 17^{th} centuries, the Republic of Venice carried out repeated diversions of watercourses draining into the Venice Lagoon. River-fed deposits settled into the lagoon causing shallowing of ship canals and,

consequently, a status of economic and environmental crisis, that forced the Republic of Venice to start a massive program of artificial river diversions which brought to strong changes in the paths of several rivers, such as the Brenta, Po, Bacchiglione, Adige, Sile, Piave and Livenza (Bondesan and Furlanetto, 2012).

Historical sources (e.g., Mozzi et al., 2004; Primon and Furlanetto, 2004; D'Alpaos, 2010a; Bondesan and Furlanetto, 2012) suggest 1143 AD as the moment in which the Brenta River was diverted along the current riverbed of the Naviglio Brenta, with two probable mouths: the first one at Fusina (the current mouth of the Naviglio Brenta), and the second one around Santa Marta, where currently the industrial area of Porto Marghera is located (Fig. 4.2A). In 1457 AD the Venetians diverted southward the downstream reach of the Brenta riverbed in the artificial "Diversivo di San Bruson" channel (Fig. 4.2A). With the aim of moving away the River from Venice city, in 1507 AD a new canal was excavated. In the area of Conche, the Brenta River was joined with the Bacchiglione River, and the two rivers flowed in the southern portion of the lagoon flowing through the "Montalbano channel" (Fig. 4.2B). In 1540 AD the outlet of the Brenta-Bacchiglione system was moved directly in the Adriatic sea in the Brondolo area. In this frame, the two riverbeds were divided in the area of Conche, and connected again downstream, about 5 km before the Brondolo mouth (Fig. 4.2C). To ensure a better drainage, the Brenta River was shifted in 1610 AD in the "Taglio Nuovissimo", in which the river flowed along the boundary between the mainland and the lagoon (the so-called "Argine di conterminazione lagunare"), which represents the Venice Lagoon boundary lines defined by the Republic of Venice (Fig. 4.2D). The Brenta River maintained the last configuration until 1840 AD when, to increase the slope of the river by the shortening of the riverbed, its outlet was shifted again toward the area Conche. From 1858 AD to 1896 AD, the Brenta River, divided from the Bacchiglione River, flowed in the "Cunetta del Brenta". It is worth noting that in these 38 years the Brenta River provided a widespread sediment accumulation in its delta. The further reclamation of the delta led to the construction of an area of

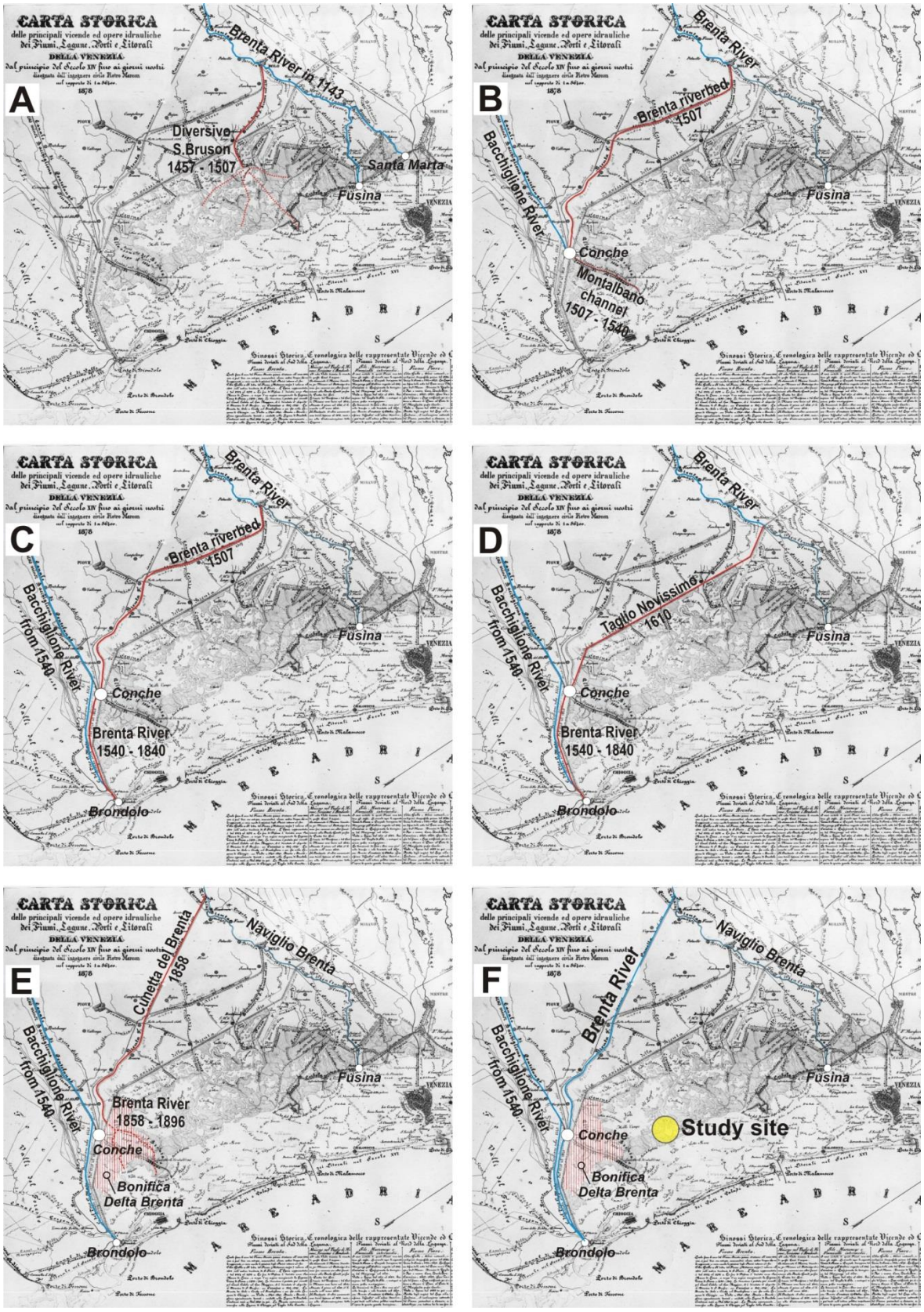

Fig. 4.2. Evolution of the Brenta River over the last millennium. (A) Brenta River in 1143 AD with the two mouths at Santa Marta and Fusina; Brenta River diversion from 1457 to 1507 AD. (B) Diversion of the river in 1507 AD. The Brenta and Bacchiglione flowed together in the southern portion of the Venice Lagoon. (C) Outlet of the Brenta-Bacchiglione system at the

Brondolo mouth from 1540 to 1840 AD. (D) Diversion of the Brenta River in 1610 AD. (E) Outlet of the Brenta River in the southern part of the Venice Lagoon from 1858 to 1896 AD. (F) Current configuration (after D'Alpaos, 2010a, modified).

27 km^2 which is nowadays part of the mainland (the so-called "Bonifica Delta Brenta") (Fig. 4.2E). At the end of the 19th century, the outlet of the Brenta River was definitively again moved to the Brondolo mouth, in which the Brenta-Bacchiglione system currently flows into the Adriatic sea. The "Naviglio Brenta", which represents one of the two small reaches of the first configuration of the Brenta River, is active and flows into the lagoon southern of Venice city (Fig. 4.2F) at the Fusina mouth (e.g., D'Alpaos 2010a, 2010b).

4.3.3 The study site

The study site is located in the southern part of the Venice Lagoon, in the Punta Cane area (Figs. 4.1B, 4.1C). A recent stratigraphical and geochronological study on a sedimentary succession in the southern part of the Venice Lagoon (Chapter 3 on this thesis) was performed by collecting 25 sediment cores distributed along a linear transect 5.2 km long cutting through subtidal-platform, tidal-flats and salt-marsh deposits and involving Valle Millecampi, Punta Cane and Fondo dei Sette Morti areas. (Fig. 4.3A). For the Punta Cane zone, that study highlighted the presence of a sedimentary succession of about 3.50 m in thickness accumulated over the past two millennia (Figs. 4.3A, 4.3B). This succession consists of a basal peaty body accumulated in a palustrine environment, which was already active during the 1st century BC. Palustrine sedimentation persisted until about the 14th century allowing the accumulation of about 2 m of peat. Around 1355^{+40}_{-45} cal AD the palustrine environment changed into a salt marsh suggesting the establishment of brackish water conditions and an increase in muddy sediment supply. Salt-marsh deposition persisted until the present day bringing to an accumulation of ~1.80 m of sediment in about 650 years. Detailed

radiocarbon and radionuclides (^{210}Pb and ^{137}Cs) datings on the salt-marsh succession (Fig. 4.3B) show a non-constant accumulation rate over time, with values ranging from 0.09 cm/year to up to 1.18 cm/year.

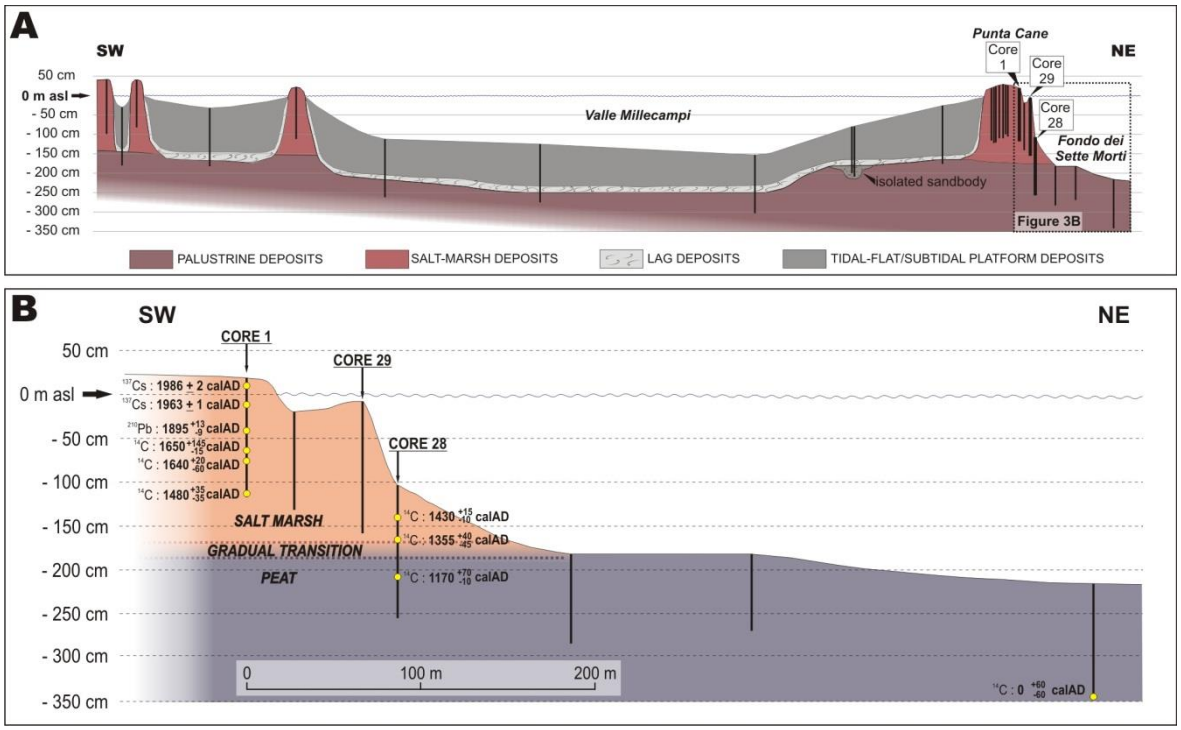

Fig. 4.3. (A) Sedimentological and stratigraphical interpretation of Valle Millecampi, Punta Cane, Fondo dei Sette Morti areas. Cores 1, 29, 28 represent the three sediment cores involved in the present study. (B) Geochronological data in the Punta Cane area. Each calibrated age is expressed as the mode value in the distribution and the two errors represent the ages interval at 68% of probability.

4.4 MATERIALS AND METHODS

To analyze the response of the salt-marsh system to changes in the sediment load provided by inputs of the Brenta River over the last ~1'000 years, we performed a series of analyses on three cores (1, 29, 28 in Figs. 4.3A, 4.3B). To detect changes along the succession, high resolution sedimentological analysis, determination of the organic matter content, detection of the inorganic fraction grain size and elemental variations were analyzed.

4.4.1 Sedimentological analysis

A high-resolution sedimentological analysis was carried out on the three study cores following the principles of modern facies analysis. This analysis aimed at defining the sedimentary distinctive features of different types of deposits and to link them with corresponding depositional environments. Deposits were differentiated on the basis of their color, grain size, texture, and sedimentary structures. Macroscopic biogenic content, mainly consisting of shells, plant debris and *in situ* vegetal remains, was also noted.

4.4.2 Determination of the organic fraction

The analysis of the organic matter content was performed on cores 1 and 29 by Loss On Ignition (LOI) at 375°C for 16 hours, on a total number of 62 samples belonging to core 1 (36 samples) and core 29 (26 samples), collected every 3 cm from the top of the cores. A total amount of 1.20 ± 0.20 g of dry sediment for each sample, dried at 60°C for 36 hours, was used to perform LOI analyses. The sediment was crumbled in a ceramic mortar and placed in a dry ceramic crucible. The LOI process started with a temperature increase of 5°C/min until reaching 375°C, and continued at a constant temperature for 16 hours (Ball, 1964; Frangipane et al., 2009; Protocol of SFU Soil Science Lab, 2011). The difference in weight, before and after the burning process, was used to estimate the amount of organic matter which was combusted. The organic content will be expressed as a percentage of the organic matter.

4.4.3 Particle size analysis

The particle size analysis was performed on the residual inorganic sediment fraction obtained after a chemical treatment with hydrogen peroxide (H_2O_2), according to Gray et al. (2010), to remove the organic component. As for the

determination of the organic matter, a total number of 62 samples, corresponding to the same stratigraphic layers used for LOI analyses (cores 1 and 29), were analyzed. Each sample, characterized by a dry weight of about 6 g, dried at 60°C for 36 hours, was treated with 35% H_2O_2 for 36 hours. At the end of the oxidation, when no visible frothing occurred, dilution with deionized water, decantation (for 24 hours), siphoning, and drying were carried out. Deionized water was added to each sample to obtain a dispersed particulate sample. The particle size analysis was carried out using a Mastersizer 2000 (Version 5.40, MALVERN INSTRUMENTS). The Mastersizer 2000 uses laser diffraction to measure the size of particles, by measuring the intensity of light scattered as a laser beam passes through the dispersed particulate sample. These data are then analyzed to calculate the size of the particles that created the scattering pattern. The grain size results will be presented as D_{50} distribution.

4.4.4 X-Ray Fluorescence

X-Ray Fluorescence (XRF) is a rapid and non-destructive analytical technique for the determination of the chemical composition in a material. Our XRF analysis was carried out on core 1 at ETH Zurich using an AVAATECH XRF core scanner, which is an energy dispersive XRF. The elemental range determined with the AVAATECH XRF core scanner starts from Aluminum (atomic number 13) to Uranium (atomic number 92) in concentrations from 100% down to ppm levels. In general, elements with higher atomic numbers have lower detection limits than lighter elements. Elements with a smaller atomic number are not traceable given that the X-ray radiation of the lighter elements is easily absorbed and therewith not able to enter the detector. The response depth of elements for incoming X-rays depends on the wavelength of emitted X-rays, the rank in the period system and the chemical composition of the sample matrix increases with increasing atomic number, as for example Al: 0.05 mm; Ca: 0.5 mm; Fe: 1 mm; Ba:

2-4 mm for average marine sediments (Jenkins and De Vries, 1970; Richter et al., 2006).

The XRF core scanner at ETH Zurich is equipped with a variable masking slit system that prevents detection of radiation from beyond the analytical area, resulting in resolution between 10 and 0.1 mm down-core and 15 to 2 mm cross-core. The optical system with the slit system has contact with the sediment surface during measurements and is flushed with Helium for a proper detection of the lighter elements. The sample, whose surface has to be smoothed as much as possible, is covered with a 4 μm thin foil "Ultralene" to prevent drying out of the sediment, the diversion of sediments and to protect the sample against dirt. The source of the radiation is an Oxford 100 Watt water-cooled X-ray tube with a 125 μm Beryllium window. The digital Canberra X-ray detector with Beryllium window contains a 1.5 mm thick Si-crystal for a better detection of elements > As. The measurement time depends strongly on the down-core resolution and the measuring time per sample. For instance, a sediment core with a length of 1 m measured in standard setting with the down-core resolution of 1 mm for all elements takes a time of 24 hours.

The XRF measurements were carried out on core 1 at 10, 30, 50 kV and at a resolution of 2 and 10 mm down-core. A digital Jai CV L105 3 CCD Color Line Scan Camera records images with a resolution of 140 ppcm (350 dpi, 70 μm).

4.5 RESULTS

4.5.1 Sedimentological analysis

The sedimentary succession is documented by a composite core obtained from the physical correlation between cores 1, 29 and 28 (Fig. 4.4). The composite core is 2.76 m thick, and its top and base are located 19 cm and 257 cm above and below the MSL, respectively. The sedimentary succession starts with 70 cm of

massive peat with abundant fragments of reeds. The peat consists of comminuted plant debris with a minimum amount of dispersed mud and very fine sand. This deposit formed in a palustrine environment in which vegetal remains were transported as debris or produced *in situ*.

The palustrine peat grades upward into salt-marsh deposits. This transition occurs within ~20 cm and is characterized by a gradual decrease in the reed-fragment content and an increase in the mud settling. Finer reeds fragments and plant debris are still present in the lowermost part of the salt-marsh deposit. The salt-marsh deposit is about 1.85 m thick and consists of a horizontally-laminated, bioturbated, brownish mud, with a variable amount of fine to very fine sand. Dark brown mud layers are common and are very rich in plant debris and roots. The latter are common in the uppermost part of the core. Light grayish very fine mud intervals are less common. They are about 15 cm thick and commonly contain scarce vegetal remains (e.g., intervals from 45 cm to 60 cm and from 95 cm to 110 cm down-core). Sand is mainly organized in millimetric, whitish, horizontal laminae which are characterized by a good grain size sorting.

The accumulation of salt-marsh deposits occurs in the highest portion of the intertidal range, where the organic matter produced by halophytic vegetation contributes to the marsh accretion together with the inorganic component. Mud settles down around high water slack, at the transition between flood and ebb tides, while the sandy laminae are generated during storm events during which waves can re-suspend sand and mud from the tidal flats and subtidal platforms in front of the marsh and deliver them onto the marsh platform. In addition, when wind-generated waves winnow the salt-marsh surface, they further suspend mud thus concentrating sand.

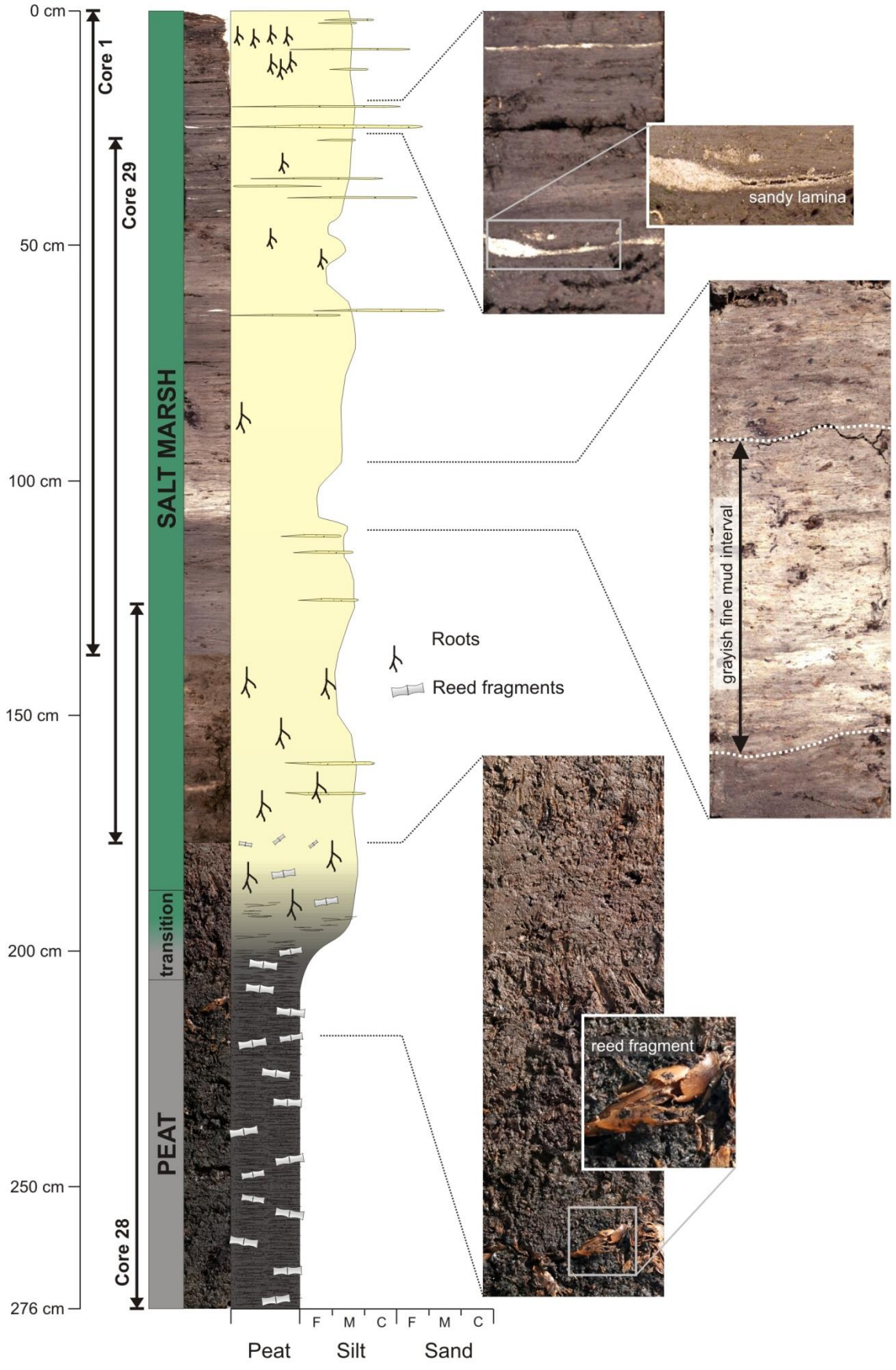

Fig. 4.4. Composite core obtained from the physical correlation between cores 1, 29, 28. Thickness, sedimentological log and main features of the deposits are shown.

4.5.2 The organic fraction

The organic matter content determined by LOI along the two studied cores (Fig. 4.5) shows a variable distribution between 8.5% and 36.1%; these percentages calculated for each sample as lost weight after burning at 375°C for 16 hours.

As to core 1 the analysis starts at 7 cm from the top of the core because the uppermost sedimentary succession was disturbed during the core recovering. As a whole, the organic content gradually decreases from the top of the core toward the bottom, with an average percentage of organic matter equal to 15.5%. More in detail, a first decreasing trend can be observed from the top up to 86÷90 cm below MSL, with value ranging between 19.9% (at 7 cm above MSL, maximum organic matter value along the core) and 8.5%, where the organic matter content reaches the minimum values. After this interval, the organic content increases again. A second marginally decreasing trend can be observed from a depth of 93 cm below MSL to the bottom of the core, with values ranging between 17.8% and 14.8%.

A different situation can be observed for the core 29 (Fig. 4.5). As a whole, the organic content tends to increase from the top of the core toward the bottom, with values ranging between 14.5% and 36.1% and an average percentage value of 20.1%. The first meter of the core shows organic values comparable with those of core 1 (minimum value: 14.5%; maximum value: 22.5%), with variable increasing/decreasing trends. At about 1.30 m below MSL the organic matter undergoes an important increase, with a percentage of organic content increasing from 19.5% to 36.1% at about 1.50 m in depth. The sample at the bottom of core 29 (1.58 m below MSL) shows instead a clear decrease, reaching a value of 26.3% of organic matter.

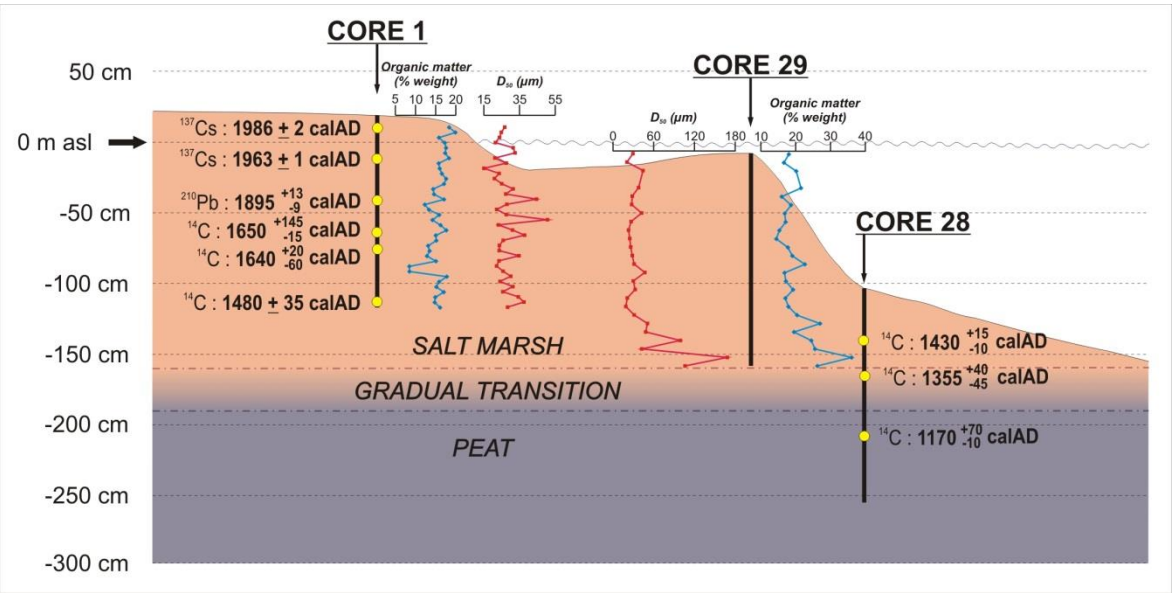

Fig. 4.5. Organic fraction content (blue lines) and D_{50} grain size (red lines) distributions for cores 1 and 29.

4.5.3 Particle size analysis

As to core 1, the grain size values for the inorganic sediment fraction range between 724 μm (maximum value) and 0.72 μm (minimum value). On average, the grain size shows a variable distribution between a medium sand (average coarser value: 360 μm) and a clay (average finer value: 0.72 μm). The median grain size D_{50} (Fig. 4.5) is in the range 15÷50 μm and shows an oscillating trend from the top of the core toward the bottom highlighting an alternation of finer and coarser interval.

As to core 29 the grain size values for the inorganic sediment fraction range between 2.19 mm (maximum value belonging to the field of granules) and 0.72 μm (minimum value). The median D_{50} distribution (Fig. 4.5) ranges between 19 μm and 168 μm. The distribution can be however divided in two intervals, determined on the base of an abrupt trend change found at about 1.30 m below MSL. The upper interval, from the top of the core to about 1.30 cm below MSL, does not show any significant change in grain size, with values ranging between 19 μm and 50 μm. The lower interval shows D_{50} distribution ranging from 43 μm and 168 μm

and highlights a clear decrease in grain size. The grain size results of the upper interval show clear affinity with those obtained for core 1. The Mastersizer, in fact, recorded a variable inorganic fraction distribution between medium sand (average coarser value: 431 μm) and clay (average finer value: 0.68 μm). On the contrary, for the lowermost interval of core 29, the values increase of more than one order of magnitude, with grain size values distributed between a very coarse sand (average coarser value: 1270 μm) and clay (average finer value: 0.84 μm).

4.5.4 X-ray Fluorescence

The results of XRF analysis are summarized in Fig. 4.6, where distribution of Si, Al, K, Fe along the core 1 was obtained at 10, 30, 50 kV and with a resolution of 10 mm down-core. Silica, aluminum, potassium and iron are typical elements in clay minerals, in feldspars and in zeolites (except for Fe), silica is the main element in quartz. Overall, the XRF trends oscillate. The signal appears to be disturbed in the first 10 cm from the top, probably due to the sediment re-working during sampling. Negative peaks which occurs, for example, at about 30 cm, 60 cm, 90cm and 120 cm in depth, can possibly be ascribed to the presence of small cracks generated by drying of the core. The XRF signal however highlights the presence of two intervals in which the concentration of the above-mentioned element reaches defined positive peaks. From the top of the core, the first peak is generated by a 10 cm thick layer that occurs between 45 cm and 55 cm down-core. The second interval (which again is about 10 cm thick) is more evident and occurs between 1.0 m and ~1.10 m down-core.

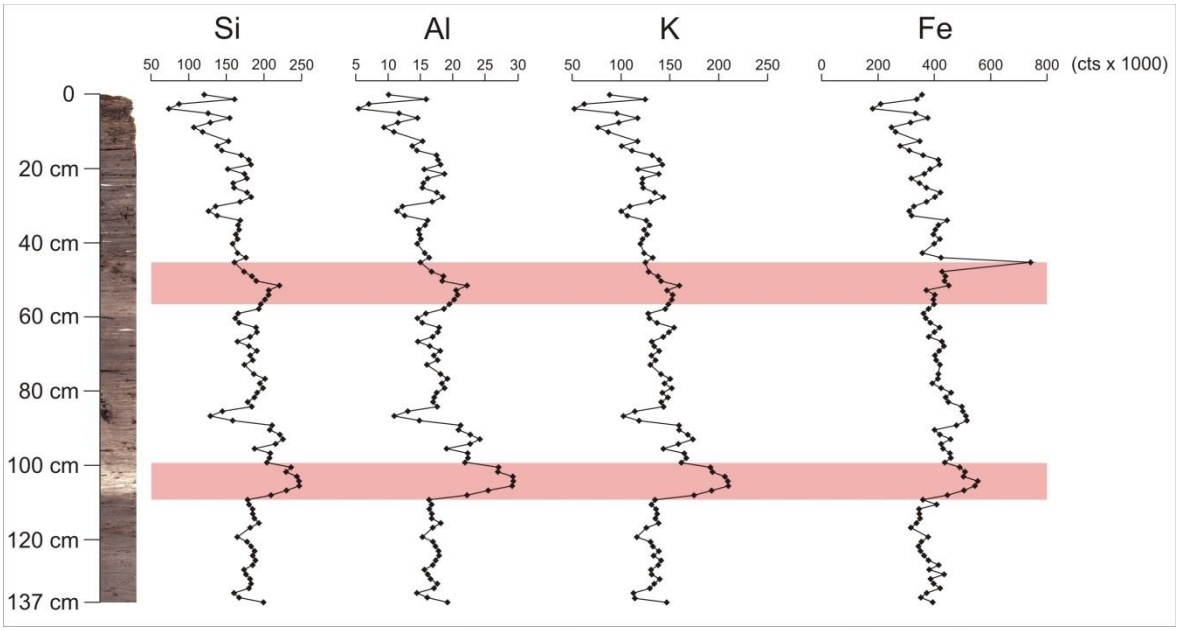

Fig. 4.6. XRF results for core 1. Silica, aluminum, potassium and iron trends along the core are reported. The two red stripes highlight the intervals in which the above-mentioned elements reach defined positive peaks.

4.6 DISCUSSION

Organic matter content and grain size analyses on cores 1 and 29 do not appear be, individually, useful indicators for determining the signature of a high sediment delivery in the Punta cane salt-marsh succession (Fig. 4.5).

The analysis of the organic content does not show significant changes along the two considered cores. However, the slightly decreasing trend in core 1 highlights the presence of a ~11 cm-thick interval (from -83 to -94 cm referred to MSL) in which the lowermost values occur. The interval corresponds to a grayish layer in the sedimentary core (Fig. 4.4) made of fine mud in which the organic material is very scattered. The organic-content analysis together with the sedimentary features of this interval support the hypothesis of a short-time change in the depositional features, in which the inorganic component largely prevails on the organic one. In core 29 instead, the oscillatory trend does not show any significant change until about 1.30 m below MSL, depth at which an important increase in the organic matter content occurs. This behavior is explained by the

fact that the lower part of core 29 is very close to the transition between the basal palustrine peat and the salt-marsh deposit which is marked by a decrease in the reed fragments, typical of the palustrine sediments, and by an increase in the inorganic fraction, fundamental component for marshes accretion. The high values in organic matter content for the lower 20 cm of core 29 represent therefore the influence of the underlying deposit, rather than an important increase in the salt-marsh organic deposition. No evidence of changes in fluvial sediment input are therefore observed.

As for the grain size of the inorganic fraction, the oscillatory trend of core 1 and the nearly vertical trend of core 29 up to the depth of about 1.40 m below MSL, do not show significant changes suggesting the presence of an important sediment supply possibly provided by the Brenta River debouching in the southern Venice Lagoon. The occurrence of small positive peaks in the grain size distribution of the inorganic fraction, corresponds to the presence of sandy laminae which, during storm events and high tide conditions, were accumulated on the salt-marsh surface by wind-generated waves. The remarkable increase at the bottom of core 29 should not be misinterpreted. Such an increase can indeed be ascribed to the presence of organic matter in the disperse particulate samples undergoing the grain size analysis (which was still visible with the unaided eye), rather than to a real increase in the size of the inorganic fraction. In fact, it is generally agreed that the H_2O_2 chemical treatment cannot totally remove the organic fraction in samples characterized by a high presence of organic matter (e.g., Mikutta et al., 2005), as in the case of the samples at hand. In this way, if the Mastersizer laser beam intercepts the organic grain along its commonly elongated shape, the scattering pattern records a grain size larger than the real one, thus providing a distorted estimate of the grain size distribution. This hypothesis is also confirmed by the results of the organic matter analysis, which highlight an increase in the organic component in the lowermost portion of core 29 because of its closeness to the underlying peaty deposits. The fact that there are no significant

visible intervals in which negative or positive peaks in organic content and size of the inorganic fraction, is quite a surprising result. No signatures of the sediment inputs provided by the Brenta River can be detected. However, one would expect the presence of a large sediment delivery provided by the Brenta River, when debouching into the lagoon, to be clearly reflected in the sedimentary succession. It is however worthwhile observing that the distance between the outlet of the river and the Punta Cane area (~5 km) is probably the main cause for the absence of the signatures we expected to find. We deem it can hardly be denied that the Brenta River flowing into the Venice Lagoon provided a large sediment supply. It is, in fact, well known, also from historical maps, that during its last diversion into the lagoon from 1858 to 1896 AD, the Brenta River led to an exceptional sediment accumulation around its debouching area. This area in fact has been reclaimed at the beginning of 20th century and is nowadays part of the mainland (the so-called "Bonifica Delta Brenta"). XRF results appear to be the most important proxy, or at least the clearest, for the determination of well-defined intervals which can represent the signature of the Brenta River system flowing into the Venice lagoon (Fig. 4.6). The occurrence of intervals with a high concentration of silica, aluminum, potassium and iron is consistent with the lito-types composition outcropping the Brenta River drainage basin, especially in its upper mountainous one.

However, the multidisciplinary approach provided results, in terms of organic content, grain size, XRF and sedimentological analysis, which wedged with the chronological model, provide an interesting output (Fig. 4.7). The red intervals in the figure represent the two XRF positive peaks. They correspond both to finer intervals in the sedimentary succession of core 1, only partially showed in the D_{50} trend, and to intervals in which the organic matter content in the salt-marsh succession is low (the lowermost XRF interval corresponds to the lowermost values in organic content in core 1). The chronological model shows a salt-marsh evolution during the last 650 years, and, consequently, the three Brenta

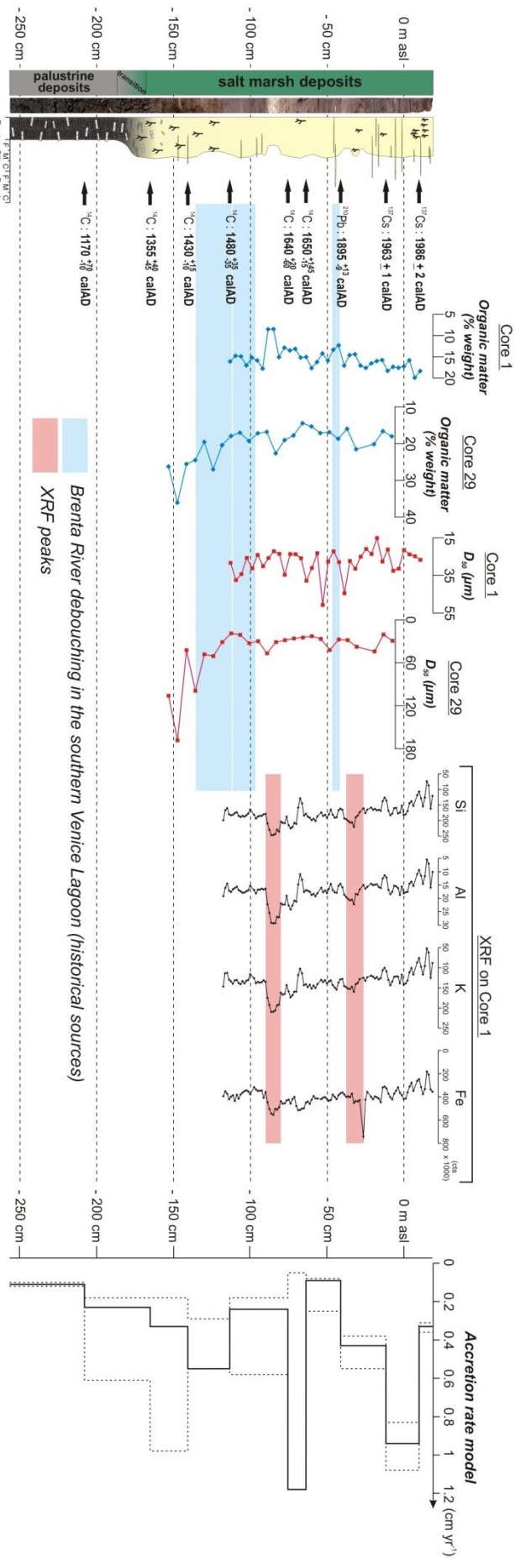

Fig. 4.7. Results of the multidisciplinary approach for the Punta Cane salt marsh succession.

River inputs into the lagoon should be recorded in the sedimentary succession. The first XRF interval, from about 80 cm to 90 cm above MSL, is located just before 1640^{+20}_{-60} cal AD, while the uppermost one, from about 25 to 35 cm, is just after 1895^{+13}_{-9} cal AD. It is clear that the red intervals, wedged with the chronological model, cannot represent the presence of the Brenta River system because of their younger ages in respect to the effective time-spans of the river flowing into the Lagoon. In fact, based on the chronological model, the blue intervals in Fig. 4.7 ideally represent the timing in which the Brenta River system flowed into the lagoon (1457 – 1507 AD; 1507 – 1540 AD; 1858 – 1896 AD; Figs. 4.2A, 4.2B, 4.2E). This multidisciplinary approach highlights the occurrence of a temporal lag between the presence of river water and sediment fluxes into the lagoon, and the evidence of their signature in the sedimentary succession. In this case, we interpret the temporal lag as the consequence of a temporary storage of the high sediment delivery provided by the River. These sediments are temporary stocked within the basin and only at later stages they are re-suspended by waves, redistributed by tidal currents and delivered onto the salt-marsh surface, where they can settle. The accumulation of the stocked sediments on the marsh surface, increases marsh elevation relative to MSL, and promotes a decreasing of organic matter production (provided by the halophytic plants which populate the marsh) which depends on marsh elevation within the tidal frame. This leads to a lower organic accumulation in the sedimentary succession.

In addition, the lack of signatures of large sediment input in the sedimentary record of the considered transect can be interpreted by considering that the main effect of the sediment pulse is to promote marsh horizontal progradation, rather than of increasing marsh elevation within the tidal frame. The Brenta River was reintroduced into the Lagoon for about 40 years (between 1858 and 1896 AD), during which it promoted the formation of 27 km^2 of marshes, now reclaimed. Previous modelling efforts (D'Alpaos et al., 2011) suggested the existence of a lag between the presence of a perturbation in the forcing (i.e., a high

sediment pulse), and the response of a salt-marsh system to the change in the forcing itself. Although our results seem to suggest the existence of a lag of this type, it is worth noting that the recalled modelling approach is based on a zero-dimensional approximation, i.e., that model considers one point as representative of the whole marsh platform. In this very case the space dependent dynamics of the considered system seems to be a relevant role in the relaxation time required for the system to reach new equilibrium conditions. The source of sediment input, in this case, is about 5 km apart from the Punta Cane marsh, and this might have an important effect.

In Fig. 4.7 is also interesting to note that during the flowing of the Brenta River into the Venice Lagoon, the accretion rates of Punta Cane salt marsh do not show significant high values. The highest accumulation rate values occur after the presence of the river.

4.7 CONCLUSIONS

We analyzed the possible response of a salt-marsh system in the southern Venice Lagoon to changes in sediment delivery rates provided by the Brenta River system. The repeated diversion of the river into the lagoon influenced the evolution of the Punta Cane salt marsh. In order to detect the signature of the presence of the Brenta River system in the sedimentary succession, sedimentological and elemental analyses were carried out, together with the determination of the organic content and grain size of the inorganic fraction along cores.

The results from our analyses suggest that a multidisciplinary approach is required in this case, any of the different analysis being sufficient alone to detect and interpret important changes in a sedimentary succession.

Sedimentological, elemental, organic content and grain size analyses, wedged with a chronological model of the Punta Cane salt marsh, show that the

marsh response to changes in sediment delivery rates is not instantaneous. A temporal lag exists between the presence of the Brenta River system into the lagoon and its identification in the salt-marsh succession. The signature of the river along the salt-marsh sequence appears with finer inorganic deposition, decreasing of organic matter accumulation and positive XRF peaks in elements which are consistent with the outcrops composition of the Brenta River drainage basin.

CHAPTER 5

CONCLUSIONS

In this work, a series of field and laboratory analyses allowed us to improve our knowledge of the biomorphodynamic evolution of salt-marsh systems. In particular, the work contributed to improve our understanding of both the evolution of salt-marsh bio-geomorphological patterns and the relative importance of physical and biological processes, and the response of salt-marsh systems to changing in the environmental forcings.

The high-resolution spatial analyses on modern sub-surface marsh sediments from the northern Venice Lagoon, unraveled the variations and the mutual feedbacks between the physical and biological processes at the marsh scale. The results emphasize that surface elevations, inorganic and organic sediment content, and grain size distribution along marsh transects are tightly related. In particular, higher elevations and coarser sediments are found along marsh edges, while the inner portion of the marsh, characterized by lower elevations, is reached only by finer sediments, suggesting that the tidal network which cuts through the tidal landscape largely controls inorganic sediment transport over the platform. In addition, the results highlight that the determination of soil organic matter and inorganic content is very sensitive to the specific analysis method (LOI, H_2O_2, H_2O_2 + NaClO), bearing important implications in determining the real values of the marsh soil organic content, the stocked organic carbon and the organic and inorganic accumulation rates. The position on the salt marsh and the distance from the channels strongly affect the rates of accumulation of the organic and inorganic components: accretion is mainly driven by the inorganic component in proximity of the channels, whereas the organic component becomes important in the inner part of the marsh.

Moreover, the accumulation of organic matter in the soil does not increase with biomass production, which is generally higher along the channel banks and lower in the inner part of the marsh. Organic matter accumulation in the soil is governed by the interplay of plant biomass productivity and decomposition. This interplay is, in turn, modulated by soil aeration, favoring decomposition, which is highest near the marsh edge and lowest in the low-lying inner zones, where the reduced decomposition rate compensates the lower biomass productivity. The analyses also provided the first estimates of soil organic carbon density and of the carbon accumulation rate (132 g C m^{-2} yr^{-1}) for marshes in the Venice Lagoon.

The multidisciplinary analyses carried out on the latest Holocene sedimentary succession in the Punta Cane area, in the southern Venice Lagoon, provided, first, new information on the evolution, at high spatial and temporal resolution, of the area over the last 2'000 years and, in addition, provided evidences of salt-marsh system dynamic response to changes in sediment supply during the last millennium.

For the first time in the case of the southern portion of the Venice Lagoon, a detailed geochronological model for the lagoonal deposits has been furnished. The study succession testifies an evolution from a palustrine freshwater environment to a lagoonal environment, in which the depositional history started with accumulation of peat deposits in a deltaic setting which progressively evolved into a salt-marsh environment in the 14th century. The evolution of the salt-marsh system is characterized by different accretion rates over time. Marsh aggradation, stemmed out from both mud settling and organic accumulation, occurred in parallel with the decrease in the salt-marsh extent and the tidal-flat expansion. Indeed, where salt-marsh deposits were locally flooded and impacted by wind-waves, wave erosion played a fundamental role, and a lag deposit developed. As a consequence of the progressive water deepening, organic-rich mud accumulated above the lag, originating tidal-flat deposits. The absence of salt-marsh deposits below the lag and the tidal-flat deposits, highlights that the disappearance of salt

marshes in this area of the Venice Lagoon has to be ascribed to the lateral erosion of their margins rather than to a progressive decrease in marsh elevations referred to MSL and the following marsh drowning.

Finally, the evidence of a possible response of a salt-marsh system to changes in sediment delivery rates provided by the repeated diversions of the Brenta River in the southern portion of the Venice Lagoon is provided. The results of a multidisciplinary approach based on sedimentological and elemental analyses on the salt-marsh succession, were wedged with the detailed age model previously presented for the area. The study reveals the existence of a temporal lag between the presence of the Brenta River into the Lagoon and its detection in salt-marsh deposits. The signature of the river along the marsh sequence appears with finer inorganic deposition, decreasing of organic matter accumulation and positive XRF peaks in elements which are consistent with the composition of the lito-types which crop out along the Brenta River drainage basin.

REFERENCES

Adam, P. (1990) *Saltmarsh Ecology*. Cambridge Univ Press, Cambridge, UK.

Allen, J.R.L. (1990) Constraints on measurements of sea-level movements from salt-marsh accretion rates. *J. Geol. Soc. London*, **147**, 5–7. doi:10.1144/gsjgs.147.1.0005.

Allen, J.R.L. (2000) Morphodynamic of Holocene salt marshes: a review sketch from the Atlantic and southern North Sea coasts of Europe. *Quat. Sci. Rev.*, **19**, 1155–1231.

Allen, J.R.L. and Thornley, D.M. (2004) Laser granulometry of Holocene estuarine silts: effects of hydrogen peroxide treatment. *The Holocene*, **14**, 290–295.

Amorosi, A., Fontana, A., Antonioli, F., Primon, S. and Bondesan, A. (2008) Post-LGM sedimentation and Holocene shoreline evolution in the NW Adriatic coastal area. *GeoActa*, **7**, 41–67.

Amos, C.L., Villatoro, M., Helsby, R., Thompson, C.E.L., Zaggia, L., Umgiesser, G., et al. (2010) The measurement of sand transport in two inlets of Venice lagoon, Italy. *Estuar., Coast., Shelf Sci.*, **87**(2), 225–236. doi:10.1016/j.ecss.2009.05.016.

Ball, D.F. (1964) Loss-on-ignition as an estimate of organic matter and organic carbon in non-calcareous soils. *J Soil Sci.*, **15**, 84–92.

Barbier, E.B., Hacker, S.D., Kennedy, C., Koch, E.W., Stier, A.C. and Silliman, B.R. (2011) The value of estuarine and coastal ecosystem services. *Ecol. Monogr.*, **81**(2), 169–193.

Barillé-Boyer, A-L., Barillé, L., Massé, H., Razet, D. and Héral, M. (2003) Correction for particulate organic matter as estimated by loss on ignition in estuarine ecosystems. *Estuar. Coast. Shelf Sci.*, **58**, 147–153. doi:10.1016/S0272-7714(03)00069-6.

Bartholy, J. (2012) Salt marsh sedimentation. In: Davis, R.A. and Dalrymple, R.W. (Eds.) *Principles of tidal sedimentology*, Springer, Berlin, 151–185.

Bellucci, L.G., Frignani, M., Cochran, J.K., Albertazzi, S., Zaggia, L., Cecconi, G., et al. (2007) ^{210}Pb and ^{137}Cs as chronometers for salt marsh accretion in the Venice Lagoon – links to flooding frequency and climate change. *J. Environ. Radioactiv.*, **97**, 85–102.

Boaga, J., D'Alpaos, A., Cassiani, G., Marani, M. and Putti, M. (2014) Plant-soil interactions in salt marsh environments: Experimental evidence from electrical resistivity tomography in the Venice Lagoon. *Geophys. Res. Lett.*, **41**, 6160–6166. doi:10.1002/2014GL060983.

Boesch, D.F. and Turner, R.E. (1984) Dependency of fishery species on salt marshes: the role of food and refuge. *Estuaries Coasts*, **7**, 460–468.

Bonardi, M., Tosi, L., Rizzetto, F., Brancolini, G. and Baradello, L. (2006) Effects of climate changes on the Late Pleistocene and Holocene sediments of the Venice Lagoon, Italy. *J. Coastal Res.*, **39**, 279–284.

Bondesan, A. and Furlanetto, P. (2012) Artificial fluvial diversions in the mainland of the Lagoon of Venice during the 16th and 17th centuries inferred by historical cartography analysis. *Géomorphol. Relief Process Environ.*, **2**, 175–200.

Brambati, A. (1988) Lagune e stagni costieri: due ambienti a confronto. In: Carrada, G.C., Cicogna, F. and Fresi, E. (Eds.) *Le lagune costiere: ricerca e gestione*. CLEM Pubbl., Massa Lubrense (Napoli), 9–33.

Brambati, A., Carbognin, L., Quaia, T., Teatini, P. and Tosi, L. (2003) The Lagoon of Venice: Geological setting, evolution and land subsidence. *Episodes*, **26**(3), 264–268.

Brancolini, G., Tosi, L., Caffau, M., Donda, F., Rizzetto, F. and Zecchin, M. (2008) Holocene evolution of the Venice Lagoon. In: *Proceedings of the 9th International Conference Littoral 2008*, November 25th–28th 2008, Venice, Italy, 1–7.

Brivio, P.A. and Zilioli, E. (1996) Assessing wetland changes in the Venice lagoon by means of satellite remote sensing data. *J. Coastal Conserv.*, **2**, 23–32.

Bromberg, K. and Silliman, B.R. (2009) Patterns of salt marsh loss within coastal regions of North America: pre-settlement to present. In: Silliman, B.R., Grosholz, T. and Bertness, M.D. (Eds.) *Human impacts on salt marshes: a global perspective*. University of California Press, Berkeley, California, USA, 253–266.

Bronck Ramsey, C. (2008) Deposition models for chronological records. *Quaternary Sci. Rev.*, **27**, 42–60.

Carbognin, L. (1992) Evoluzione naturale e antropica della Laguna di Venezia. *Mem. Descr. Carta Geol. D'Italia*, **42**, 123–134.

Carbognin, L. and Tosi, L. (2002) Interaction between climate changes, eustacy and land subsidence in the North Adriatic Region, Italy. *Mar. Ecol.*, **23**, 38–50.

Carbognin, L., Teatini, P. and Tosi, L. (2004) Eustacy and land subsidence in the Venice Lagoon at the beginning of the new millennium. *J. Marine Syst.*, **51**, 345–353. doi:10.1016/j.jmarsys.2004.05.021.

Carbognin, L., Teatini, P. and Tosi, L. (2005) Land subsidence in the Venetian area: known and recent aspects. *Giorn. Geol. Appl.*, **1**, 5–11. doi:10.1474/GGA.2005-01.0-01.0001.

Carniello, L., Defina, A. and D'Alpaos, L. (2009) Morphological evolution of the Venice lagoon: Evidence from the past and trend for the future. *J. Geophys. Res. – Earth Surface*, **114**, F04002. doi:10.1029/2008JF001157.

Carniello, L., D'Alpaos, A. and Defina, A. (2011) Modeling wind waves and tidal flows in shallow micro-tidal basins. *Estuar. Coast. Shelf Sci.*, **114**, F04002. doi:10.1016/j.ecss.2011.01.001.

Chapman, V.J. (1976) *Coastal vegetation*. 2nd ed., Pergamon Press, Oxford.

Chmura, G.L., Anisfed, S.C., Cahoon, D.R. and Lynch, J.C. (2003) Global carbon sequestration in tidal, saline wetland soils. *Global Biogeochem. Cy.*, **17**, 1111. doi:10.1029/2002GB001917.

Christiansen, T., Wiberg, P.L. and Milligan, T.G. (2000) Flow and sediment transport on a tidal salt marsh surface. *Estuar. Coast. Shelf Sci.*, **50**, 315–331. doi:10.1006/ecss.2000.0548.

Cola, S., Sanavia, L., Simonini, P. and Schrefler, B.A. (2008) Coupled thermohydromechanical analysis of venice lagoon salt marshes. *Water resour. Res.*, **44**, W00C05. doi:10.1029/2007WR006570.

Costanza, R., d'Arge, R., de Groot, R., Farber, S., Grasso, M., Hannon, B., et al. (1997) The value of the world's ecosystem services and natural capital. *Nature*, **387**, 253–260. doi:10.1038/387253a0.

Costanza, R., Pe´rez-Maqueo, O., Martinez, M.L., Sutton, P., Anderson, S.J. and Mulder, K. (2008) The value of coastal wetlands for hurricane protection. *Ambio*, **37**, 241–248.

Craft, C.B,, Seneca, E.D. and Broome, S.W. (1991) Loss on ignition and Kjeldahl digestion for estimating organic carbon and total nitrogen in estuarine marsh soils: Calibration with dry combustion. *Estuaries*, **14,** 175–179.

Cronk, J.K. and Fennessy, M.S. (2001) *Wetland Plants: Biology and Ecology*. CRC Press/Lewis Publishers, Boca Raton, FL, 440 pp.

D'Alpaos, A. (2011) The mutual influence of biotic and abiotic components on the long-term ecomorphodynamic evolution of salt-marsh ecosystems. *Geomorphology*, **126**, 269–278.

D'Alpaos, L. (2010a) *Fatti e misfatti di idraulica lagunare. La laguna di Venezia dalla diversione dei fiumi alle nuove opere alle bocche di porto*. Istituto Veneto di Scienze, Lettere ed Arti, Venezia, 329 pp.

D'Alpaos, L. (2010b) *L'evoluzione morfologica della Laguna di Venezia attraverso la lettura di alcune mappe storiche e delle sue carte idrografiche*. Europrint, Quinto di Treviso, 109 pp.

D'Alpaos, A. and Marani, M. (2015) Reading the signatures of biologic-geomorphic feedbacks in salt-marsh landscapes. *Adv. Water Resour.* doi:10.1016/j.advwatres.2015.09.004.

D'Alpaos, A., Lanzoni, S., Marani, M., Fagherazzi, S. and Rinaldo, A. (2005) Tidal network ontogeny: channel initiation and early development. *J. Geophys. Res. – Earth Surface*, **110**, F02001. doi:10.1029/2004JF000182.

D'Alpaos, A., Lanzoni, S., Marani, M. and Rinaldo, A. (2007) Landscape evolution in tidal embayments: Modeling the interplay of erosion, sedimentation, and vegetation dynamics. *J. Geophys. Res.*, **112**, F01008. doi:10.1029/2006JF000537.

D'Alpaos, A., Lanzoni, S., Rinaldo, A. and Marani, M. (2009) Intertidal eco-geomorphological dynamics and hydrodynamic circulation. In: Perillo, G.M.R., Wolanski, E., Cahoon, D.R. and Brinson, M.M. (Eds.) *Coastal Wetlands: An Integrated Ecosystem Approach*. Elsevier, Oxford, UK Burlington, 159–184.

D'Alpaos, A., Mudd, S.M. and Carniello, L. (2011) Dynamic response of marshes to perturbations in suspended sediment concentrations and rates of relative sea level rise. *J. Geophys. Res.*, **116**, F04020. doi:10.1029/2011JF002093.

D'Alpaos, A., Da Lio, C. and Marani, M. (2012) Biogeomorphology of tidal landforms: physical and biological processes shaping the tidal landscape. *Ecohydrology*, **5**, 550–562.

D'Alpaos, A., Carniello, L. and Rinaldo, A. (2013) Statistical mechanics of wind wave-induced erosion in shallow tidal basins: Inferences from the Venice Lagoon. *Geophys. Res. Lett.*, **40**, 3402–3407. doi:10.1002/grl.50666.

D'Odorico, P., Laio, F., Porporato, A., Ridolfi, L., Rinaldo, A. and Rodriguez-Iturbe, I. (2010). Ecohydrology of terrestrial ecosystems. *Bioscience*, **60**(11), 898–907. doi:10.1525/bio.2010.60.11.6.

Da Lio, C., D'Alpaos, A. and Marani, M. (2013) The secret gardener: vegetation and the emergence of biogeomorphic patterns in tidal environments. *Phil. Trans. R. Soc. A*, **371**, 20120367. doi:10.1098/rsta.2012.0367.

Dadey, K.A., Janecek, T. and Klaus, A. (1992) Dry-bulk density: its use and determination. In: Taylor, B., Fujioka, K., et al. (Eds.) *Proceeding of the Ocean Drilling Program, Scientific Results*. College Station, TX (Ocean Drilling Program), **126**, 551–554. doi:10.2973/odp.proc.sr.126.157.1992.

Dankers, N. and Laane, R. (1983) A comparison of wet oxidation and loss on ignition of organic material in suspended matter. *Environ. Technol. Lett.*, **4**, 283–290.

Davy, A., Figueroa, E. and Bakker, J. (2009) Human modification European salt marshes. In: Silliman, B.R., Grosholz, T. and Bertness, M.D. (Eds.) *Human impacts on salt marshes: a global perspective*. University of California Press, Los Angeles, CA, USA, 311–336.

Day, J.W., Rismondo, A., Scarton, F., Are, D. and Cecconi, G. (1998a) Relative sea level rise and Venice lagoon wetlands. *J. Coastal Conserv.*, **4**, 27–34.

Day, J.W., Scarton, F., Rismondo, A. and Are, D. (1998b) Rapid deterioration of a salt marsh in Venice lagoon, Italy. *J. Coastal Res.*, **14**(2), 583–590.

Day, J.W., Rybczyk, J., Scarton, F., Rismondo, A., Are, D. and Cecconi, G. (1999) Soil Accretionary Dynamics, Sea-level Rise and the Survival of Wetlands in Venice Lagoon: A Field and Modelling Approach. *Estuar. Coast. Shelf Sci.*, **49**, 607–628.

Day, J.W., Shaffer, G.P., Britsch, L.D., Reed, D.J., Hawes, S.R. and Cahoon, D. (2000) Pattern and process of land loss in the Mississippi Delta: A spatial and temporal analysis of wetland habitat change. *Estuaries*, **23**, 425–438.

Day, J.W., Christian, R.R., Boesch, D.M., Yáñez-Arancibia, A., Morris, J., Twilley, R.R., et al. (2008) Consequences of climate change on the ecomorphology of coastal wetlands. *Estuar. Coast.*, **31**, 477–491. doi:10.1007/s12237-008-9047-6.

Day, J.W., Cable, J.E., Cowan, J.H., Delaune, R.D., de Mutsert, K., Fry, B., et al. (2009) The Impact of Pulsed Reintroduction of River Water on a Mississippi Delta Coastal Basin. *J. Coastal Res.*, **54**, 225–243.

Delaune, R.D. and Pezeshki, S.R. (2003) The role of soil organic carbon in maintaining surface elevation in rapidly subsiding U.S. Gulf of Mexico coastal marshes. *Water Air Soil Poll.*, **3**, 167–179.

Dietrich, W.E. and Perron, J.T. (2006) The search for a topographic signature of life. *Nature*, **439**, 411–418. doi:10.1038/nature04452.

Donkin, M.J. (1991) Loss-on-ignition as an estimator of soil organic carbon in A-horizon forestry soils. *Commun. Soil Sci. Plan.*, **22**, 233–241.

Dorigo, W. (1983) *Venezia. Origini, ipotesi e ricerche sulla formazione della città*. Electa Fantoni Grafica di Venezia, Venezia, vol. 1–2–3.

Dorigo, W. (1994) *Venezie sepolte nella terra del Piave: Duemila anni fa fra il doce e il salso*. Viella, Roma, 440 pp.

Duarte, C.M., Middelburg, J.J. and Caraco, N. (2005) Major role of marine vegetation on the oceanic carbon cycle. *Biogeosciences*, **2**, 1–8.

Duarte, C.M., Losada, I.J., Hendriks, I.E., Mazarrasa, I. and Marbà, N. (2013) The role of coastal plant communities for climate change mitigation and adaption. *Nat. Clim. Change*, **3**, 961–968. doi:10.1038/nclimate1970.

Fagherazzi, S., Carniello, L., D'Alpaos, L. and Defina, A. (2006) Critical bifurcation of shallow microtidal landforms in tidal flats and salt marshes. *P. Natl. Acad. Sci. USA*, **103**(22), 8337-8341. doi:10.1073/pnas.0508379103.

Fagherazzi, S., Kirwan, M.L., Mudd, S.M., Guntenspergen, G.R., Temmerman, S., D'Alpaos, A., et al. (2012) Numerical models of salt marsh evolution: ecological, geomorphic, and climatic factors. *Rev. Geophys.*, **50**, RG1002. doi:10.1029/2011RG000359.

Favero, V. (1985) Evoluzione della laguna di Venezia ed effetti indotti da interventi antropici sulla rete fluviale circumlagunare. In: *Ministero dei LL. PP. – Magistrato delle Acque – Laguna, fiumi, lidi; cinque secoli di gestione delle acque nelle Venezie*. Atti del Convegno indetto dal Magistrato delle Acque, Venezia, 10-12 giugno 1983, 402–409.

Favero, V. and Serandrei Barbero, R. (1978) La sedimentazione olocenica nella piana costiera tra Brenta e Adige. *Atti 69° Congresso Soc. Geol. It.*, 67–75.

Favero, V. and Serandrei Barbero, R. (1980) Origine ed evoluzione della Laguna di Venezia – Bacino meridionale. *Lavori Soc. Ven. Sc. Nat.*, **5**, 49–71.

Favero, V., Parolini, R. and Scattolin M. (1988) *Morfologia storica della laguna di Venezia*. Comune di Venezia, Assessorato all'Ecologia. Arsenale Editrice, Venezia, 79 pp.

Fedi, M.E., Cartocci, A., Manetti, M., Taccetti, F. and Mandò, P.A. (2007) The ^{14}C AMS facility at LABEC, Florence. *Nucl. Instrum. Meth. B*, **259**, 18–22.

Fontana, A., Mozzi, P. and Bondesan, A. (2004) L'evoluzione geomorfologica della pianura veneto-friulana. In: Bondesan, A. and Meneghel, M. (Eds.) *Geomorfologia della provincia di Venezia*. Esedra editrice, Padova, 113–138.

Francalanci, S., Bendoni, M., Rinaldi, M. and Solari, L. (2013) Ecomorphodynamic evolution of salt marshes: Experimental observations of bank retreat processes. *Geomorphology*, **195**, 53–65. doi:10.1016/j.geomorph.2013.04.026.

Frangipane, G., Pistolato, M., Molinaroli, E., Guerzoni, S. and Tagliapietra, D. (2009) Comparison of loss on ignition and thermal analysis stepwise methods for determination of sedimentary organic matter. *Aquat. Conserv.*, **19**, 24–33.

French, J.R., Spencer, T., Murray, A.L. and Arnold, N.S. (1995) Geostatistical analysis of sediment deposition in two small tidal wetlands, Norfolk, United Kingdom. *J. Coastal Res.*, **11**, 308–321.

Frignani, M. and Langone, L. (1991) Accumulation rates and ^{137}Cs distributions in sediments off the Po River delta and the Emilia-Romagna coast (northwestern Adriatic Sea, Italy). *Cont. Shelf Res.*, **6**, 525–542.

Gatto, P. and Carbognin, L. (1981) The lagoon of Venice: Natural environmental trend and man-induced modification. *Hydrol. Sci. Bull.*, **26**, 379–391.

Gedan, K.B. and Silliman, B.R. (2009) Patterns of salt marsh loss within coastal regions of North America: pre-settlement to present. In: Silliman, B.R., Grosholz E.D. and Bertness, M.D. (Eds.) *Human impacts on salt marshes: a global perspective.* University of California Press, Los Angeles, CA, USA, 253–265.

Gedan, K.B., Silliman, B.R. and Bertness, M.D. (2009) Centuries of human-driven change in salt marsh ecosystems. *Annu. Rev. Mater. Sci.*, **1**, 117–141.

Gedan, K.B., Kirwan, M.L., Wolanski, E., Barbier, E.B. and Silliman, B.R. (2011) The present and future role of coastal wetland vegetation in protecting shorelines: answering recent challenges to the paradigm. *Clim. Change*, **106**(1), 7–29. doi:10.1007/s10584-010-0003-7.

Gee, G.W and Bauder, J.W. (1986) Particle-size analysis. In: Klute, A. (Ed.) *Methods of Soil Analysis, Part 1. Physical and Mineralogical Methods.* Agronomy Monograph No. 9, 2nd ed. American Society of Agronomy/Soil Science Society of America, Madison, WI, 383–411.

Gray, A.B., Pasternack, G.B. and Watson, E.B. (2010) Hydrogen peroxide treatment effects on the particle size distribution of alluvial and marsh sediments. *The Holocene*, **20**, 293–301.

Heiri, O., Lotter, A.F. and Lemcke, G. (2001) Loss on ignition as a method for estimating organic and carbonate content in sediments: reproducibility and comparability of results. *J. Paleolimnol.*, **25**, 101–110.

Horne, J.C., Ferm, J.C., Caruccio, F.T. and Baganz, B.P. (1978) Depositional models in coal exploration and mine planning in Appalachian region. *Am. Assoc. Petr. Geol. Bull.*, **62**, 2379–2411.

Howard, P.J.A. and Howard, D.M. (1990) Use of organic carbon and loss-on-ignition to estimate soil organic matter in different soil types and horizons. *Biol. Fert. Soils*, **9**, 306–310.

Howes, N.C., FitzGerald, D.M., Hughes, Z.J., Georgiou, I.Y., Kulp, M.A., Miner, M.D., et al. (2010) Hurricane-induced failure of low salinity wetlands. *P. Natl. Acad. Sci. USA*, **107**, 14014–14019. doi:10.1073/pnas.0914582107.

Hu, Z., van Belzen, J., van der Wal, D., Balke, T., Wang, Z.B., Stive, M., et al. (2015) Windows of opportunity for salt marsh vegetation establishment on bare tidal flats: The importance of temporal and spatial variability in hydrodynamic forcing. *J. Geophys. Res.-Biogeo.*, **120**, 1450–1469, doi:10.1002/2014JG002870.

Hupp, C.R., Osterkamp, W.R. and Howard, A.D. (1995) *Biogeomorphology – Terrestrial and freshwater systems*. Elsevier, Amsterdam, The Netherlands, 347 pp.

Jenkins, R. and De Vries, J.L. (1970) Practical X-ray Spectrometry. Macmillan, London.

Jones, C., Lawton, J. and Shachak, M. (1994) Organisms as ecosystem engineers. *Oikos*, **69**, 373–386.

Kirwan, M.L. and Guntenspergen, G.R. (2012) Feedbacks between inundation, root production, and shoot growth in a rapidly submerging brackish marsh. *J. Ecol.*, **100**, 764–770.

Kirwan, M.L. and Mudd, S.M. (2012) Response of salt-marsh carbon accumulation to climate change. *Nature*, **489**, 550–553. doi:10.1038/nature11440.

Kirwan, M.L. and Murray, A.B. (2005) Response of an ecomorphodynamic model of tidal marshes to varying sea level rise rates. In: Parker, G. and García, M.H. (Eds.) *River, Coastal and Estuarine Morphodynamics: RCEM 2005*, Taylor and Francis Group, London, ISBN 0415392705, 629–634.

Kirwan, M.L. and Murray, A.B. (2007) A coupled geomorphic and ecological model of tidal marsh evolution. *P. Natl. Acad. Sci. USA*, **104**, 6118–6122.

Kirwan, M.L. and Murray, A.B. (2008) Tidal marshes as disequilibrium landscapes? Lags between morphology and Holocene sea level changes. *Geophys. Res. Lett.*, **35**, L24401. doi:10.1029/2008GL036050.

Kirwan, M.L. and Temmerman, S. (2009) Coastal marsh response to historical and future sea-level acceleration. *Quat. Sci. Rev.*, **28**, 1801–1808. doi:10.1016/j.quascirev.2009.02.022.

Kirwan, M.L., Murray, A.B. and Boyd, W.S. (2008) Temporary vegetation disturbance as an explanation for permanent loss of tidal wetlands. *Geophys. Res. Lett.*, **35**, L05403. doi:10.1029/2007GL032681.

Kirwan, M.L., Guntenspergen, G.R., D'Alpaos, A., Morris, J.T., Mudd, S.M. and Temmerman, S. (2010) Limits of the adaptability of coastal marshes to rising sea level. *Geophys. Res. Lett.*, **37**, L23401. doi:10.1029/2010GL045489.

Kirwan, M.L., Murray, A.B., Donnelly, J.P. and Corbett, D.R. (2011) Rapid wetland expansion during European settlement and its implication for marsh survival under modern sediment delivery rates. Geology, 39(5), 507-510. doi:10.1130/G31789.1.

Larsen, L.G., Moseman, S., Santoro, A.E., Hopfensperger, K. and Burgin, A. (2010) A complex-system approach to predicting effects of sea level rise and nitrogen loading on nitrogen cycling in coastal wetland ecosystem. In: Kemp, P.F. (Ed.) *Eco-DAS VIII Symposium Proceedings*. Waco, Tex, Assoc. Sci. Limnol. Oceanogr., 67–92.

Leonard, L.A. and Croft, A.L. (2006) The effect of standing biomass on flow velocity and turbulence in Spartina alterniflora canopies. *Estuar. Coast. Shelf Sci.*, **69**, 325–336.

Leonard, L.A. and Luther, M.E. (1995) Flow hydrodynamics in tidal marsh canopies. *Limnol. Oceanogr.*, **40**(8), 1474–1484.

Li, H. and Yang, S.L. (2009) Trapping effect of tidal marsh vegetation on suspended sediment, Yangtze Delta. *J. Coastal Res.*, **254**, 915–924. doi:10.2112/08-1010.1.

Lucchini, F., Frignani, M., Sammartino, I., Dinelli, E. and Bellucci, L.G. (2001) Composition of Venice Lagoon sediments: distribution, sources, setting and recent evolution. *GeoActa*, **1**, 1–14.

MacKenzie, R.A. and Dionne, M. (2008) Habitat heterogeneity: importance of salt marsh pools and high marsh surfaces to fish production in two Gulf of Maine salt marshes. *Mar. Ecol.-Prog. Ser.*, **368**, 217–230.

Madricardo, F. and Donnici, S. (2014) Mapping past and recent landscape modifications in the Lagoon of Venice through geophysical surveys and historical maps. *Anthropocene*, **6**, 86–96. doi:10.1016/j.ancene.2014.11.001.

Madricardo, F., Donnici, S., Lezziero, A., De Carli, F., Buogo, S., Calicchia, P., et al. (2007) Palaeoenvironment reconstruction in the Lagoon of Venice through wide-area acoustic surveys and core sampling. *Estuar. Coast. Shelf Sci.*, **75**, 205–213. doi:10.1016/j.ecss.2007.02.031.

Marani, M., Belluco, E., D'Alpaos, A., Defina, A., Lanzoni, S. and Rinaldo, A. (2003) On the drainage density of tidal networks. *Water Resour. Res.*, **39**, 1040. doi:10.1029/2001WR001051.

Marani, M., Belluco, E., Ferrari, S., Silvestri, S., D'Alpaos, A., Lanzoni, S., et al. (2006) Analysis, synthesis and modelling of high-resolution observations of saltmarsh ecogeomorphological patterns in the Venice lagoon. *Estuar. Coast. Shelf Sci.*, **69**(3–4), 414–426. doi:10.1016/j.ecss.2006.05.021.

Marani, M., D'Alpaos, A., Lanzoni, S., Carniello, L., Rinaldo, A. (2007) Biologically-controlled multiple equilibria of tidal landforms and the fate of the Venice Lagoon. *Geophys. Res. Lett.*, **34**, L11402. doi:10.1029/2007GL030178.

Marani, M., D'Alpaos, A., Lanzoni, S., Carniello, L. and Rinaldo, A. (2010) The importance of being coupled: Stable states and catastrophic shifts in tidal biomorphodynamics. *J. Geophys. Res.*, **115**, F04004. doi:10.1029/2009JF001600.

Marani, M., D'Alpaos, A., Lanzoni, S. and Santalucia, M. (2011) Understanding and predicting wave erosion of marsh edges. *Geophys. Res. Lett.*, **38**, L21401. doi:10.1029/2011GL048995.

Marani, M., Da Lio, C. and D'Alpaos, A. (2013) Vegetation engineers marsh morphology through multiple competing stable states. *P. Natl. Acad. Sci. USA*, **110**(9), 3259–3263. doi:10.1073/pnas.1218327110.

Mariotti, G. and Carr, J. (2014) Dual role of salt marsh retreat: Long-term loss and short-term resilience. *Water Resour. Res.*, **50**(4), 2963–2974. doi:10.1002/2013WR014676.

Mariotti, G. and Fagherazzi, S. (2010) A numerical model for the coupled long-term evolution of salt marshes and tidal flats. *J. Geophys. Res.*, **115**, F01004. doi:10.1029/2009JF001326.

Mariotti, G. and Fagherazzi, S. (2013) Critical width of tidal flats triggers marsh collapse in the absence of sea-level rise. *P. Natl. Acad. Sci. USA*, **110**(14), 5353–5356. doi:10.1073/pnas.1219600110.

Mayor, J. and Hicks, C. (2009) Potential impacts of elevated CO_2 on plant interactions, sustained growth, and carbon cycling in salt marsh ecosystems. In: Silliman, B.R., Grosholz, T. and Bertness, M.D. (Eds.) *Human impacts on salt marshes: a global perspective*. University of California Press, Berkeley, California, USA, 207–230.

McClennen, C.E. and Housley, R.A. (2006) Late-Holocene channel meander migration and mudflat accumulation rates, Lagoon of Venice, Italy. *J. Coastal Res.*, **22**(4), 930–945.

Mcleod, E., Chmura, G.L., Bouillon, S., Salm, R., Björk, M., Duarte, C.M., et al. (2011) A blueprint for blue carbon: toward an improved understanding of the role of vegetated coastal habitats in sequestering CO_2. *Front. Ecol. Environ.*, **9**(10), 552–560. doi:10.1890/110004.

Mendelsshon, I.A., McKee, K.L. and Patrick, W.H. (1981) Oxygen Deficiency in Spartina alterniflora roots: Metabolic Adaptation to Anoxia. *Science*, **214**, 439–441.

MichczyÒski, A. (2007) Is it possible to find a good point estimate of a calibrated radiocarbon date? *Radiocarbon*, **49**, 393–401.

Mikutta, R., Kleber, M., Kaiser, K. and Jahn, R. (2005) Review: Organic matter removal from soils using hydrogen peroxide, sodium hypochlorite, and disodium peroxodisulfate. *Soil Sci. Soc. Am. J.*, **69**, 120–135.

Mitsch, W.J. and Gosselink, J.G. (2000) *Wetlands*. 3rd edition, John Wiley, New York, USA

Moffett, K.B., Robinson, D.A. and Gorelick, S.M. (2010) Relationship of salt marsh vegetation zonation to spatial patterns in soil moisture, salinity, and topography. *Ecosystems*, **13**, 1287–1302.

Möller, I., Spencer, T., French, J.R., Leggett, D. and Dixon, M. (1999) Wave transformation over salt marshes: A field and numerical modelling study from North Norfolk, England. *Estuar. Coast. Shelf Sci.*, **49**, 411–426. doi:10.1006/ecss.1999.0509.

Möller, I., Kudella, M., Rupprecht, F., Spencer, T., Paul, M., van Wesenbeeck, B.K., et al. (2014) Wave attenuation over coastal salt marshes under storm surge conditions. *Nat. Geosci.*, **7**, 727–731. doi:10.1038/NGEO2251.

Mook, D.H. and Hoskin, C.M. (1982) Organic determination by ignition, caution advised. *Estuar. Coast. Shelf Sci.*, **15**, 697–699.

Morgan, P.A., Burdick, D.M. and Short, F.T. (2009) The functions and values of fringing salt marshes in Northern New England, USA. *Estuaries Coasts*, **32**, 483–495.

Morris, J.T., Sundareshwar, P.V., Nietch, C.T., Kjerfve, B. and Cahoon, D.R. (2002) Responses of coastal wetlands to rising sea level. *Ecology*, **83**, 2869–2877.

Mozzi, P., Furlanetto, P. and Primon, S. (2004) Tra Naviglio Brenta e Bacchiglione. In: Bondesan, A. and Meneghel, M. (Eds.) *Geomorfologia della provincia di Venezia*. Esedra editrice, Padova, 269–298.

Mudd, S.M. (2011) The life and death of salt marshes in response to anthropogenic disturbance of sediment supply. *Geology*, **39**, 511–512. doi:10.1130/focus052011.1.

Mudd, S.M., Fagherazzi, S., Morris, J.T. and Furbish, D.J. (2004) Flow, sedimentation, and biomass production on a vegetated salt marsh in South Carolina: Toward a predictive model of marsh morphologic and ecologic evolution. In: Fagherazzi, S., Marani, M. and Blum, L.K. (Eds.) *The Ecogeomorphology of Salt Marshes*. Coast. Estuar. Stud., Am. Geophys. Un., Washington, DC, **59**, 165–188.

Mudd, S.M., Howell, S. and Morris, J.T. (2009) Impact of dynamic feed-backs between sedimentation, sea-level rise, and biomass production on near surface marsh stratigraphy and carbon accumulation. *Estuar. Coast. Shelf Sci.*, **82**, 377–389.

Mudd, S.M., D'Alpaos, A. and Morris, J.T. (2010) How does vegetation affect sedimentation on tidal marshes? Investigating particle capture and hydrodynamic controls on biologically mediated sedimentation. *J. Geophys. Res.*, **115**, F03029. doi:10.1029/2009JF001566.

Murray, A.B., Knaapen, M.A.F., Tal, M. and Kirwan, M.L. (2008) Biomorphodynamics: physical-biological feedbacks that shape landscapes. *Water Resour. Res.*, **44**(11), W11301. doi:10.1029/2007WR006410.

Murray, B.C., Pendleton, L., Jenkins, W.A. and Sifleet, S. (2011) Green Payments for Blue Carbon. Economic Incentives for protecting Threatened Coastal habitats. *Duke Nicholas Institute Report*, NI R 11-04.

Nellemann, C., Corcoran, E., Duarte, C.M., Valdés, L., De Young, C., Fonseca, L., et al. (2009) *Blue Carbon. The role of healthy oceans in binding carbon. A rapid response assessment.* GRID-Arendal, United Nations Environment Programme. ISBN:978-82-7701-060-1.

Neubauer, S.C. (2008) Contributions of mineral and organic components to tidal freshwater marsh accretion. *Estuar. Coast. Shelf Sci.*, **78**, 78–88.

Ninfo, A., Fontana, A., Mozzi, P. and Ferrarese, F. (2009) The map of Altinum, ancestor of Venice. *Science*, **325**, 577–577.

Nyman, J.A., Walters, R.J., Delaune, R.D. and Patrick, W.H. (2006) Marsh vertical accretion via vegetative growth. *Estuar. Coast. Shelf Sci.*, **69**, 370–380.

Pendleton, L., Donato, D.C., Murray, B.C., Crooks, S., Jenkins, W.A., Sifleet, S., et al. (2012) Estimating global "Blue Carbon" emissions from conversion and degradation of vegetated coastal ecosystem. *PLoS ONE*, **7**(9), e43542. doi:10.1371/journal.pone.0043542.

Pennings, S.C., Grant, M. and Bertness, M.D. (2005) Plant zonation in low-latitudes salt marshes: Disentangling the roles of flooding, salinity and competition. *J. Ecol.*, **93**, 159–167.

Perillo, G.M.E., Wolanski, E., Cahoon, D.R. and Brinson, M.M. (2009) *Coastal Wetlands: An Integrated Ecosystem Approach*. Elsevier, Oxford, UK Burlington.

Primon, S. and Furlanetto P. (2004) La laguna sud. In: Bondesan, A. and Meneghel, M. (Eds.) *Geomorfologia della provincia di Venezia*. Esedra editrice, Padova, 307–326.

Protocol of Simon Fraser University Soil Science Lab, compiled by Robertson, S. (2011) *Direct estimation of organic matter by loss on ignition: Methods*. Property of SFU Soil Science Lab.

Ratliff, K., Braswell, A. and Marani, M. (2015) Spatial response of coastal marshes to increased atmospheric CO_2, *P. Natl. Acad. Sci. USA*, **112**(51), 15580–15584. doi:10.1073/pnas.1516286112.

Ravera, O. (2000) The Lagoon of Venice: the result of both natural factors and human influence. *J. Limnol.*, **59**(1), 19–30.

Reed, D.J. (2002) Sea-level rise and coastal marsh sustainability: geological and ecological factors in the Mississippi delta plain. *Geomorphology*, **48**, 233–243.

Reed, D.J., Spencer, T., Murray, A.L., French, J.R. and Leonard, L. (1999) Marsh surface sediment deposition and the role of tidal creeks: Implications for created and managed coastal marshes. *J. Coastal Conserv.*, **5**, 81–90. doi:10.1007/BF02802742.

Reimer, P.J., Baillie, M.G.L., Bard, E., Bayliss, A., Beck, J.W., Blackwell, P.G., et al. (2009) IntCal09 and Marine09 radiocarbon age calibration curves, 0–50,000 years cal BP. *Radiocarbon*, **51**, 1111–1150.

Reinhardt, L., Jerolmack, D., Cardinale, B.J., Vanacker, V. and Wright, J. (2010) Dynamic interactions of life and its landscape: feedbacks at the interface of geomorphology and ecology. *Earth Surf. Proc. Land.*, **35**(1), 78–101. doi:10.1002/esp.1912.

Richter, T.O., Van Der Gaast, S., Koster, B., Vaars, A., Gieles, R., De Stigter, H.C., et al. (2006) The Avaatech XRF Core Scanner: technical description and application to NE Atlantic sediments. In: Rothwell, R.G. (Ed.) New Techniques in Sediment Core Analysis, Geological Society, London, 39–50.

Rizzetto, F. and Tosi, L. (2011) Aptitude of modern salt marshes to counteract relative sea-level rise, Venice Lagoon (Italy). *Geology*, **39**(8), 755–758. doi:10.1130/G31736.1.

Sanchez-Cabeza, J.A., Masqué, P., Radakovitch, O., Heussner, S., Brand, T., Lindsay, F., et al. (1994) Data quality assurance in Euromarge-NB: ^{210}Pb intercomparison exercises. In: *First Workshop of the Mediterranean Targeted Project*, Barcelona, Spain, November 21st–23rd , 1994.

Santisteban, J.I., Mediavilla, R., López-Pamo, E., Dabrio, C.J., Ruiz Zapata, M.B., Gil García, M.J., et al. (2004) Loss on ignition: a qualitative or quantitative method for organic matter and carbonate mineral content in sediments? *J. Paleolimnol.*, **32**, 287–299.

Sfriso, A., Favaretto, M., Ceoldo, S., Facca, C. and Marcomini, A. (2005) Organic carbon changes in the surface sediments of the Venice lagoon. *Environ. Int.*, **31**, 1002–1010. doi:10.1016/j.envint.2005.05.010.

Sheehan, M.R. and Ellison, J.C. (2014) Intertidal morphology change following Spartina anglica introduction, Tamar Estuary, Tasmania. *Estuar. Coast. Shelf Sci.*, **149**, 24–37.

Sifleet, S., Pendleton, L. and Murray, B.C. (2011) State of the Science on Coastal Blue Carbon. A summary for Policy Makers. *Duke Nicholas Institute Report*, NI R 11-06.

Silliman, B., Bertness, M. and Grosholz, E. (2009) *Human Impacts on Salt Marshes: A Global Perspective*. University Presses of California, Columbia and Princeton, University of California Press.

Silvestri, S. and Marani, M. (2004) Salt-marsh vegetation and morphology: Basic physiology, modelling and remote sensing observations. In: Fagherazzi, S., Marani, M. and Blum, L.K. (Eds.) *Coastal and Estuarine Studies. The Ecogeomorphology of tidal marshes*, AGU, Washington, D.C., **59**, 5–26.

Silvestri, S., Marani, M. and Marani, A. (2003) Hyperspectral remote sensing of salt marsh vegetation, morphology and soil topography. *Phys. Chem. Earth*, **28**, 15–25.

Silvestri, S., Defina, A. and Marani, M. (2005) Tidal regime, salinity and salt marsh plant zonation. *Estuar. Coast. Shelf Sci.*, **62**, 119–130.

Southerland, R.A. (1998) Loss-on-ignition estimates of organic matter and relationships to organic carbon in fluvial bed sediments. *Hydrobiologia*, **389**, 153–167.

Strozzi, T., Teatini, P., Tosi, L., Wegmüller, U. and Werner, C. (2013) Land subsidence of natural transitional environments by satellite radar interferometry on artificial reflectors. *J. Geophys. Res.*, **118**, 1177–1191. doi:10.1002/jgrf.20082.

Surian, N. and Cisotto, A. (2007) Channel adjustments, bedload transport and sediment sources in a gravel-bed river, Brenta River, Italy. *Earth Surf. Process. Landforms*, **32**, 1641–1656. doi:10.1002/esp.1591.

Surian, N., Ziliani, L., Comiti, F., Lenzi, M.A. and Mao, L. (2009) Channel adjustments and alteration of sediment fluxes in gravel-bed rivers of north-eastern Italy: potentials and limitations for channel recovery. *River Res. Applic.*, **25**, 551-567. doi:10.1002/rra.1231.

Teatini, P., Tosi, L., Strozzi, T., Carbognin, L., Wegmüller, U. and Rizzetto, F. (2005) Mapping regional land displacements in the Venice coastland by an integrated monitoring system. *Remote Sens. Environ.*, **98**, 403–413. doi:10.1016/j.rse.2005.08.002.

Teatini, P., Tosi, L., Strozzi, T., Carbognin, L., Cecconi, G., Rosselli, R., et al. (2012) Resolving land subsidence within the Venice Lagoon by persistent scatterer SAR interferometry. *Phys. Chem. Earth Pts. A/B/C*, **40–41**, 72–79. doi:10.1016/j.pce.2010.01.002.

Temmerman, S., Govers, G., Meire, P. and Wartel, S. (2003) Modelling long-term tidal marsh growth under changing tidal conditions and suspended sediment concentration, Scheldt estuary, Belgium. *Mar. Geol.*, **193**, 151–169. doi:10.1016/S0025-3227(02)00642-4.

Temmerman, S., Govers, G., Meire, P. and Wartel, S. (2004) Simulating the long-term development of levee-basin topography on tidal marshes. *Geomorphology*, **63**, 39–55. doi:10.1016/j.geomorph.2004.03.004.

Temmerman, S., Bouma, T.J., Van de Koppel, J., Van der Wal, D., De Vries, M.B. and Herman, P.M.J. (2007) Vegetation causes channel erosion in a tidal landscape. *Geology*, **35**, 631–634. doi:10.1130/G23502A.1.

Temmerman, S., Meire, P., Bouma, T.J., Herman, P.M.J., Ysebaret, T. and De Vriend, H.J. (2013) Ecosystem-based coastal defence in the face of global change. *Nature*, **504**, 79–83. doi:10.1038/nature12859.

Tosi, L., Carbognin, L., Teatini, P., Strozzi, T. and Wegmüller, U. (2002) Evidence of the present relative land stability of Venice, Italy, from land, sea, and space observations. *Geophys. Res. Lett.*, **29**(12), 1562. doi:10.1029/2001GL013211.

Tosi, L., Rizzetto, F., Bonardi, M., Donnici, S., Serandrei-Barbero, R. and Toffoletto, F. (2007a) *Note illustrative della Carta geologicad'Italia alla scala 1:50.000. 128 – Venezia*. APAT, Dipartimento Difesa del suolo, Servizio Geologico d'Italia, Casa Editrice SystemCart, Roma, 164 pp., 2 allegati cartografici.

Tosi, L., Rizzetto, F., Bonardi, M., Donnici, S., Serandrei-Barbero, R. and Toffoletto, F. (2007b) *Note illustrative della Carta geologicad'Italia alla scala 1:50.000. 148-149 – Chioggia-Malamocco*. APAT, Dipartimento Difesa del suolo, Servizio Geologico d'Italia, Casa Editrice SystemCart, Roma, 164 pp., 2 allegati cartografici.

Tosi, L., Rizzetto, F., Zecchin, M., Brancolini, G. and Baradello, L. (2009a) Morphostratigraphic framework of the Venice Lagoon (Italy) by very shallow water VHRS surveys: Evidence of radical changes triggered by human-induced river diversions. *Geophys. Res. Lett.*, **36** (9), L09406. doi:10.1029/2008GL037136.

Tosi, L., Teatini, P., Carbognin, L. and Brancolini, G. (2009b) Using high resolution data to reveal depht-dependent mechanisms that drive land subsidence: The Venice coast, Italy. *Tectonophysics*, **474**, 271–284. doi:10.1016/j.tecto.2009.02.026.

Viles, H. (1988) *Biogeomorphology*. Basil Blackwell, Oxford.

Weliky, K., Suess, E., Ungerer, C.A., Müller, P.J. and Fischer, K. (1983) Problems with accurate carbon measurements in marine sediments and particulate organic matter in sea water: a new approach. *Limnol. Oceanogr.*, **28**, 1252–1259.

Woodwell, G.M., Rich, P.H. and– Mall, C.S.A. (1973) Carbon in estuaries. In: Woodwell, G.M. and Pecari, E.V. (Eds.) *Carbon in the biosphere*, U.S. AEC, 221–240.

Yang, S.L. (1998) The role of Scirpus marsh in attenuation of hydrodynamics and retention of fine sediment in the Yangtze Estuary. *Estuar. Coast. Shelf Sci.*, **47**, 227–233. doi:10.1006/ecss.1998.0348.

Zecchin, M., Baradello, L., Brancolini, G., Donda, F., Rizzetto, F. and Tosi, L. (2008) Sequence stratigraphy based on high-resolution seismic profiles in the late Pleistocene and Holocene deposits of the Venice area. *Mar. Geol.*, **253**, 185–198. doi:10.1016/j.margeo.2008.05.010.

Zecchin, M., Brancolini, G., Tosi, L., Rizzetto, F., Caffau, M. and Baradello, L. (2009) Anatomy of the Holocene succession of the southern Venice lagoon revealed by very high-resolution seismic data. *Contin. Shelf Res.*, **29**, 1343–1359. doi:10.1016/j.csr.2009.03.006.

Zecchin, M., Caffau, M. and Tosi, L. (2011) Relationship between peat bed formation and climate changes during the last glacial in the Venice area. *Sediment. Geol.*, **238**, 172–180. doi:10.1016/j.sedgeo.2011.04.011.

Zecchin, M., Tosi, L., Caffau, M., Baradello, L. and Donnici, S. (2014) Sequence stratigraphic significance of tidal channel system in a shallow lagoon (Venice, Italy). *The Holocene*, 1–13. doi:10.1177/0959683614526903.